12-2017

The Influence of Varying Fiber Stacking Sequence on the Tensile, Impact, and Water Absorption Properties of Unidirectional Flax/E-Glass Fiber Reinforced Epoxy Composite

Mohammed F. Al-Edhari
Utah State University

THE INFLUENCE OF VARYING FIBER STACKING SEQUENCE ON THE TENSILE, IMPACT, AND WATER ABSORPTION PROPERTIES OF UNIDIRECTIONAL FLAX/E-GLASS FIBER REINFORCED EPOXY COMPOSITE

by

Mohammed F. Al-Edhari

A thesis submitted in partial fulfillment
of the requirements for the degree

of

MASTER OF SCIENCE

in

Mechanical Engineering

Approved:

Thomas H. Fronk, Ph.D. Major Professor	Ling Liu, Ph.D. Committee Member
Nick Roberts, Ph.D. Committee Member	Mark R. McLellan, Ph.D. Vice President for Research and Dean of the School of Graduate Studies

UTAH STATE UNIVERSITY
Logan, Utah

2017

ABSTRACT

The Influence of Varying Fiber Stacking Sequence on the Tensile, Impact, and Water Absorption Properties of Unidirectional Flax/E-Glass Fiber Reinforced Epoxy Composite

by

Mohammed F. Al-Edhari, Master of Science

Utah State University, 2017

Major Professor: Thomas H. Fronk, Ph.D.
Department: Mechanical and Aerospace Engineering

This thesis includes the study of the mechanical performance of two different types of fibers reinforced hybrid composites. Two kinds of fibers, natural fiber (flax) and synthetic fiber (E-glass), are used to reinforce epoxy resin. To evaluate the effective properties of the hybrid composites, a micromechanical analysis of the structure genome (SG) of a unidirectional fiber hybrid composites is performed using finite element analysis (FEA). Both fibers are assumed to be circular and packed in a hexagonal pattern. The effects of varying volume fractions and fiber locations, of the two fibers, on the elastic properties of the hybrid composites are studied using FEA. Rule of hybrid mixtures (RoHM) and Halpin-Tsai equations, which are analytical equations, are used as a preliminary prediction of the elastic constants of the hybrid composites. Then, the comparison is made between FEA and analytical results. The predicted elastic constants through numerical homogenization are in good a agreement with analytical results. The effect of changing fiber locations on the tensile strength of hybrid composite is investigated using tensile tests. Impact strength of single fiber composites and flax/glass fiber hybrid composites, in which various stacking sequences of flax and glass fibers are used, are obtained using Charpy impact tests. Moisture absorption test was performed by immersing single fiber composites and various

stacking sequences of hybrid composites in deionized water at room temperature for a week. To investigate the effect of water absorption on the tensile properties of composite, tensile test was done on various stacking sequences of the hybrid composite. FEA and analytical equations showed that Young's and shear moduli increased and the axial Poison's ratio decreased linearly with the glass fiber content. Also, FEA showed that changing fiber locations have no effect on the effective properties of the hybrid composite. However, changing fiber stacking sequences showed a significant effect on tensile strength, impact strength, and water absorption properties of the hybrid composites. It was concluded that better design of the hybrid composite was achieved when glass fibers placed on the extreme positions and flax fibers in the middle. Positive hybrid effect is achieved from hybridization of E-glass fiber with flax fiber.

(124 pages)

PUBLIC ABSTRACT

The Influence of Varying Fiber Stacking Sequence on the Tensile, Impact, and Water Absorption Properties of Unidirectional Flax/E-Glass Fiber Reinforced Epoxy Composite

by

Mohammed F. Al-Edhari, Master of Science

Utah State University, 2017

Major Professor: Thomas H. Fronk, Ph.D.
Department: Mechanical and Aerospace Engineering

This thesis includes the study of the mechanical performance of two different types of fibers reinforced hybrid composites. Two kinds of fibers, natural fiber (flax) and synthetic fiber (E-glass), are used to reinforce epoxy resin. To evaluate the effective properties of the hybrid composites, a micromechanical analysis of the structure genome (SG) of a unidirectional fiber hybrid composites is performed using finite element analysis (FEA). Both fibers are assumed to be circular and packed in a hexagonal pattern. The effects of varying volume fractions and fiber locations, of the two fibers, on the elastic properties of the hybrid composites are studied using FEA. Rule of hybrid mixtures (RoHM) and Halpin-Tsai equations, which are analytical equations, are used as a preliminary prediction of the elastic constants of the hybrid composites. Then, the comparison is made between FEA and analytical results. The predicted elastic constants through numerical homogenization are in good a agreement with analytical results. The effect of changing fiber locations on the tensile strength of hybrid composite is investigated using tensile tests. Impact strength of single fiber composites and flax/glass fiber hybrid composites, in which various stacking sequences of flax and glass fibers are used, are obtained using Charpy impact tests. Moisture absorption test was performed by immersing single fiber composites and various

stacking sequences of hybrid composites in deionized water at room temperature for a week. To investigate the effect of water absorption on the tensile properties of composite, tensile test was done on various stacking sequences of the hybrid composite. FEA and analytical equations showed that Young's and shear moduli increased and the axial Poison's ratio decreased linearly with the glass fiber content. Also, FEA showed that changing fiber locations have no effect on the effective properties of the hybrid composite. However, changing fiber stacking sequences showed a significant effect on tensile strength, impact strength, and water absorption properties of the hybrid composites. It was concluded that better design of the hybrid composite was achieved when glass fibers placed on the extreme positions and flax fibers in the middle. Positive hybrid effect is achieved from hybridization of E-glass fiber with flax fiber.

To my parents who could not see this thesis completed, to my siblings, and to all my teachers

ACKNOWLEDGMENTS

My huge appreciation goes to my sponsor "the Higher Committee for Education Development in Iraq" (HCED) for providing me the scholarship to pursue masters degree in mechanical engineering at Utah State University.

It has been a great honor to work with Dr. Thomas H. Fronk who has dedicated a lot of his time and effort for this research. His supervision, support, intelligence, enthusiasm, and useful advice helped in all the time of research. Without his guidance and persistence help this thesis would not be done.

I am so grateful to Dr. Ling Liu and Dr. Nick Roberts for being on my supervisory committee. My sincere appreciation goes to staff of the MAE department, Chris Spall, Karen Zobell, Terry Zollinger, and Mike Morgan for everything run smoothly.

I owe debt of gratitude to Dr. Andrew Sorensen, Dr. Marc Maguire, and Dr. Robert Thomas in Civil Engineering department at Utah State University for their generous offer of letting me use the impact tester in SMASH Lab. I thank my friend Madher Alfindee, PhD student in Chemistry Science department at Utah State University, who provided de-ionized water for the research.

I must express my sincere gratitude and huge appreciation to my parents, siblings, and all teachers. Without whom I cannot reach to the point I am now.

I extend my thanks to all friends especially those who stood behind me and support me after the death of my parents.

Mohammed F. Al-Edhari

CONTENTS

LIST OF TABLES

LIST OF FIGURES

ACRONYMS

FEA	Finite Element Analysis
SG	Structure Genome
MSG	Mechanics of Structure Genome
RVE	Representative Volume Element
RoHM	Rule of Hybrid Mixtures
RoM	Rule of Mixtures
SEM	Scanning Electron Microscope
VARTM	Vacuum Assisted Resin Transfer Modeling

CHAPTER 1

Introduction

1.1 Motivation

Composite materials are used in a wide range of applications. They have been successfully used for structural applications in the aircraft, automotive, marine, and infrastructure industries. The reason behind the invention of composite materials comes from the demand of high strength and low weight materials [1, 2]. Since the desire for stronger and lighter materials continues to grow, composites will be in ever-increasing demand. The evidence of increasing demands for composites can be clearly noticed in the aerospace industry, as composites are gradually substituting metal components as both primary and secondary structures in todays aircraft. For example, 50% of the Boing 787 weight is made up of composites and 25% of the Airbus $A380$ weight is made up of composites [3]. The increased use of composite materials is due to many excellent properties they exhibit compared to metals such as higher strength and stiffness, lower cost, lower weight, and better corrosion and fatigue resistance [2]. However, most of the existing composites are based on synthetic fibers as reinforcement such as carbon, glass, boron, kevlar, and aramid fibers which are petroleum-based fibers, energy consuming, and non-biodegradable [4]. Emissions of toxic gases such as carbon dioxide due to burning of these composites and polluting the soil due to non-biodegradability of these composites lead to adding pollution to the environment [5]. For these reasons, it is necessary to find another source of fibers with lower impact on the environment. Natural fibers present good alternatives to synthetic fibers [4, 6].

Natural fibers show good alternative to synthetic fibers because they possess the advantages of low density, low-cost, high specific strength, recyclability, and the sources of these fibers are green or eco-friendly [7, 8]. Furthermore, the energy needed to produce natural fibers is much lower than the energy needed to produce synthetic fibers [2, 9]. However, the

poor wettability, poor adhesion, poor compatibility to the matrix, and the poor dimensional stability due to their hydrophilic nature are the biggest challenges of using natural fibers to reinforce polymeric resin [10, 11]. Although several natural fibers show good mechanical properties such as flax, hemp, and kenaf, the use of natural fibers is still limited to non-structural applications due to their lower stiffness, strength, and thermo-physical and impact properties compared to synthetic fibers reinforced polymeric resins and conventional materials [12, 13].

In order to improve the properties that lacked in natural fiber composites, natural fibers are usually combined with one or more than one type of synthetic fibers. The mechanical properties are improved by adding stiffer and stronger synthetic fiber to natural fiber reinforced polymeric resin. The moisture absorption behavior is enhanced due to the barrier provided by the more impermeable synthetic fiber [14]. Hybridization with glass fiber provides a method to improve the mechanical properties of natural fiber composites. Mishra et al. [8] stated that hybrid natural/glass composites with $5.7wt\%$ of glass fiber leads to improve the mechanical properties and the dimensional stability of composite. Davoodi et al. [15] claimed that hybridization of natural fibers with glass fiber leads to improve the mechanical properties over natural fibers alone.

Hybridization is usually classified into two types: interlaminate and intralaminate. Interlaminate, or simply laminate, composed of layers made of different fibers, whereas, in intralaminate, more than one type of fiber embedded in a single matrix [16]. In this thesis, only intralaminate hybridization is of interest. The behavior of the developed hybrid composites is a weighed sum of the individual components in which there is a more favorable balance between the inherent advantages and disadvantages. The advantage of using a hybrid composite is that one type of fiber can improve the property lacking in the other [17]. As a result from hybridization, balance in cost and performance could be attained through proper material design [18]. The properties of the hybrid composite highly depend on the fiber contents, length of individual fibers, fiber orientations, bonding between fibers and matrix, and dispersion of both fibers. The strength of the hybrid composite mainly depends

on the failure strain of both fibers in unidirectional direction. Maximum hybrid results can be achieved when the fibers are highly strain compatible [19].

The mechanical properties in the fiber direction of the hybrid composite consisting of two types of fibers can be predicted by the rule of hybrid mixture.

$$P^H = P^m V^m + P^{f1} V^{f1} + P^{f2} V^{f2} \tag{1.1}$$

Where P^H is the property to be investigated, P^m is the property of the matrix, P^{f1} is the property of the first fiber, and P^{f2} is the property of the second fiber. V^m, V^{f1}, V^{f2} are the volume fractions of the matrix, first fiber, and second fiber respectively .

$$V^m + V^{f1} + V^{f2} = 1 \tag{1.2}$$

It has been shown that the rule of hybrid mixture gives good results in the fiber direction [20, 21]. A positive or negative hybrid effect is defined as a positive and negative deviation of a certain property from the rule of hybrid mixture [22]. In this thesis, the term hybrid effect is used to describe the improvement in the mechanical properties of a composite containing two different types of fibers.

1.2 Thesis Statement

In this thesis, a unidirectional flax fiber and E-glass fiber are selected to make the hybrid composite. E-glass fiber is selected to be combined with fiber fiber to reinforce polymeric resin for structural application purposes with the aim of improving tensile, impact, and water absorption properties of composite compared to flax fiber reinforced polymeric resin. Also, to produce composite lighter in weight, cheaper, and less impact on environment compared to glass fiber reinforced polymeric resin. The reason behind choosing flax fiber among all other natural fibers is because flax fiber appears to have the best potential combination of low-cost, low weight, and high strength and stiffness for structural applications [23–25].

Most of the research in natural/synthetic fiber hybrid composites that have been found

in the literature are based on experiments. There are many parameters that can alter the mechanical properties of the developed hybrid composites such as the relative volume fraction and fibers locations. The effect of changing these parameters in the hybrid composite are studied in this thesis. It is time-consuming and costly to study the effect of changing these parameters in the hybrid composite by using experiments. The FEA offers the opportunity of saving time and money to study the effect of changing these parameters. That is why it is of interest in this thesis to use micromechanical analysis on SG of hybrid composite. The results of hybridizing flax fiber with glass fiber reinforced polymeric resin is compared to flax fiber and glass fiber reinforced polymer individually. Analytical equations are also used as a preliminary prediction of the effective elastic properties of the composites. The FEA and analytical results of the hybrid composite are compared with the experimental results. The experimental results are obtained from the conventional tensile tests. The water absorption properties of the devolved hybrid composite are investigated by immersing the hybrid composite specimens in de-ionized water for a week. The effect of water absorption on the tensile properties of the composites are considered in this thesis. Finally, Charpy impact test of notched specimen are carried out on flax fiber composite, glass fiber composite, and flax/glass fiber hybrid composite. All the tests are performed for different staking sequences of flax and glass fiber in the polymeric resin. The best design of the hybrid composite are decided based on the water absorption, tensile, and impact tests.

1.3 Literature Review

In the present thesis, the term hybrid composite refers to the incorporation of two different types of fibers embedded into a single matrix. Hybrid composite materials are used in wide range of applications due to their low cost, low strength to weight ratio, and ease of manufacturing [26]. Hybridization of two different types of fibers provides an option of achieving a blend of properties such as stiffness, strength and ductility, which cannot be achieved by single fiber reinforced composites [6].

Many factors can help to increase the hybrid effect. These factors include the strength ratio, failure strain ratio, stiffness ratio, strength of low elongation fiber, fiber dispersion,

the relative volume fraction of fibers, the orientation of fibers, adhesion between fibers and matrix, and the length of individual fibers [22,27]. Well dispersed fibers and small fraction of low elongation fiber lead to maximize the hybrid effect [22]. Fu et al. showed that the tensile properties of hybrid composite increased as the length of fiber increased and it was unchanged after a length of fiber reached to a specific length [27]. Hybrid composites can be designed by a combination of two different types of synthetic fibers, a synthetic fiber and a natural fiber, and two different types of natural fibers.

1.3.1 Overview of Synthetic and Natural Fibers

In the field of composites, fibers are hair-like materials that can usually be used to reinforce polymeric resin. There are two different types of fibers, synthetic and natural fibers. Synthetic fibers are human made fibers such as carbon, glass, kevlar, boron, and aramid. In another hand, natural fibers are these fibers which are obtained from natural resources such as plant, animal, and mineral resources. There are many different types of natural fibers, they are distinguished by their origin. Fig.1.1 shows types of natural fibers and examples for each type [18, 28]. As can be noticed in Fig. 1.1, plant natural fibers can be classified according to their location in the plant. Typical mechanical properties of commonly used natural and synthetic fibers are presented in the Table 1.1. The properties listed in Table 1.1 are collected from references [9, 29, 30]. As can be seen in Table 1.1, mechanical properties of natural fibers are varied in wide range distribution. These wide range of variations in mechanical properties of natural fibers can be attributed to many reasons. First, it can be demonstrated by the variability in their chemical composition and structure (the chemical constituent content, microfibrillar angle, size of the lumen, length of the fiber, diameter of the fiber, and defects) due to many factors including: age of the plant, quality of the soil where they planted and the environmental conditions during planting and growth [31–33]. The location of fibers in the plant also has influence on the mechanical properties of fibers. For instance, Charlet et al. [34] showed that flax fibers in the middle of stem have better mechanical properties than other locations. Thirdly, it can be referred to different testing method or different environmental conditions during

testing (speed loading, number of sample tested, relative humidity, and temperature) [35]. Moreover, mechanical testing can be performed at bundle of fibers or single fiber. When mechanical testing carried out at bundle of fibers, slippage might occur at adjacent fibers. Consequently, mechanical properties of bundle are lower than those of single fiber.

Table 1.1: Typical mechanical properties of natural and synthetic fibers

Fiber	Density (g/cm^3)	Tensile modulus(GPa)	Tensile strength (MPa)	Strain at break (%)
Cotton	1.5-1.6	5.5-12.6	400	2-10
Jute	1.3-1.5	10-55	393-800	1.5-1.8
Hemp	1.35	30-60	580-1110	1.6-4.5
Flax	1.5	50-70	343-1035	1.2-3
Kenaf	1.45	22-60	295-930	2.7-6.9
Coir	1.2	6	175	15-25
Sisal	1.3-1.5	9.4-28	507-855	2-2.5
Banana	1.35	27-32	529-914	5-6
Bamboo	0.6-1.1	11-36	140-441	1.3-8
OPEFB	0.7-1.55	3.2	248	2.5
Pineapple	1.5	60-82	170-1627	1-3
Hardwood	0.3-0.88	5.2-15.6	51-120.7	-
Softwood	0.3-0.59	3.6-14.3	45.5-11.7	4.4
Silk	1.3	5-25	100-1500	15-60
Wool	1.3	2.3-5.5	50-315	13.2 -35
E-glass	2.5	70-73	2000-3500	2.5
S-glass	2.5	86	4570	2.8
Carbon	1.74	263	4000	1.4-1.8

1.3.2 Synthetic-Synthetic Fiber Hybrid Composite

Among all the possible combinations of synthetic/synthetic fiber, the glass/carbon fiber hybrid composites are the most common. The carbon fiber is strong, relatively stiff, and expensive while the glass fiber is cheaper and has better fracture property, but it lacks the strength and stiffness of carbon fiber. By combining carbon fiber and glass fiber, the tensile modulus decreases, fracture strain increases, and the cost of the composite decreases when

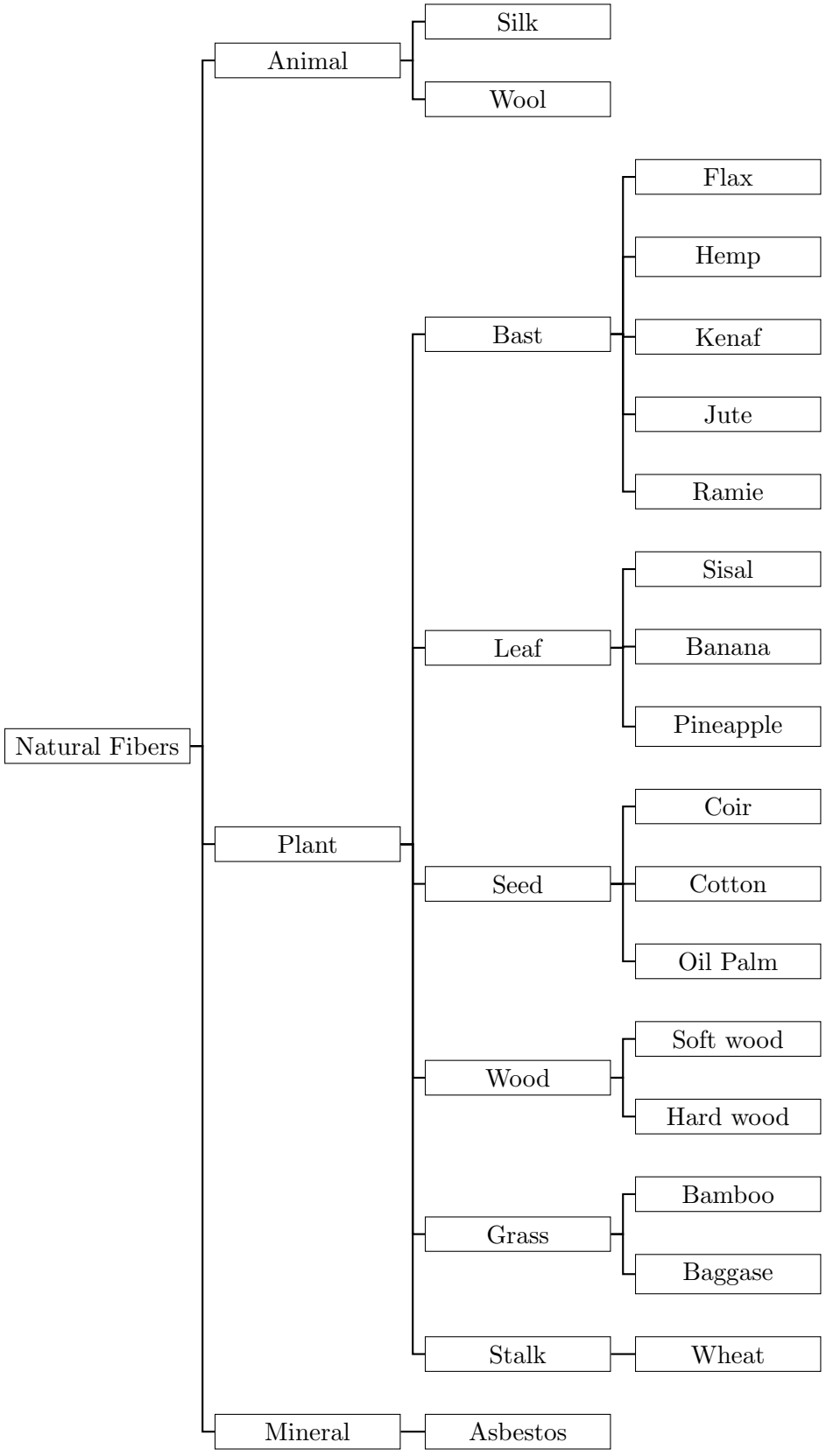

Fig. 1.1: Classification of natural fibers according to their origin.

compared to carbon fiber composite. When compared to glass fiber composite, fracture strain decreases while the tensile strength and tensile modulus increase. Tensile strength and modulus of the hybrid composite increase while the failure strain decreases with increasing the fiber content of carbon fiber [27].

Banerjee et al. [36] performed micromechanical analysis of the RVE of E-glass/carbon fiber reinforced epoxy resin. The elastic constants and strength properties were evaluated by using analytical formula and the results were compared with the FEA results. In their study, the effect of changing fiber locations on the mechanical properties for the same volume fractions was studied. They found that the overall stiffness and elastic constant for a given volume fraction is not affected by changing fiber locations. They reported that the elastic constants in the fiber direction varying linearly with the variation of volume fraction of carbon fiber.

The hybridization of glass fiber with carbon mat in thermoplastic matrix was reported by Kim et al. [21]. The aim of their study is to reduce the weight of the conventional glass mat thermoplastic bumper beam. The glass fiber mat thermoplastic was substituted with glass/carbon mat thermoplastic. Various designs of glass/carbon mat thermoplastic was devised for the bumper beam and the final design of glass/carbon mat thermoplastic was selected by considering the weight, the impact performance, and the content of carbon fiber. They reported that carbon fiber reinforced plastic possesses a higher specific strength under high impact load than that of glass fiber reinforced plastic. Since the density of carbon fiber is lower than the density of glass fiber and the tensile strength and modulus of carbon fiber are higher than those of glass fiber, they found that the density decreased and tensile modulus and strength of composite increased by substituting of glass fiber by carbon fiber. They reported that the final design of glass/carbon mat thermoplastic have better impact performance compared to the glass mat thermoplastic with reducing the weight by 33%.

Fu et al. [27] established that in the glass/carbon fiber hybrid composites, carbon fibers are usually expected to fail first because the elongation at failure of carbon fibers are less

than that of glass fibers. When carbon fibers fail, the load would transfer to glass fibers. Upon the failure of glass fibers, the matrix must sustain the applied load. The composite failure eventually occurs due to the failure of the matrix.

1.3.3 Natural - Synthetic Fiber Hybrid Composite

A variety of the natural/synthetic fiber combinations to reinforce polymeric resin are found in the literature, but in the most common, natural fiber/glass fiber are incorporated together into a polymeric resin. Hybridization of glass fiber with natural fibers provides an opportunity to improve the mechanical properties of natural composites [37]. Hybridization with glass fiber also has a great influence on the water absorption property of composites [38].

Morye and Wool [2] have looked into the properties of flax/glass fiber composite. They observed that the developed hybrid composite has better tensile, flexural, and impact properties than that of flax fiber composite. In their study, variability in the mechanical properties due to varying glass fiber content with keeping the total volume fraction of the hybrid composite the same was achieved. They showed that the tensile and flexural strength of the hybrid composite increased with glass fiber content. The impact property also increased with glass fiber content. They reported that the water uptake of the hybrid composite was less than that of flax fiber composite.

Zhang et al. [20] have revealed that the hybridization of flax fiber with glass fiber showed positive response on the tensile properties of the hybrid composite. Variability in mechanical properties due to varying the volume fractions and stacking sequence were found. They concluded that the tensile properties of the hybrid composite increased with increasing the volume fraction of glass fiber. It was shown that the stacking sequence had great influence on the tensile strength of flax/glass fiber reinforced composite, but not on the tensile modulus if the volume fractions in the hybrid system were the same.

Davoodi et al. [15] have made an attempt to find out the flexural and impact properties of kenaf/glass fiber reinforced epoxy resin. They found improvement in the flexural strength and flexural modulus when glass fibers added to kenaf fiber composite. They reported

that the average impact property of the hybrid system was nearly half of the glass mat thermoplastic.

The tensile, flexural , thermal, impact, and water absorption properties of sisal/glass fiber polypropylene composite were studied by Jarukumjorn et al. [39]. They observed that the effect of adding glass fiber into sisal fiber reinforced polypropylene composite was not much on the mechanical properties. They found a significant increase in the heat distortion temperature, thermal decomposition temperature, and reduction in water absorption property with the increment in glass fiber content.

Mishra et al. [8] studied the moisture absorption property of sisal/glass and pineapple/glass fiber reinforced polyester composites. Composites were designed by varying the fiber content of glass fiber and by subjecting the natural fibers to different chemical treatment. They found that the water uptake of the hybrid composites were less than that of sisal fiber and pineapple fiber composites. They reported that the water uptake of chemically treated hybrid composites were less than that of the untreated hybrid composites.

Panthapulakkal and Sain [40] studied the mechanical properties of hemp/glass fiber reinforced polypropylene composite. The aim of their study is to determine the tensile, flexural, and impact properties of the hemp/glass fiber reinforced polypropylene composite. They observed that the addition of glass fiber into hemp fiber reinforced polypropylene composite enhanced the tensile, flexural, and impact properties of short hemp fiber composites. The strength properties of the hybrid composite were increased with increasing the glass fiber content. Water absorption property of the hybrid system improved with the addition of glass fiber. They reported that the bending stiffness of the hybrid composite can be compared with that of $40wt\%$ of long glass fiber polypropylene reinforced composites.

Bakar et al. [41] have observed enhancement in tensile properties of oil palm/glass fiber reinforced epoxy resin. They mentioned that the effect of hybridization of glass fiber in oil palm-epoxy composite resulted in increasing the tensile strength and modulus and elongation at break of the hybrid composite. They found that the impact strength of the hybrid composite increased with the addition of glass fiber.

Pothan et al. [42] have done an investigated study on the hybrid composites prepared from banana and glass fibers reinforced polyester resin to obtain tensile and impact properties at different ratios of the fiber content. It was concluded that the tensile strength of the hybrid composite increased linearly with increasing the glass fiber content. They were noticed that the highest impact property of the hybrid system when the volume fraction of the glass fiber was 11%. The impact strength decreased with further increase in the volume fraction of the glass fiber.

1.3.4 Natural - Natural Fiber Hybrid Composite

Composites consisted of two different types of natural fibers are less common. The main purpose of natural/natural fiber hybrid composite is to reduce the cost, the energy needed, density, and to produce biodegradable composites [18]. Idicula et al. [43] studied the mechanical performance of short randomly oriented banana and sisal hybrid fiber reinforced polyester composites. They found a positive hybrid effect in the flexural strength and flexural modulus of the hybrid composites. They also found that the tensile strength showed a positive hybrid effect and the maximum tensile strength was found to be in the hybrid composite having a ratio of banana and sisal 4:1. The impact strength of the hybrid composite was less than that of the sisal fiber polyester composites because of the porous nature and the high spiral angle of the sisal fiber.

Jacob et al. [44] have designed sisal/oil palm reinforced natural rubber composite. They concluded that the combination of these two fibers resulted in increasing modulus. Chemical modification of both oil palm and sisal fibers resulted in improvement in interfacial adhesion and mechanical properties.

Composites made of oil palm empty fruit bunches(OPEFB)/jute fibers reinforced epoxy hybrid composites were made by Jawaid et al. [45]. Their attempt is to investigate the hybridization effect by changing the volume fractions and stacking sequence of fibers. Flexural and impact testing were performed on the composites. In their study, it was found that pure jute composites have the highest flexural strength and modulus among pure OPEFB composites and all hybrid composites. Since jute fibers have better flexural properties than

OPEFB, they observed increasing in flexural properties with increasing the weight fraction of jute fibers. They showed that changing stacking sequences of fibers in the resin have influence on the flexural strength and modulus. They concluded that OPEFB/jute hybrid composites have better flexural properties when jute fibers placed in the extreme positions. They interpreted this by saying that jute fibers have better flexural properties than OPEFB. They observed that pure OPEFB composites have higher impact strength than those composites made of pure jute or hybrid fibers. They showed that changing stacking sequences of fibers effect the impact strength of the hybrid composites. Composite made of OPEFB/jute/OPEFB staking sequence have higher impact strength than those composites made of jute/OPEFB/jute stacking sequence.

The tensile, flexural, impact and water absorption properties of banana/sisal fiber reinforced epoxy resin were investigated by Venkateshwaran et al. [46]. They showed that increasing fiber length and weight fraction of fibers lead to increase the mechanical properties of composites up to a certain limit. Further increasing of fiber length or weight fraction causes decreasing in mechanical properties. They justified this by saying that increasing fiber length and weight fraction cause poor interracial boding between fibers and resin. The mechanical properties of composites made of pure sisal compared with mechanical properties of composite made of only banana fiber and sisal/banana fiber. They noted that sisal fiber composites have better mechanical properties than banana fiber composites and banana/sisal fiber hybrid composites. They showed that adding sisal fibers in the composite resulted in increasing the tensile strength, flexural strength, and impact strength. This is due to the fact that sisal fibers have better mechanical properties than banana fibers. They observed that water uptake property of the hybrid composite was minimum when sisal and jute combined in the resin in the same amount.

Mehdi [47] has looked into the static and dynamic mechanical properties of kenaf fiber/wood flour reinforced polypropylene hybrid composite. In this research article, equal proportions of kenaf fibers and wood flour are combined to reinforce the polypropylene. The static and dynamic properties of the hybrid composites were compared with the properties

of kenaf fiber composites and wood flour composites. It was found that tensile and flexural properties of kenaf fiber composites were the highest while the tensile and flexural properties of wood flour composites were the lowest. The value of tensile properties and flexural modulus of the hybrid composites lied in between. Interestingly, the value of flexural strength of the hybrid composites was close to that of kenaf fiber composite. It was shown that kenaf fiber composites exhibit higher glass-transition temperature value compared to wood flour composites and to the hybrid composites. The value of glass-transition temperature of the hybrid composites was identical to that of wood flour composites.

1.3.5 Properties of Flax and Glass Fibers

The mechanical properties of flax fiber and E-glass fiber are given in Table 1.1. As can be seen, the longitudinal tensile properties and elongation at break of flax fiber is less than that of glass fiber. However, the density of flax fiber is lower than that of glass fiber. Therefore, hybridization flax fiber with glass fiber might yield composites with lighter in weight, higher in specific strength and modulus, and greener than glass fiber composites.

1.4 Overview

This thesis is divided into eight chapters followed by references at the end. The chapters are as follows:

1. Introduction
2. Research Objectives
3. Approach
4. Micromechanics Modeling of Composites
5. Structure and Effective Elastic Constants of Flax Fiber
6. Effective Elastic Constants of Hybrid Composite
7. Experimentation

8. Summary, Conclusion, and Future Work

The first chapter discusses the motivation behind this work, literature review, and some conclusions from the past research. Chapter 2 lists the research objectives. Chapter 3 explains the approach that is followed to complete the objectives. Chapter 4 shows how to determine the homogenized properties of composite using micromechanical analysis on SG and analytical equations. Chapter 5 discusses the structure of flax fiber and finding the effective mechanical properties of flax fiber based on the fiber constituents properties. The FEA and analytical equations are employed to predict the effective properties of flax fiber composite, glass fiber composite, and flax/glass fiber hybrid composite in chapter 6. Chapter 7 explains the experimental work that is carried out to fabricate composite specimens and to determine the tensile, impact, and water absorption properties of the hybrid composite. Chapter 8 provides a summary of this work, observations and conclusions from this research study, and suggestions for future work.

CHAPTER 2

Objectives

The objectives listed below are considered the minimum requirements for this thesis and once accomplished, the thesis is complete.

- Determine the effective elastic constants of flax fiber composite, E-glass fiber composite, and flax/glass fiber hybrid composite using FEA and analytical equations.
- Investigate the effect of varying fiber volume fraction and fiber locations on the effective properties of flax/E-glass fiber hybrid composite using FEA.
- Investigate the effect of changing fiber layer locations on the tensile, impact, and water absorption properties of flax/E-glass fiber hybrid composite through tensile, impact, and water absorption tests.
- Study the effect of subjecting composite specimens to water immersion tests on the tensile properties.
- Quantify the hybridization effect of flax/E-glass fiber hybrid composite and compare the results with flax fiber and glass fiber composites individually.

CHAPTER 3

Approach

The objectives listed in the previous chapter are proposed to be achieved by the following approach. This tasks can be divided into three categories, numerical modeling, analytical modeling, and experiment.

Numerical Modeling:

- Calculate the effective properties of flax fiber. This task can be achieved by
    1. Draw a Structural Genome (SG) representing the cell wall layers of flax fiber and calculate the effective elastic constants of these layers.
    2. Draw a SG of technical flax fiber consisting of cell wall layers and calculate the elastic constants of the fiber.
- Generate a SG based model of unidirectional flax/E-glass fiber reinforced hybrid composite by ABAQUS and calculate the effective properties of the hybrid composite through mechanics of structure genome (MSG) modeling of the structure at the meso-scale. This homogenization model provides the elastic constants of the hybrid composite.
- Find out the effect of changing volume fraction of flax and E-glass fiber with maintaining the total volume fraction the same on the effective properties of the hybrid composite. The total volume fraction of both fibers is assumed to be 40%. This step is achieved by following-
    1. Start with a composite that is only reinforced by flax fiber.
    2. Decrease the volume fraction of flax fiber by 5% and increase the volume fraction of E-glass fiber by 5% until the composite is only reinforced by E-glass fiber.

- Study the effect of changing fiber locations on the effective mechanical properties of the hybrid composites using the FEA. This can be done by placing flax and E-glass fiber in different locations in the SG. This task can show the effect of changing fiber locations on the effective properties of composite.

Analytical Modeling:

- Predict the elastic constants of the hybrid composite in the fiber direction and in the transverse directions by using the rule of hybrid mixture (RoHM) and Halpin-Tsai equations. Analytical results are compared with the FEA results.

Experimentation:

- Carry out a tensile test on hybrid composites for different flax and E-glass fiber layer locations and evaluate Young's modulus and tensile strength. The results obtained from tensile tests are compared, whenever applicable, with the FEA and analytical results. This task helps to examine the hybridization effect and decide the best location of flax and E-glass fiber layers in tensile composite specimens.

- Perform water absorption tests on flax fiber composite, E-glass fiber composite, and various stacking sequence of flax/E-glass fiber hybrid composites. This task can be achieved by immersing composite specimens in de-ionized water at room temperature (23°C) for a week and determine the percentage of moisture uptake of the composite specimens every 24 hours. The immersed composite specimens are then used for tensile tests. The results obtained from wet specimens are compared with dry specimens results. The purpose of this task is to investigate the effect of subjecting composite specimens to water immersion on the tensile properties.

- Perform Charpy impact test on single fiber composites and various stacking sequence of fiber layers of the hybrid composites and calculate the impact strength. This task can help to show the hybridization effect and the influence of varying fiber layer locations on the impact strength of composites.

CHAPTER 4

Micromechanics Modeling of Composites

4.1 Introduction

In this chapter, an introduction to micromechanical modeling of composite using FEA and analytical equations are discussed. As it is known for mechanical engineers, composite materials are structures made of two or more different materials in specific proportions. Generally speaking, composites consist of fiber reinforcement embedded in a polymeric resin. Diameter of fibers are usually few microns. Due to the mismatch in mechanical properties between fibers and matrix in microscopic level, composites are considered anisotropic and heterogeneous materials. To evaluate the effective properties of composite, micromechanical analysis are usually performed at meso-scale through homogenization theories. In the FEA, Mechanics of Structural Genome (MSG) is the homogenization theory that is used to find the effective properties of composite. The homogenized properties of composite are also predicted using analytical equations including RoM and Halpin-Tsai equation.

4.2 Micro-Mechanical Analysis of Composite

Homogenized properties of composite predicted using FEA and analytical equations. Analytical equations include RoM to predict the longitudinal elastic constants and Halpin-Tsai equations to obtain the transverse properties of composite.

4.2.1 Finite Element Analysis (FEA)

Finite element can be employed to find the homogenized properties of composite materials. To predict the effective elastic constants of composite, a numerical homogenization was carried out on SG. A 2D SG of composite generated using ABAQUS. A S4 (A four-node doubly curved general purpose shell, finite element membrane strain) element was selected in the analysis. A four-node element is shown in Fig. 4.1. The SG of composite is analyzed

using ABAQUS. To predict the elastic constants of composite, a numerical homogenization was carried out using SwiftComp on SG. SwiftComp is a multiscale composite modeling Python code developed by AnalySwift to determine the effective properties. It can be used stand alone or in interface with ABAQUS or ANSYS. In this thesis, SwiftComp is used in interface with ABAQUS.

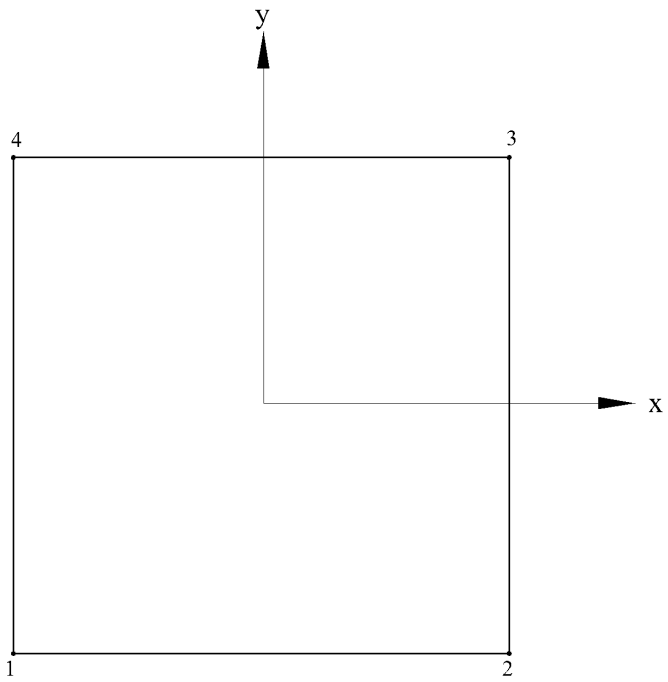

Fig. 4.1: S4 element

Numerical Homogenization Theory

Composite materials is defined as a mixture of two or more different materials in specific proportions. Generally, composite is made up of fiber reinforcement embedded in a polymeric resin. This is why composites usually have heterogeneous microstructure due to different mechanical properties of fiber and matrix in micro-scale level. For this reason, it is necessary to start modeling the composite from the fiber size (often the size of few microns) and matrix. The field of micromechanics offers an opportunity to understand and analyze composites materials. Effective properties of composites can be predicted from

homogenizing composite constituents using micromechanical analysis. The micromechanical analysis is performed on SG. SG can be defined as the smallest mathematical building block of a structure that contains all the constitutive information of a structure [50].

Both SG and RVE can provide the homogenized properties of composite structure. However, there are few differences between them,

1. SG uses continuum hypothesis to determine the effective elastic constants.

2. The constitutive modeling over the 2D SG can provide the complete set of 3D elastic constants of structure. On other hand, only in-plane properties can be achieved from 2D RVE based models. If all the elastic constants are needed for a structure, a 3D RVE are usually used for this purpose [48] or 2D RVE with six different loadings and boundary conditions [36].

3. Boundary conditions in terms of displacement and tractions are the main requirements in RVE based models. However, the effective properties obtained from the SG are independent of boundary and loading conditions of macroscopic structure.

4. RVE must have straight edges while SG can have arbitrary shapes.

MSG is limited to Kirchhoff–Love plate/shell model and structure must be made of linear elastic materials. In this thesis, micromechanical analysis is carried out using 2D FEA shell elements. Here, 2D notation refers to the two coordinates needed for the analysis.

Mechanics of Structure Genome

SG must be govern by a physical theory. The theory behind SG is called Mechanics of Structure Genome (MSG) which is an updated version of the Variational Asymptotic Method for Unit Cell Homogenization (VAMUCH) developed by Yu, W [50] . MSG requires the necessary information to link the microstructure scale and the macroscopic scale of composite and provides the elastic constants of structure. To obtain the effective elastic properties, kinematics, kinetics, and constitutive relations are required in the analysis. Kinematics include the strain-displacement relations and compatibility equations while kinetics

include stress and equations of motion. Both kinematics and kinetics can be expressed within the framework of continuum mechanics. Constitutive relations relate stress and strain. The following derivations are drawn from this research article [50].

Kinematics

The first step to formulate MSC is using kinematics. Kinematics include the displacement field and strain field of the original structures in terms of those in the macroscopic structural model. Cauchy's continuum used in formulating MSG.

Coordinate Systems

x_i notation is used as global coordinates to describe the macroscopic structure of the composite. An orthogonal coordinates system of arc-length are used. When the structures can be dimensionally reducible, Greek indices are used to describe the eliminated coordinates, corresponding to the dimensions that are neglected in the macroscopic structural model. Latin indices are used to describe the remaining coordinates in macroscopic structural model. For plate/shell-like structures, the in-plane coordinates x_1 and x_2 remain, while the through thickness coordinate x_3 is eliminated in the final plate/shell model. y_i notation is used to describe the local coordinate of SG. Microscopic coordinate can be related to macroscopic coordinate through (y_i=x_i/ϵ), where ϵ is small parameter that enables zoom-in view of the SG at a size similar to the macroscopic structure. For 2D SG, y_2 and y_3 are needed. In multiscale structural modeling, field function of original structure can be expressed as a function of remaining macrocoordinates x_k and microcoordinates y_j. According to Bensoussan et al. [51], the partial derivative of field function can be written as,

$$\frac{\partial f(x_k, y_j)}{\partial x_i} = \frac{\partial f(x_k, y_j)}{\partial x_i}\Big|_{y_j=const.} + \frac{1}{\epsilon}\frac{\partial f(x_k, y_j)}{\partial y_i}\Big|_{x_k=const.} \tag{4.1}$$

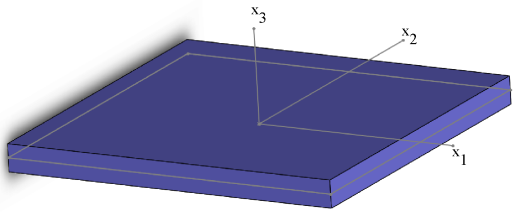

Fig. 4.2: Macrocoordinates (x_1, x_2, x_3)of plate/shell

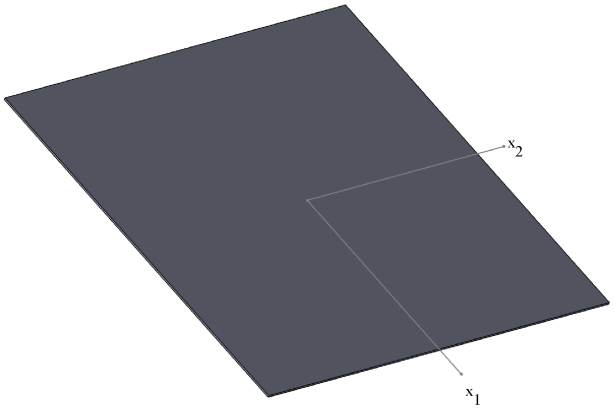

Fig. 4.3: Remaining macrocoordinates (x_1, x_2)of plate/shell

Undeformed and Deformed Configurations

b_k notation is used to describe the unit vector tangent to the macroscopic coordinates of the undeformed configuration, which is function of x_k only. For plate/shell-like structure, b_1 and b_2 are chosen to be tangent to the plate/shell reference surface and b_3 as a unit vector tangent to the eliminated thickness coordinate x_α. As it can be seen from Fig 4.4, any material point of macroscopic structure can be described by its position vector r from a fixed point O in an inertial frame such that,

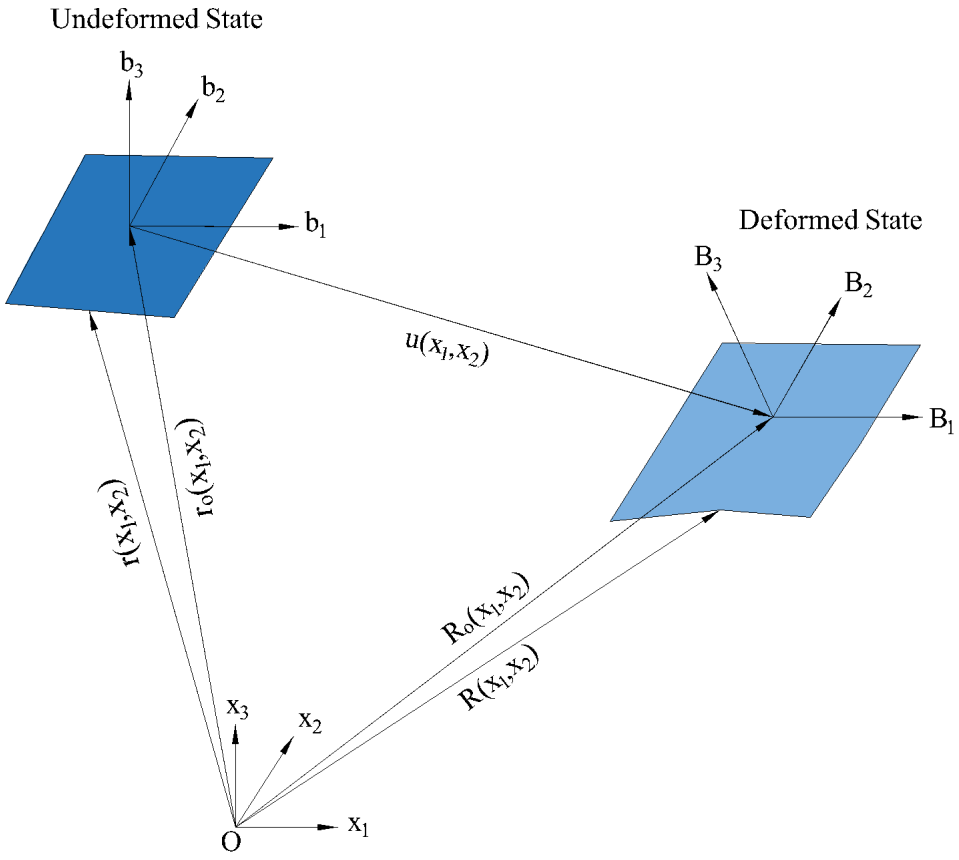

Fig. 4.4: Deformation of plate/shell structure

$$r(x_k, y_\alpha) = r_o(x_k) + \epsilon y_\alpha b_\alpha(x_k) \tag{4.2}$$

Where r_o is the position vector from point O to a material point of the original structure. Because x_k refers to arc-length orthogonal coordinate, b_k can be written as

$$b_k = \frac{\partial r_o}{\partial x_k} \tag{4.3}$$

When the structure deforms, the material point that retained position vector r in the uniformed configuration now possesses position vector R in the deformed configuration,

$$R(x_k, y_j) = R_o(x_k) + \epsilon y_\alpha B_\alpha(x_k) + \epsilon w_i(x_k, y_j) B_i(x_k) \tag{4.4}$$

Where R_o refers to the position vector of the deformed structure, B_i denotes to the orthogonal triad of the deformed configuration and ϵw_i represents the fluctuating functions to include all the possible deformations other than those described by R_O and B_i. The triads b_i and B_i can be related using direction cosine matrix (C_{ij}) so that

$$B_i = C_{ij} b_j \tag{4.5}$$

R is written in Eq. 4.4 in terms of R_o, B_i, and w_i which gives six time redundancy. Therefore, six constraints are required to remove this redundancy. These needed constraints can be obtain from how R_o and B_i defined in terms of R. R_o can be expressed as,

$$R_o = \langle\langle R \rangle\rangle - \langle\langle \epsilon y_\alpha \rangle\rangle B_\alpha(x_k) \tag{4.6}$$

Where $\langle\langle\rangle\rangle$ represents the averaging over the SG. If y_α is selected in such a way that ensure $\langle\langle \epsilon y_\alpha \rangle\rangle = 0$, R_o in this case defined as the averaging of position vector of the original structure. Thereupon, the constraint on the fluctuating functions can be expressed,

$$\langle\langle w_i \rangle\rangle = 0 \tag{4.7}$$

For plate/shell-like structure, B_3 can be selected as a normal to reference surface of the deformed structure. It is necessary to point out that the selection of B_3 in this case

is not based upon the classical lamination theory (CLT) developed by Kirchhoff-love. In Kirchhoff assumption, plane section originally plane and perpendicular to the mid-plane remain plane and perpendicular through deformation.

$$B_3.R_{o,1} = 0 \tag{4.8a}$$

$$B_3.R_{o,2} = 0 \tag{4.8b}$$

The last constrain can be assigned from the rotation of B_1 and B_2 around B_3 such that

$$B_1.R_{o,2} = B_2.R_{o,1} \tag{4.9}$$

Strain and the Local Rotation Tensor

The rotation can be divided into two parts, large rotation which is equal to the global rotation and local rotation. Local rotation is defined as the rotation of selected material point of original structure subtracting the rotation of triad b_i to B_i. If the local strain is small, the Jaumann-Biot-Cauchy strain tensor can be used according to decomposition of the rotation tensor [52].

$$\Gamma_{ij} = \frac{1}{2}(F_{ij} + F_{ji}) - \delta_{ij} \tag{4.10}$$

Where δ_{ij} refers to Kronecker delta and F_{ij} is the mixed-basis component of the decomposition gradient tensor and it can be written as

$$F_{ij} = B_i.G_a g^a.b_j = B_i.(G_k g^k + G_\alpha g^\alpha).b_j \tag{4.11}$$

Here G_a and g^a represent the 3D covariant vector of the deformed configuration and the 3D contravariant base vector of the undeformed configuration respectively.

The contravariant base vector can be given as [53]

$$g^a = \frac{1}{2\sqrt{g}} e_{ijk} g_j \times g_k \tag{4.12}$$

Here e_{ijk} is the 3D permutation symbol and $g = det(g_i.g_j)$.

From the undeformed configuration, the covariant base vectors are tangent to the remaining coordinate curves,

$$g_i = \frac{\partial r}{\partial x_i} = b_i + \epsilon y_\alpha \frac{\partial b_\alpha}{\partial x_i} = b_i + \epsilon y_\alpha k_i \times b_\alpha = b_i + e_{j\alpha k} \epsilon y_\alpha k_{ij} b_k \tag{4.13}$$

With k_i is the initial curvature vector corresponding to the remaining macrocoordinate. According to Yu and Hodges [54], the initial curvature vector of shells can be written as

$$k_{ij}^{2D} = \alpha_{jk} k_{ik} \tag{4.14}$$

where α_{ij} is the 2D permutation symbol.

From the undeformed configuration, the covariant base vectors are tangent to the eliminating coordinate curves,

$$g_\alpha = \frac{\partial r}{\partial x_\alpha} = \frac{\partial (\epsilon y_\alpha)}{\partial x_\alpha} b_\alpha = b_\alpha \tag{4.15}$$

From the deformed configuration, the contravariant base vector are tangent to the remaining coordinate curves,

$$G_i = \frac{\partial R}{\partial x_i} = \frac{\partial R_o}{\partial x_i} + \epsilon y_\alpha \frac{\partial B_\alpha}{\partial x_i} + \epsilon \frac{\partial w_i}{\partial x_i} B_i + \epsilon w_i \frac{\partial B_i}{\partial x_i} \tag{4.16}$$

From the deformed configuration, the contravariant base vector are tangent to the eliminating coordinate curves,

$$G_\alpha = \frac{\partial R}{\partial x_\alpha} = \frac{\partial (\epsilon y_\alpha)}{\partial x_\alpha} B_\alpha + \epsilon \frac{\partial w_i}{\partial x_\alpha} B_i = B_\alpha + \frac{\partial w_i}{\partial y_\alpha} B_i \tag{4.17}$$

It is necessary to address the macroscopic strain. Macroscopic strain is required for the macroscopic structural analysis. According to Yu et al. [55] and Pietraszkiewicz and Eremeyev [56], Lagrangian stretch tensor and Lagrangian curvature strain tensor can be given as,

$$\epsilon_{mn} = B_n . \frac{\partial R_o}{\partial x_m} - \delta_{mn} \tag{4.18a}$$

$$\kappa_{mn} = \frac{1}{2} e_{nij} B_j . \frac{\partial B_i}{\partial x_m} - k_{mn} \tag{4.18b}$$

Where ϵ_{mn} and κ_{mn} are Lagrangian stretch tensor and Lagrangian curvature strain tensor respectively. Corresponding to the kinematic of nonlinear Cosserat continuum, this definition allows six degree of freedoms (three translations and three rotations). For plate/shell like structure, if Eq. 4.9 is used, then the symmetry $\epsilon_{12} = \epsilon_{21}$ is obtained as a constrain for the kinematics of the final plate/shell model. This definition produces 2D generalized strain and subsequently agrees with Reissner-Mindlin model. If Eq. 4.9 is applied which means that B_3 is normal to the reference surface of the plate/shell, this leads to produce the 2D generalized strain and meets the Kirchhoff-Love theory of plate/shell structures.

To make the definition of covariant vector G_i easier, Eq. 4.18 can be written as,

$$\frac{\partial R_o}{\partial x_m} = B_m + \epsilon_{mn} B_n \tag{4.19a}$$

$$\frac{\partial B_i}{\partial x_m} = (\kappa_{mn} + k_{mn}) B_j \times B_i \tag{4.19b}$$

From Eqs 4.8, $\epsilon_{13} = \epsilon_{23} = 0$ can be achieved for plate and shell structures.

By substituting Eq.4.19 to Eq.4.16, the covariant base vector of the deformed shape can be written,

$$G_k = (\delta_{kl}+\epsilon_{kl}+\epsilon\frac{\partial w_l}{\partial x_k}B_l)+\epsilon(e_{ij\alpha}(y_\alpha+w_\alpha)(\kappa_{kj}+k_{kj})+\frac{\partial w_\alpha}{\partial x_k}\delta_{\alpha i}+e_{ijl}w_l(\kappa_{kj}+k_{kj}))B_i \quad (4.20)$$

By using the expression for g^a and G_a and removing nonlinear terms due to the multiplication of the curvature strains and the fluctuating functions, the 3D strain field can be given in the following matrix form,

$$\Gamma = \Gamma_h w + \Gamma_\epsilon \bar{\epsilon} + \epsilon\Gamma_l w + \epsilon\Gamma_R w \quad (4.21)$$

Where $\Gamma = \lfloor\ \Gamma_{11}\ \Gamma_{22}\ \Gamma_{33}\ 2\Gamma_{23}\ 2\Gamma_{13}\ 2\Gamma_{12}\ \rfloor^T$ refers to the strain field of the original structure, $w = \lfloor\ w_1\ w_2\ w_3\ \rfloor^T$ denotes the fluctuating functions, and $\bar{\epsilon} = \lfloor\ \epsilon_{11}\ \epsilon_{22}\ 2\epsilon_{12}\ \kappa_{11}\ \kappa_{22}\ \kappa_{12}\rfloor^T$ represents strain of macroscopic structural model with ϵ_{ij} referring to the in-plane strains and κ_{ij} referring to the curvature strains. Γ_h is an operator matrix which relies on the dimensionality of SG. Γ_ϵ and Γ_l are two operator matrices where they depend on the macroscopic structural model. Γ_R is an operator matrix which exists when the original structure possesses initial curvatures.

Γ_h for 2D shell-like structure can be given as,

$$\Gamma_h = \begin{bmatrix} 0 & 0 & 0 \\ 0 & \frac{1}{S_2}\frac{\partial}{\partial y_2} & 0 \\ 0 & 0 & \frac{\partial}{\partial y_3} \\ 0 & \frac{\partial}{\partial y_3} & \frac{1}{S_2}\frac{\partial}{\partial y_2} \\ \frac{\partial}{\partial y_3} & 0 & 0 \\ \frac{1}{S_2}\frac{\partial}{\partial y_2} & 0 & 0 \end{bmatrix} \quad (4.22)$$

Γ_ϵ for plate/shell like structure is,

$$\Gamma_\epsilon = \begin{bmatrix} \frac{1}{S_1} & 0 & 0 & \frac{\epsilon y_3}{S_1} & 0 & 0 \\ 0 & \frac{1}{S_2} & 0 & 0 & \frac{\epsilon y_3}{S_2} & 0 \\ 0 & 0 & 0 & 0 & 0 & 0 \\ 0 & 0 & 0 & 0 & 0 & 0 \\ 0 & 0 & 0 & 0 & 0 & 0 \\ 0 & 0 & \frac{1}{2}(\frac{1}{S_1} + \frac{1}{S_2}) & 0 & 0 & \frac{1}{2}(\frac{\epsilon y_3}{S_1} + \frac{\epsilon y_3}{S_2}) \end{bmatrix} \tag{4.23}$$

Γ_l for plate/shell like structure is,

$$\Gamma_l = \begin{bmatrix} \frac{1}{S_1}\frac{\partial}{\partial x_1} & 0 & 0 \\ 0 & \frac{1}{S_2}\frac{\partial}{\partial x_2} & 0 \\ 0 & 0 & 0 \\ 0 & 0 & \frac{1}{S_2}\frac{\partial}{\partial x_2} \\ 0 & 0 & \frac{1}{S_1}\frac{\partial}{\partial x_1} \\ \frac{1}{S_2}\frac{\partial}{\partial x_2} & \frac{1}{S_1}\frac{\partial}{\partial x_1} & 0 \end{bmatrix} \tag{4.24}$$

Γ_R for shell mode is,

$$\Gamma_R = \begin{bmatrix} 0 & \frac{-k_{13}}{S_1} & \frac{k_{12}}{S_1} \\ \frac{k_{23}}{S_2} & 0 & \frac{-k_{21}}{S_2} \\ 0 & 0 & 0 \\ 0 & \frac{k_{21}}{S_2} & 0 \\ \frac{-k_{12}}{S_1} & 0 & 0 \\ \frac{k_{13}}{S_1} & \frac{-k_{23}}{S_2} & 0 \end{bmatrix} \tag{4.25}$$

Where $S_1 = \sqrt{g_1} = 1 + \epsilon y_3 k_{12}$ and $S_2 = \sqrt{g_2} = 1 - \epsilon y_3 k_{23}$ for shell-like structures and κ is the initial curvatures. By substituting operator matrices in Eqs 4.22 - 4.22 to Eq. 4.21,

the 3D field strain can be obtained as,

$$\Gamma_{11} = \epsilon_{11} + x_3\kappa_{11} + w_{1,1} \tag{4.26a}$$

$$\Gamma_{22} = \epsilon_{22} + x_3\kappa_{22} + w_{2,2} \tag{4.26b}$$

$$\Gamma_{33} = w_{3,3} \tag{4.26c}$$

$$2\Gamma_{23} = w_{2,3} + w_{3,2} \tag{4.26d}$$

$$2\Gamma_{13} = w_{1,3} + w_{3,1} \tag{4.26e}$$

$$2\Gamma_{12} = 2\epsilon_{12} + 2x_3\kappa_{12} + w_{1,1} + w_{2,1} \tag{4.26f}$$

Variational Statement for SG

SC concepts can be applied to nonlinear materials. However, MSG is used for linear elastic materials. The relation between strain energy and virtual work of the applied loads can be given as,

$$\delta U = \overline{\delta W} \tag{4.27}$$

with δ is the Lagrangian variation, U is the strain energy, and $\overline{\delta W}$ is the virtual work of the applied load.

The strain energy of linear elastic materials can be written as,

$$U = \frac{1}{2}\int_{\Omega} \langle \Gamma^T D \Gamma \rangle d\Omega \tag{4.28}$$

Where Ω is the volume of macroscopic structural model, D is the stiffness matrix.

If the load applied from tractions and body force. The virtual work achieved by these loads can be given as,

$$\overline{\delta W} = (\int \langle p \rangle . \delta R + \int_s Q . \delta R ds) d\Omega \tag{4.29}$$

Where p refers to the applied force per unit volume $p = p_i B_i$, Q denotes the applied traction force per unit area $Q = Q_i B_i$ and s represents the boundary curve of the SG. δR refers to the Lagrangian variation of displacement,

$$\delta R = \overline{\delta q_i} B_i + \epsilon y_\alpha \delta B_\alpha + \epsilon \delta w_i B_i + \epsilon w_i \delta B_i \tag{4.30}$$

The multiplication of the fluctuating functions and virtual rotations in Eq.4.30 can be omitted because they are very small. Therefore, Eq.4.30 can be rewritten as,

$$\delta R = \overline{\delta q_i} B_i + \epsilon y_\alpha \delta B_\alpha + \epsilon \delta w_i B_i \tag{4.31}$$

The virtual displacements and rotations of the macroscopic structural model can be obtained from

$$\overline{\delta q_i} = \delta R_o . B_i \tag{4.32a}$$

$$\delta B_\alpha = \overline{\delta \psi_j} B_j \times B_\alpha \tag{4.32b}$$

Where $\overline{\delta q_i}$ contains the virtual displacement and $\overline{\delta \psi_j}$ contain the virtual rotation in the B_i system. Both of them are function of the remaining macroscopic coordinate (x_k) only.

By substituting Eqs.4.32 in Eq. 4.31, Eq. 4.31 can be rewritten as,

$$\delta R = (\overline{\delta q_i} + \epsilon e_{j\alpha i} y_\alpha \overline{\delta \psi_i} + \epsilon \delta w_i) B_i \tag{4.33}$$

The virtual work due to applied loads can be divided into virtual work does not contain fluctuating functions w_i and virtual work contain fluctuating functions.

$$\overline{\delta W} = \overline{\delta W_H} + \epsilon \overline{\delta W^*} \tag{4.34}$$

Where $\overline{\delta W_H}$ and $\overline{\delta W^*}$ can be given as,

$$\overline{\delta W_H} = \int_\Omega (f_i \overline{\delta q_i} + m_i \overline{\delta \psi_i}) d\Omega \tag{4.35a}$$

$$\overline{\delta W^*} = \int_\Omega (\langle p_i \delta w_i \rangle + \oint Q_i \delta w_i ds) d\Omega \tag{4.35b}$$

Where f_i and m_i are generalized forces and moments defines as

$$f_i = (\langle p_i \rangle + \int Q_i ds) \tag{4.36a}$$

$$m_i = e_{i\alpha j}(\langle \epsilon y_\alpha p_j \rangle + \int \epsilon y_\alpha Q_j ds) \tag{4.36b}$$

If body and traction forces are assumed to be independent of fluctuating function, $\overline{\delta W^*}$ can be written as,

$$\overline{\delta W^*} = \delta \int (\langle p_i w_i \rangle + Q_i w_i ds) d\Omega \tag{4.37}$$

By substituting the strain energy expression in Eq.4.28 and virtual work in Eq.4.34 along with Eq.4.35, Eq.4.27 can be written as,

$$\int \delta[\frac{1}{2}(\langle \Gamma^T D \Gamma \rangle - \epsilon(\langle p_i w_i \rangle + \int Q_i w_i ds))] d\Omega - (f_i \overline{\delta q_i} + m_i \overline{\delta \psi_i}) d\Omega = 0 \tag{4.38}$$

Eq. 4.38 is not easy to solve because fluctuating functions w_i are unknown functions in macro- and microcoordinates. This issue can be solved by variational asymptotic method (VAM) developed by Berdinchevsky [56]. VAM offers an opportunity to get the fluctuating functions through an asymptotic analysis of the variational statement in Eq.4.38. It

can be done in terms of ϵ which is small parameter and inseparable in the composite to build asymptotic macroscopic structure models. According to VAM, the least two terms in Eq.4.38 that are not function of fluctuating function can be neglected. Then, the fluctuating function is governed by the following equation,

$$\delta(\frac{1}{2}\langle\Gamma^T D\Gamma\rangle - \epsilon(\langle p_i w_i\rangle + \int Q_i w_i ds)) = 0 \tag{4.39}$$

According to VAM, the small terms that can cause complexity can be omitted which is in this case the terms multiplied by ϵ. Therefore, Eq.4.39 can be rewritten and given as,

$$\delta\frac{1}{2}\langle(\Gamma_h w + \Gamma_\epsilon\bar{\epsilon})^T D(\Gamma_h w + \Gamma_\epsilon\bar{\epsilon})\rangle = 0 \tag{4.40}$$

Eq.4.40 can be solved exactly and analytically. Numerical methods such as FEA can be suggested for finding the homogenized properties of composite and for structural analysis of composite. Here, w can be formulated using shape function over SG,

$$w(x_k, y_j) = S(y_j)V(x_k) \tag{4.41}$$

w in Eq.4.41 can be found by given a macroscopic strain ($\bar{\epsilon}$) and V as a function of remaining macrocoordinates (x_k). S are the shape functions which depend on the type of element used in FEA. By substituting Eq.4.41 into Eq.4.40, it can be obtained,

$$U = \frac{1}{2}(V^T EV + 2V^T D_{h\epsilon}\bar{\epsilon} + \bar{\epsilon}^T D_{\epsilon\epsilon}\bar{\epsilon}) \tag{4.42}$$

Where,

$$E = \langle(\Gamma_h S)^T D(\Gamma_h S)\rangle \tag{4.43a}$$

$$D_{h\epsilon} = \langle(\Gamma_h S)^T D\Gamma_\epsilon\rangle \tag{4.43b}$$

$$D_{\epsilon\epsilon} = \langle\Gamma_\epsilon^T D\Gamma_\epsilon\rangle \tag{4.43c}$$

Minimizing U in Eq. 4.42 by subjecting the SG to the constrains, it gives linear expression as shown in the following statement,

$$EV = -D_{h\epsilon}\bar{\epsilon} \tag{4.44}$$

It can be noticed from Eq.4.44 that V changes linearly with $\bar{\epsilon}$. Thus, V can be correlated with $\bar{\epsilon}$ through following equation

$$V = V_o\bar{\epsilon} \tag{4.45}$$

By substituting Eq.4.45 into Eq.4.42, the strain energy stored in the SG can be determined from the following expression,

$$U = \frac{1}{2}\bar{\epsilon}^T(V_o^T D_{h\epsilon} + D_{\epsilon\epsilon})\bar{\epsilon} \equiv \frac{\omega}{2}\bar{\epsilon}^T\overline{D}\bar{\epsilon} \tag{4.46}$$

Where $\overline{D}$ is effective stiffness matrix of the macroscopic structural model. For the Kirchhoff-Love plate/shell model, $\overline{D}$ is 6×6 stiffness matrix.

The equation that govern the original structure can be achieved by substituting Eq.4.46 into Eq.4.38 as shown below,

$$\int(\delta\frac{1}{2}\bar{\epsilon}^T\overline{D}\bar{\epsilon} - f_i\overline{\delta q_i} - m_i\overline{\psi_i})d\Omega = 0 \tag{4.47}$$

The above equation governs the macroscopic structural model because it contains fields which are function of macrocoordinates x_k. The first term in this equation represent the energy stored over the macroscopic structural model while the remaining terms represent the virtual work done by generalized forces and moments.

When $\bar{\epsilon}$ achieved from the macroscopic structural analysis, the fluctuating function can be determined from the following expression,

$$w = SV_o\bar{\epsilon} \tag{4.48}$$

The local displacement can be calculated from the following expression,

$$u_i = \overline{u_i} + x_\alpha(C_{\alpha i} - \delta_{\alpha i}) + \epsilon w_j C_{ji} \tag{4.49}$$

with u_i representing the local displacement and $\overline{u_i}$ representing the macroscopic displacement. For SGs possessing microcoordinates (y_k) with respect to remaining macrocoordinates (x_k) in the macroscopic structural model, $\overline{u_i}$ can be given as,

$$\overline{u_i} = \overline{u_i}(x_{ko}) + x_k \overline{u_{i,k}} \tag{4.50}$$

where x_{ko} and $\overline{u_{i,k}}$ denote the center of the SG and the displacement gradient along the x_k calculated at x_{ko}.

The local strain can be achieved from the the following equation,

$$\Gamma = (\Gamma_h S V_o + \Gamma_\epsilon)\bar{\epsilon} \tag{4.51}$$

The local stress can be calculated using Hooke's law,

$$\sigma = D\Gamma \tag{4.52}$$

4.2.2 Analytical Equations

Another way to find the macroscopic properties of composite is by using analytical equations. RoM is usually used to find the longitudinal tensile modulus and Poisson's ratio of composite while Halpin-Tsai equations are used to find the transverse tensile moduli and shear moduli.

Rule of Mixtures (RoM)

RoM is used to predict various properties of composite. Its usage is limited to continuous and unidirectional or perfectly aligned fibers. Properties such as axial Young's modulus, axial Poisson's ratio, and mass density can be predicted by RoM. In this study,

longitudinal Young's modulus and Poisson's ratio are predicted using RoM. RoM is based on Voigt model. In Voigt model, it is assumed that uniform strain is present in composite in a longitudinal direction. The unit cell used in RoM is different from FEA unit cell. Fig. 4.5 demonstrates the RoM unit cell which it shows a section cut of single layer of composite. The Fig.4.5 shows the longitudinal direction denoted by 1 and transverse direction denoted by 2.

The longitudinal Young's modulus for single fiber reinforced polymeric composite can be written as,

$$E_1^c = E_1^f V^f + E^m V^m \tag{4.53}$$

Where E and V denote Young's modulus and volume fraction respectively. Superscripts c, f, and m refer to composite, fiber, and matrix respectively.

The longitudinal Poisson's ratio can be given as,

$$\nu_{12}^c = \nu_{12}^f V^f + \nu^m V^m \tag{4.54}$$

With ν refers to Poisson's ratio.

4.2.3 Halpin-Tsai Equations

The Halpin-Tsai model is based on self-consistent field method provided by Hill. In the self-consistent method, a single ellipsoidal inclusion embedded in an infinite medium is assumed. Perfect boding between inclusion and the medium is also assumed. Halpin-Tsai equations used to predict the transverse properties of composite material by considering the geometry, orientation of the fiber, and the elastic properties of the fibers and matrix. These equations are also called semi-empirical relations because they contain parameters that have some physical significance. The transverse moduli can be determine from Eq. 4.55 [57],

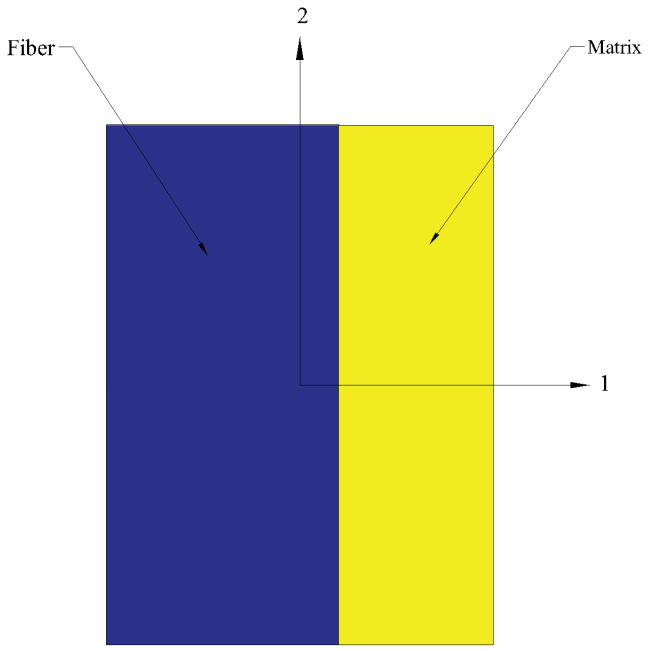

Fig. 4.5: RoM model for unidirectional composite

$$M = M_m \frac{1 + \xi \eta V_f}{1 - \eta V_f} \tag{4.55}$$

Where

$$\eta = \frac{\frac{M_f}{M_m} - 1}{\frac{M_f}{M_m} + \xi} \tag{4.56}$$

and M $= E_y$ or G_{xy}, $M_f = E_f$ or G_f and $M_m = E_m$ or G_m. ξ is considered as reinforcement measure which depends on the aspect ratio of the reinforcement.

CHAPTER 5

Structure and Elastic Constants of Flax Fiber

5.1 Introduction

In this chapter, structure and the elastic constants of flax fiber are presented. FEA was employed as a primary prediction of the elastic constants of flax fiber. To predict the effective properties of flax fiber, a numerical homogenization was carried out by using MSG on SG. RoM and Halpin-Tsai equations were also used to find the elastic constants of cell wall layers. Then, the comparison was made between FEA results and analytical results.

5.2 Structure of Flax Fiber

Plant natural fibers generally have a very complex multiscale structure, which needs to be analyzed in macroscale, microscale, and nanoscale [58]. On a macroscopic scale, it can be observed a bundle of flax fibers which consists of 10-40 of elementary flax fibers as shown in Fig.5.1. These elementary fibers are glued together in the bundle by pectin (middle lamellae (M)) [32].

On microscopic scale, flax fiber possesses non-uniform geometrical characteristics. The fibers have a polygonal cross section with 5-7 sides as shown on the SEM image (Fig.5.2). The longitudinal view of flax fiber from SEM showed non-constant transverse dimensions. The fiber is thin in some regions and thick in other regions. The average diameter of the flax fibers is about 20 μm.

Plant natural fibers have a hierarchical structure. They consists of two concentric cell walls with a small hole in the middle called the lumen, which contributes to the water uptake as shown in Fig. 5.3 [32,59]. The size of the lumen is 0-5 % of the volume flax fiber [60]. The external wall is called primary wall (P). The thickness of the primary wall is small compared to the total thickness of the fiber. The inner wall is called the secondary wall, which consists

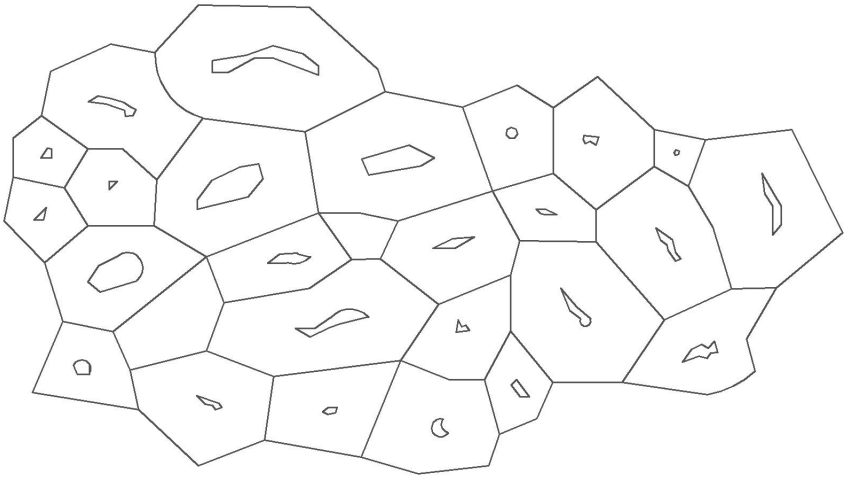

Fig. 5.1: Bundle of flax fibers

of three layers namely, S1, S2, and S3. The thickness of these secondary layers ranges from tenths micron to several microns. The S2 layer is the thickest layer, it represents 76 % of the total thickness of the fiber [61]. Thus, the feature of this layer has a great influence on the properties of flax fiber. The cell wall layers mainly composed of three constituents, cellulose, hemicellulose, and lignin. In general, plant natural fibers are composite in nature. Cellulose is the essential component of cell walls, it contributes to strength and stiffness of the natural fiber. Therefore, cellulose acts as a reinforcing agent. Hemicellulose and lignin together act as a binding agent. The content of these chemical constituents are different in each layer of the cell wall as shown in Table 5.1. Additional components such as pectin, oil, wax, and structural water can be found in the microstructure of flax fibers [32].

On nanometer scale, each layer of the cell wall consists of many microfibrils, which represent the unit cell of the cell wall [32]. The diameter of the microfibrils is from 10 to 20 nm. The microfibrils constituted of cellulose. The cellulose microfibrils of cell wall layers oriented at different angles with respect to the fiber axis (Table 5.1). The microfibrils are discontinuous and randomly distributed in the primary layer [62]. The microfibrils in S1

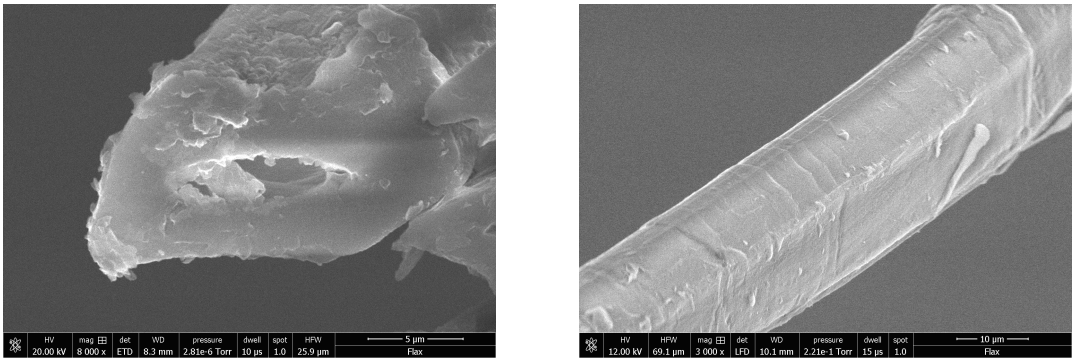

Fig. 5.2: Polygonal cross section of flax fiber

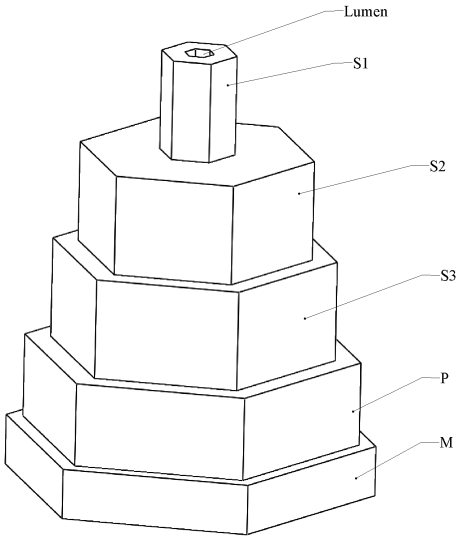

Fig. 5.3: Structure of flax fiber cell walls

and S3 layers are oriented in a flat helix, whereas in the S2 layer are oriented in a steep helix. They are arranged in a helix of opposite sign in the S1 and S3 layers (so-called S and Z helices), while they are arranged in the Z-helix in the S2 layer [63] as shown in Fig. 5.4. The orientation of the microfibrils possess a great influence on the mechanical properties of the natural fibers.

Table 5.1: Thickness, microfibril angle (θ) and the composition of cell wall layers of flax fiber
[61, 64]

Layer	Relative thickness(%)	$\theta(^\circ)$	Cellulose(%)	Hemicellulose(%)	Lignin(%)
M	6	-	0	34	66
P	2	Random	22	26	52
S1	8	$\pm$ 50 - $\pm$ 70	35	30	35
S2	76	6 - 10	64 -71	26 - 33	3
S3	8	$\pm$ 60 - $\pm$ 90	45	35	20

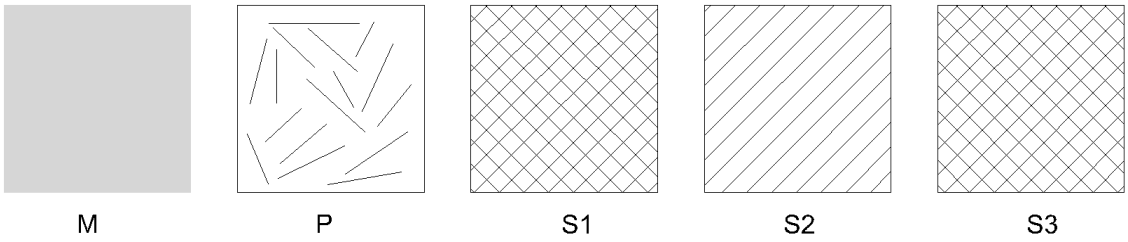

Fig. 5.4: Schematic configuration of cell wall layers

5.3 Constituents of Flax Fiber

The chemical composition and location of constituents within the fiber define the properties of plant natural fibers. The main constituents of plant natural fibers are cellulose, hemicellulose, lignin, pectin, and wax.

5.3.1 Cellulose

Cellulose is an organic polymer known as a polysaccharide $(C_6H_{10}O_5)_n$ consisting of linear chains of D-glucose units joined together by β 1 $\longrightarrow$ 4 glyosidic linkage [65, 66]. Hydrogen bonds between the different macromolecule define the physical properties of the fiber including the capability to form crystalline structure. Cellulose has a semi-crystalline structure, there are regions where cellulose is highly crystalline and others where cellulose is amorphous.

Cellulose is the most abundant organic polymer on Earth [66]. It is the major chemical

and structural component of the primary and secondary cell walls of plant fibers and the strongest and stiffest constituent of such fibers. Thus, cellulose content and orientation within the fiber determine the properties of the fibers. However, cellulose gives the hydrophilic nature to plant fiber due to its structure of semi-crystalline polysaccharide with a large amount of hydroxyl group.

5.3.2 Hemicellulose

Like cellulose, hemicellulose belongs to the group of heterogeneous polysaccharides [67]. Unlike cellulose, hemicellulose has entirely amorphous structure, little strength, and it is easily to be hydrolyzed by dilute acid or base. Cellulose consists of 7000-15000 glucose units and is an unbranched polymer. In other hand, hemicellulose has 500-3000 sugar units and is a branched polymer. Further comparison between cellulose and hemicellulose displayed in Table 5.2.

Table 5.2: Comparison between Cellulose and Homocellulose

	Cellulose	Hemicellulose
Monomer	Pure glucose	Mixed sugar
Polymer chain length	Long	Short
Polymer topology	Linear	Branched
Polymer morphology	Crystalline and amorphous	Amorphous
Solubility	Low	High
Hydrophilic	Less	More

5.3.3 Lignin

Lignin is a highly complex polymer (phenolic group), aromatic, and having amorphous structure [68]. It is normally found in the secondary cell walls of plant natural fibers. It is a polymer of phenylpropane units but has the least water absorption among the plant natural fiber constituents. Despite of insolubility of lignin in water, it is soluble in weak alkaline solutions such as sodium hydroxide. Sodium hydroxide is usually used to separate lignin

from cellulose. Existence of lignin in cell wall is important because it gives the rigidity and it does not rot easily [69]. Together with hemicellulose, these two constituents form a matrix surrounding the cellulose fibrils.

5.3.4 Pectin

Pectin is a structural heteropolysaccharide found in the primary cell walls of plant fibers [70]. The word pectin derived from a Greek word pektickos which means congealed or curdled. In plant natural fiber, its function is to expand or grow and bind cells together. It exhibits highly hydrophilic behavior. The solubility of pectin depends on the temperature and composition.

5.3.5 Wax

Most of the waxes in plants are mixtures of substituted long chains of aliphatic hydrocarbons. Waxes contain alkaline, primary and secondary alcohol, fatty acids, aldehydes, ketones, and other ingredients [71].

5.4 Elastic Constants

The purpose of this section is to evaluate the values of elastic constants of flax fiber by taking into account different microfibril angles and cellulose content of S2 layer. S2 layer is the only layer considered in computing the elastic constants of flax fiber because this layer is the thickest layer, it has more cellulose content than other layers, and the microfibrils are almost unidirectional in this layer. A 2D SG of cellulose, hemicellulose, and lignin is homogenized to calculate the effective properties of each cell wall layer by considering the volume fraction of S2 layer constituents. This step was accomplished using FEA and the analytical equations.

5.4.1 Elastic Constants of S2 Layer

A 2D SG was adopted to calculate the elastic properties of S2 layer as shown in Fig.5.5. In this schema, the central core, the middle layer, and the external layer of the SG represent

microfibrils (cellulose), hemicellulose, and lignin respectively. Cellulose and hemicellulose exhibit transversely isotropic properties and lignin exhibit isotropic properties. Table 5.3 shows the elastic properties of the fiber constituents in the microfibril direction, where subscript x indicates the longitudinal direction and y indicates the transverse plane normal to the longitudinal direction. The effective properties of cell wall layers were predicted using FEA and analytical equations. Analytical equations including RoM and Halpin-Tsai equations, RoM was used to calculate the longitudinal properties and Halpin-Tsai equation was used to calculate the transverse properties of the secondary wall layers.

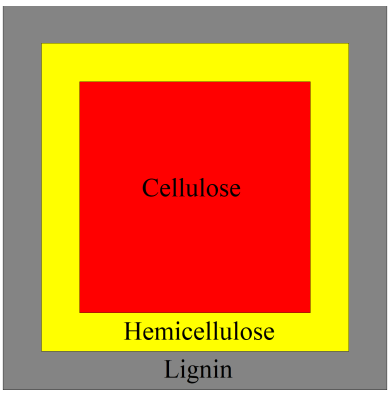

Fig. 5.5: A 2D unit cell

Table 5.3: Mechanical properties of constituents [62]

Constituents	E_x(MPa)	E_y(MPa)	G_{xy}(MPa)	ν_{xy}	ν_{yz}
Cellulose	138000	27200	4400	0.235	0.48
Hemicellulose	7000	3500	1800	0.2	0.4
Lignin	2000	2000	770	0.3	0.3

In FEA, a 2D SG of S2 layer was generated using ABAQUS. It is assumed that fiber constituents of the cell walls are repeated in a square unit cell pattern. A S4(A 4-node doubly curved general-purpose shell, finite membrane strains) element was chosen in the analysis. Fig.5.6 shows the meshed of the 2D SG of S2 layer.

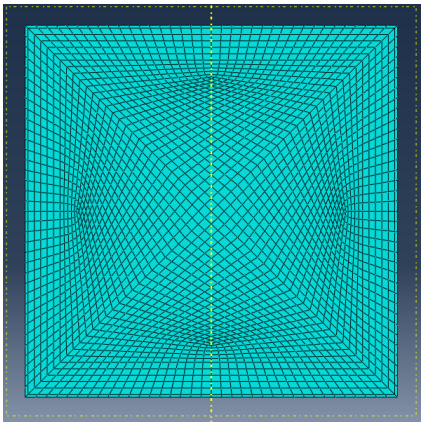

Fig. 5.6: The meshed SG of S2 layer

Elastic constants were also evaluated using RoM and Halpin-Tsai equations. Two step of homogenization was followed to calculate the elastic properties of S2 layer using Halpin-Tsai equation as shown in Fig 5.7. First, cellulose and hemicellulose are homogenized to calculate the equivalent material properties of these two constituents. Then, this material is considered as a reinforcement to lignin. The second step of homogenization gives the effective properties of each secondary wall layer.

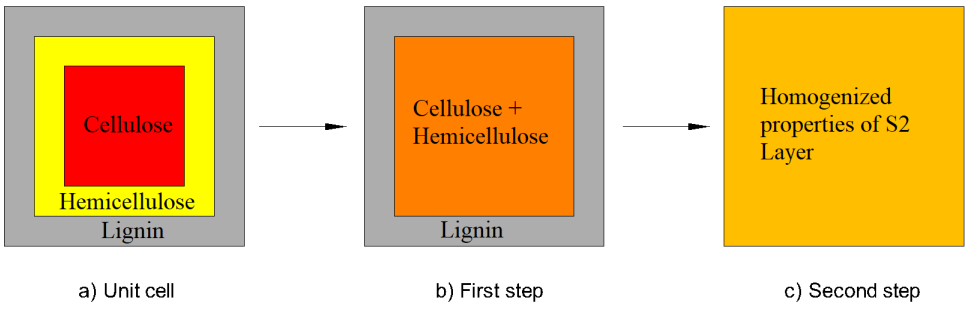

Fig. 5.7: A two-step homogenization procedure of unit cell

RoM and Halpin-Tsai equation are given in Eqs. 4.53 -4.55.

ξ for very high fiber content [72]:

$$\xi(E_x) = 2 + 40V_f^{10} \tag{5.1}$$

$$\xi(G_{xy}) = 1 + 40V_f^{10} \tag{5.2}$$

The computed elastic constants of S2 layer through 2D FEA SG model are compared with those values obtained from analytical equations given in Eqs.4.53-4.55. The comparison between FEA results and analytical equations results is shown later in this chapter.

Different possible combination of microfibril angles (θ) and S2 layer constituent contents in the S2 layer were selected to determine the effect of θ and cellulose content on the mechanical properties of flax fiber.

Effect of θ on Elastic Constants

The elastic constants of S2 layer were calculated in the microfibril direction. To achieve elastic constants of flax fiber in the fiber direction, the computed mechanical properties of S2 needed to be transformed from microfibril direction to the fiber direction. Microfibril orientation is very important structure property which it has profound effect on the mechanical properties of flax fiber. As shown in Fig.5.8, x-y coordinate aligned with the microfibril direction and 1-2 coordinate aligned with fiber direction. For S2 layer, its stiffness matrix in 1-2 coordinate system is:

$$\bar{C} = T_1^{-1}(\theta) C T_2(\theta) \tag{5.3}$$

Where θ, C , T_1 and T_2 refer to microfibril angles, stiffness matrix in x-y coordinate, and transformation matrices respectively.

$$C = \begin{bmatrix} \frac{1-\nu_{yz}\nu_{zy}}{E_y E y \Delta} & \frac{\nu_{yx}+\nu_{yz}\nu_{zx}}{E_y E_z \Delta} & \frac{\nu_{zx}+\nu_{yx}\nu_{zy}}{E_y E_z \Delta} & 0 & 0 & 0 \\ \frac{\nu_{yx}+\nu_{yz}\nu_{zx}}{E_y E_z \Delta} & \frac{1-\nu_{xz}\nu_{zx}}{E_x E_z \Delta} & \frac{\nu_{zy}+\nu_{xy}\nu_{zx}}{E_x E_z \Delta} & 0 & 0 & 0 \\ \frac{(\nu_{zx}+\nu_{yx}\nu_{zy})}{E_y E_z \Delta} & \frac{(\nu_{zy}+\nu_{xy}\nu_{zx})}{E_x E_z} & \frac{(1-\nu_{xy}\nu_{yx})}{E_x E_y \Delta} & 0 & 0 & 0 \\ 0 & 0 & 0 & \frac{E_y}{2(1+\nu_{xy})} & 0 & 0 \\ 0 & 0 & 0 & 0 & G_{xz} & 0 \\ 0 & 0 & 0 & 0 & 0 & G_{xy} \end{bmatrix} \tag{5.4}$$

Where:

$$\Delta = (1 - \nu_{xy}\nu_{yx} - \nu_{yz}\nu_{zy} - \nu_{xz}\nu_{zx} - 2\nu_{yx}\nu_{zy}\nu_{xz})/(E_x E_y E_z)$$

$$T_1 = \begin{bmatrix} m^2 & n^2 & 0 & 0 & 0 & 2mn \\ n^2 & m^2 & 0 & 0 & 0 & -2mn \\ 0 & 0 & 1 & 0 & 0 & 0 \\ 0 & 0 & 0 & m & -n & 0 \\ 0 & 0 & 0 & n & m & 0 \\ -mn & mn & 0 & 0 & 0 & m^2 - n^2 \end{bmatrix} \tag{5.5}$$

$$T_2 = \begin{bmatrix} m^2 & n^2 & 0 & 0 & 0 & mn \\ n^2 & m^2 & 0 & 0 & 0 & -mn \\ 0 & 0 & 1 & 0 & 0 & 0 \\ 0 & 0 & 0 & m & -n & 0 \\ 0 & 0 & 0 & n & m & 0 \\ -2mn & 2mn & 0 & 0 & 0 & m^2 - n^2 \end{bmatrix} \tag{5.6}$$

Where m and n refer to cosθ and sinθ respectively.

As a result of stiffness matrix transformation, orthotropic elastic properties are achieved for S2 layer. Orthotropic elastic constants of S2 are shown in Figs. 5.9 - 5.12. These Figs.

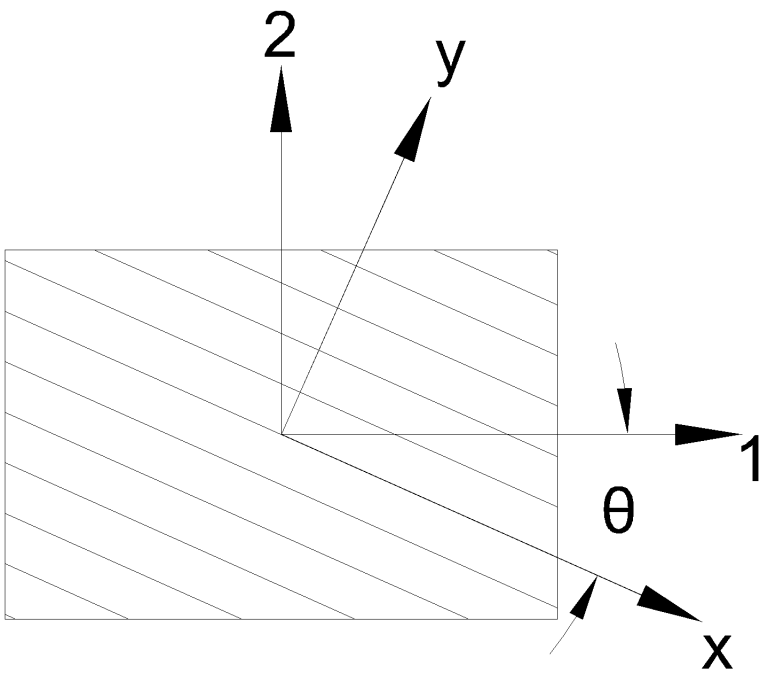

Fig. 5.8: Schematic representation of S2 layer showing microfibril and fiber axes

plotted at volume fractions of cellulose, hemicellulose, and lignin equal to 68%, 29%, and 3% respectively.

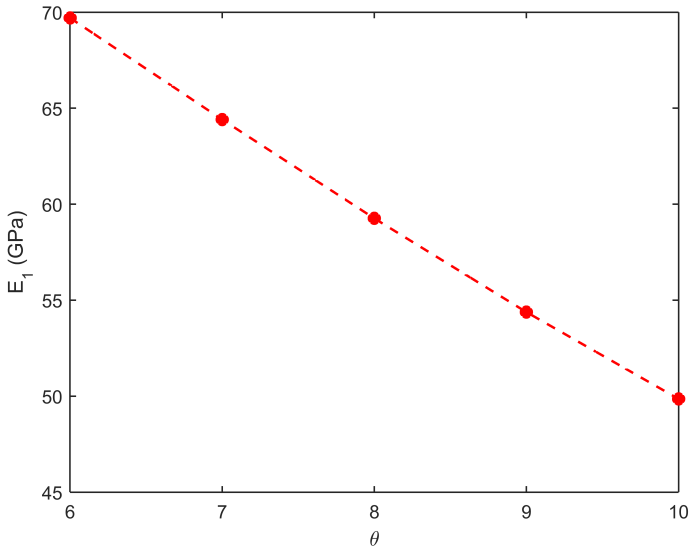

Fig. 5.9: E_1 Versus θ

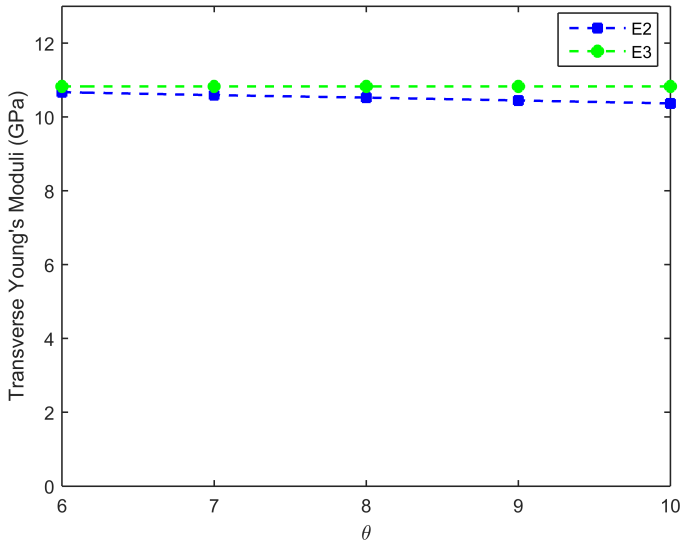

Fig. 5.10: Transverse Young's moduli Versus θ

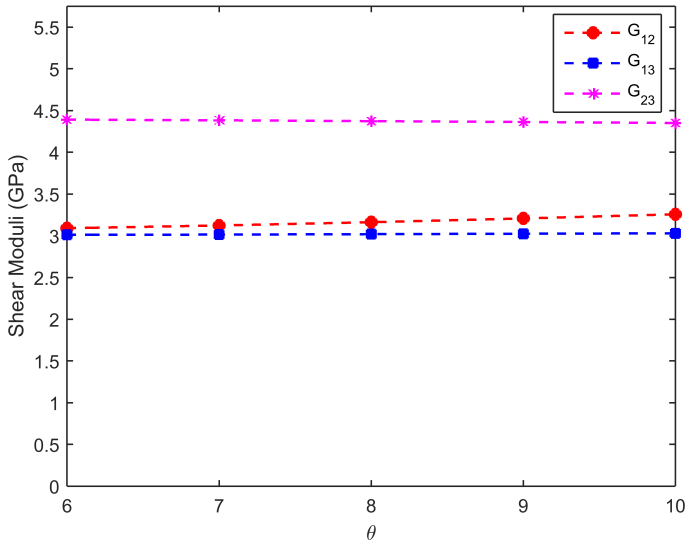

Fig. 5.11: Shear moduli Versus θ

Observation

Increase in θ:

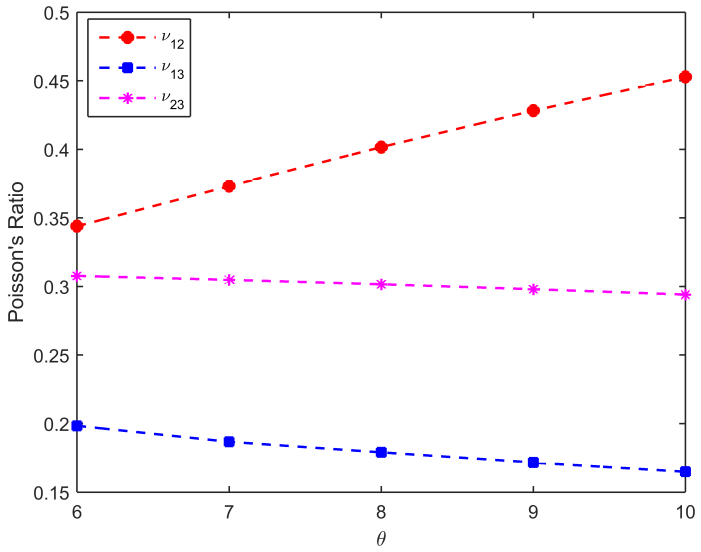

Fig. 5.12: Poisson's Ratio Versus θ

1. The longitudinal modulus decreased linearly with increasing θ. The Longitudinal Young's modulus dropped by 28.5% when θ was changed from 6° -10°.

2. Transverse Young's moduli and all shear moduli were less effected with increasing θ.

3. The longitudinal Poisson's ratio increased linearly with increasing θ. The longitudinal Poisson's ratio increased by 31.67% when θ increased from 6°-10°. Transverse Poisson's ratio decreased with increasing θ.

Effect of Cellulose Content on Elastic Constants

Cellulose content is the second important structure property where the mechanical properties of flax fiber changes significantly with changing cellulose content. The effective elastic constants computed using 2D FEA and semi-emperical relations for different combination of S2 layer constituents are shown in Figs.5.13-5.17. These calculations were done at θ=0°.

Observation

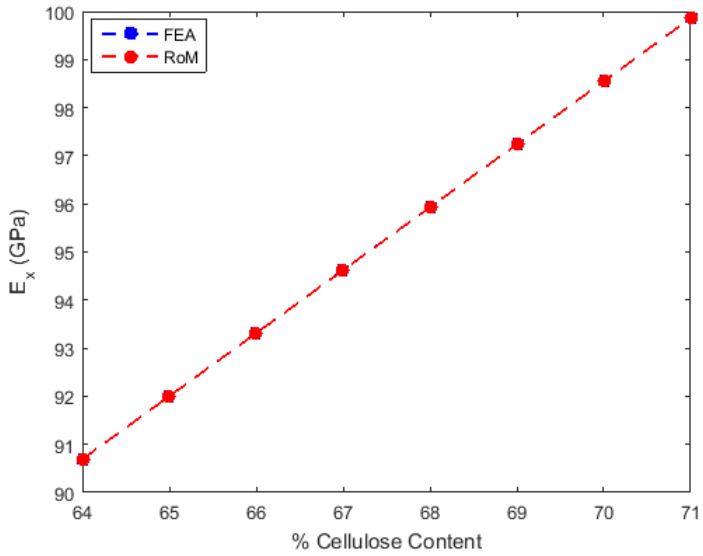

Fig. 5.13: Young's modulus in Longitudinal direction

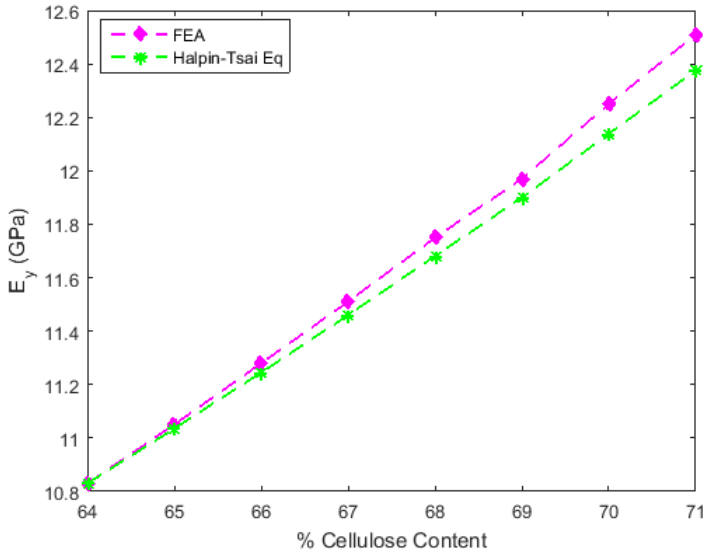

Fig. 5.14: Transverse Young's modulus

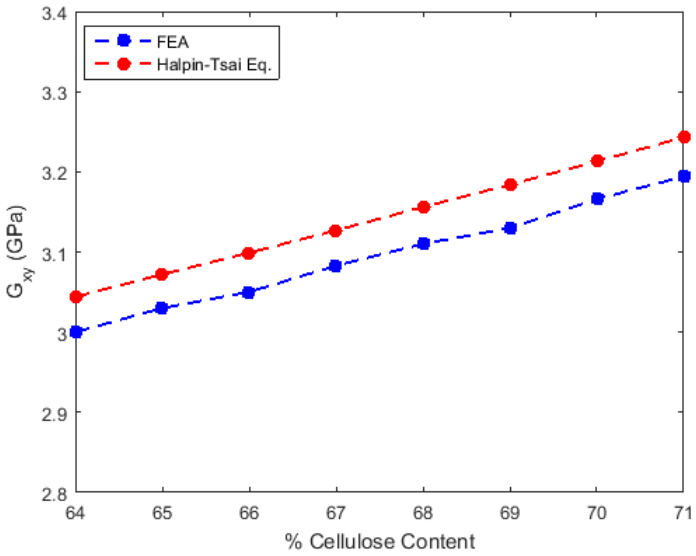

Fig. 5.15: Longitudinal Shear modulus

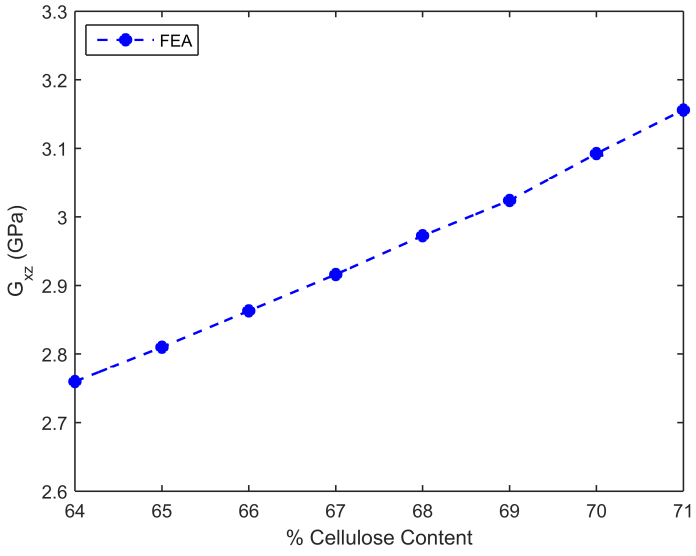

Fig. 5.16: Transverse Shear modulus

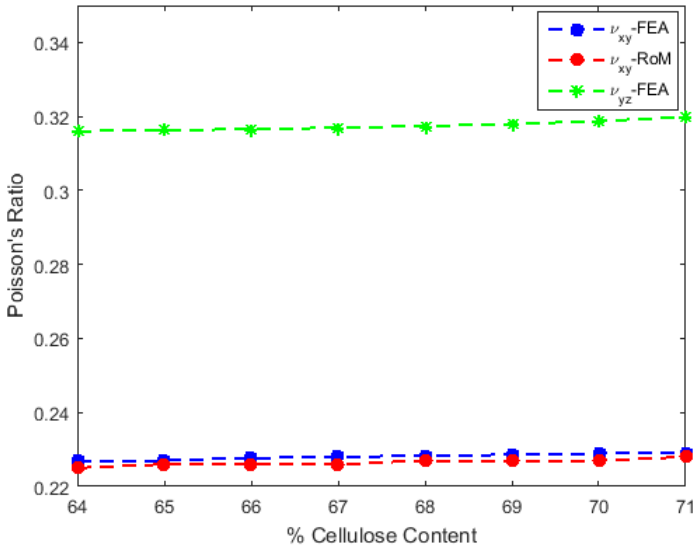

Fig. 5.17: Poisson's ratio

1. Axial Young's modulus and Poisson's ratio computed from RoM are consistent with FEA. Transverse Young's modulus computed from Halpin-Tsai equations gives a discrepancy about 18 % compared to FEA. The source of this discrepancy due to the fact that Halpin-Tsai equations depends on the aspect ratio of composite constituents. For this particular problem, it is found the value of $\xi(E_y)$ that gives a good agreement to 2D FE results equal to 1.775. However, shear modulus computed from Halpin-Tsai equations are in good agreement with 2D FE results.

2. The longitudinal and transverse Young's moduli increased linearly with increasing cellulose content.

3. Shear moduli and Poisson's ratios were least effected with increasing cellulose content.

5.4.2 Elastic Constants of Flax Fiber

Elastic constants of S2 layer are determined at nanoscale for different θ and flax fiber constituents in the previous section. These properties are applied to 2D FEA of regular hexagon cross-section of flax fiber as shown in Fig.5.16. Although SEM images showed that flax fibers exhibit polygonal cross-section with 5-7 sides and the length of each side

is not the same, flax fibers are assumed to have regular hexagonal cross-section. Qing and Mishnaevsky [62] performed a 3D FEA model of regular and irregular hexagon cross-section fiber. They concluded that axial Young's modulus do not highly depend on the variation of the cross-section of fiber while transverse Young's moduli are more sensitive to the shape of the cross-section.

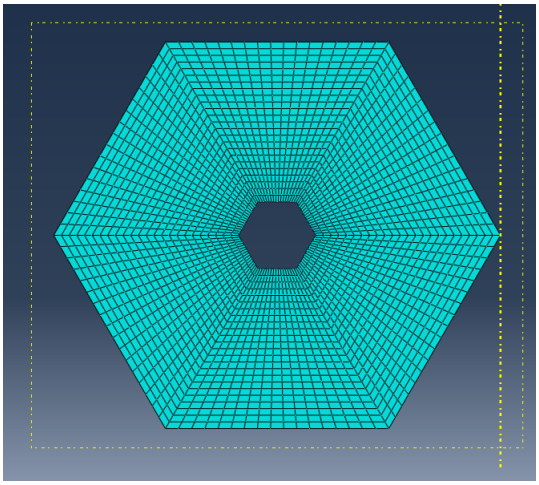

Fig. 5.18: RVE of flax fiber

Fig.5.18 shows a 2D SG of hexagonal cross-section flax fiber with a length of each side is equal to 10 μm and the diagonal of the fiber is equal to 20 μm. The size of the lumen is assumed to be 3 % of the total area of flax. θ and volume fractions of cellulose, hemicellulose, and lignin of S2 layer that are used in finding the elastic constants of flax fiber equivalent to 10°, 68%, 29%, and 3% respectively.

Table 5.4: Elastic constants of flax fiber using only S2 layer (Moduli in GPa)

E_1	E_2	E_3	ν_{12}	ν_{13}	ν_{23}	G_{12}	G_{13}	G_{23}
50	10.28	10.76	0.46	0.1628	0.285	3.16	2.94	3.89

CHAPTER 6

Elastic Constants of Hybrid Composite

6.1 Introduction

In the following sections, a micromechanical analysis of SG of a unidirectional flax/E-glass fiber hybrid composite is performed using FEA and compared to analytical methods. To minimize time and computational efforts, both fibers are assumed to have circular cross-section. The fibers are also assumed to be packed in a hexagonal pattern. To study the effect of volume fractions of both fibers on the effective properties of the hybrid composite, different possible combinations of flax and glass fibers are chosen with maintaining total volume fraction of both fibers. In order to find the effect of fiber locations on the mechanical properties of the hybrid composite, flax and glass fibers are placed in different locations in the SG.

6.2 Model for Hybrid Composite

Based on the processing conditions and applications, fibers can be oriented in various ways in the matrix. They may be randomly oriented in plane, partially aligned, and approximately unidirectional. In this thesis, it is assumed that both fibers are unidirectionally oriented, perfectly bonded to the epoxy matrix, and arranged in a hexagonal pattern. A hexagonal pattern was chosen because it can give more accurate transverse properties than that of a square pattern. The hexagonal SG is illustrated in Fig.6.2. Its dimensions can be calculated from the following equation:

$$V_f = \frac{\text{Area of fibers}}{\text{Area of matrix+ Area of fibers}} \tag{6.1a}$$

$$V_f = \frac{3.\frac{\pi r^2}{6}}{\frac{1}{2}L.L.sin(\frac{\pi}{3})} \tag{6.1b}$$

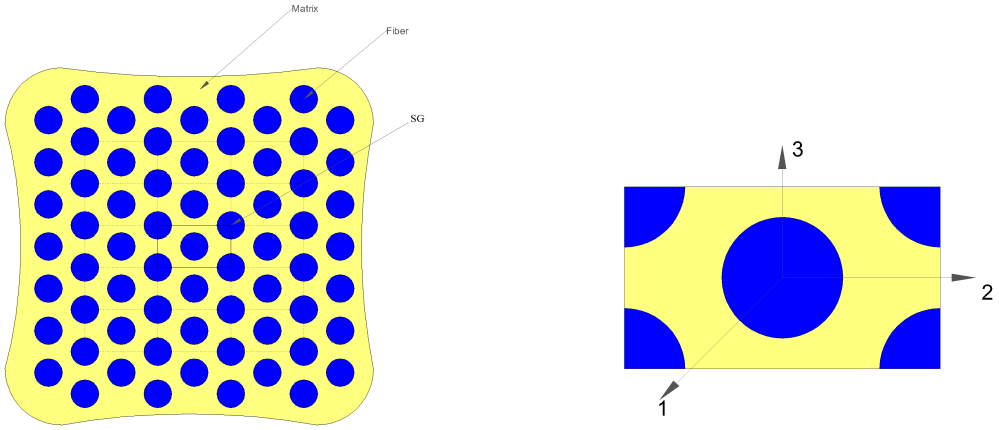

(a) Fibers distribution in a heaxongal pattern (b) Hexagonal SG

Fig. 6.1: Hexagonal-packed array model

A cross-section of flax/glass fiber reinforced epoxy composite is depicted in Fig.6.1. The blue circles represent fibers and yellow region represent epoxy. Both fibers are assumed to be solid and have the same radii of 20 μ. This assumption can give more flexibility in generating finite element mesh.

6.3 Elastic Properties of the Unidirectional Fiber Hybrid Composite

The micromechanical SG of the composite is analyzed using FEA. ABAQUS software was used in the FEA. A S4 element was selected in the analysis. Fig.6.2 shows the meshed SG of flax/E-glass fiber reinforced epoxy resin. The effective properties of the hybrid composite were calculated through numerical homogenization. The material properties of the composite constituents are listed in Table 6.1. As it can be noticed from this table, flax fiber possesses orthotropic properties while E-glass and epoxy possess isotropic properties. The resulted hybrid composite follow orthotropic properties behavior. The reason for this is that flax fiber shows orthotropic properties which effect the overall behavior of the hybrid composite.

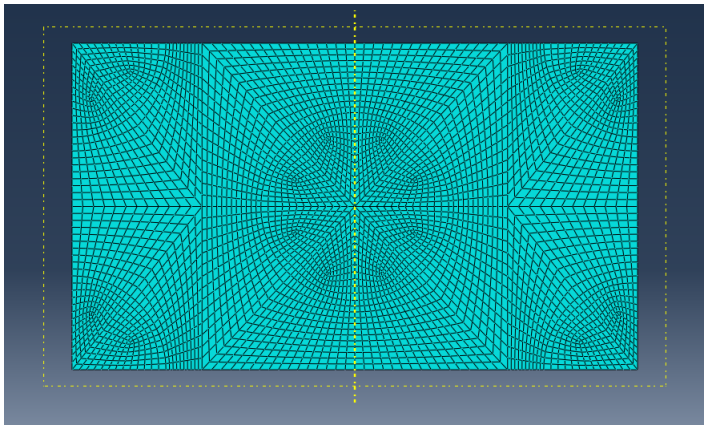

Fig. 6.2: The meshed SG of the hybrid composite

Table 6.1: Elastic constants of composite constituents

Property	Flax fiber	E-glass fiber	Epoxy
$E_1(GPa)$	50	80	3.5
$E_2(GPa)$	10.28	80	3.5
$E_3(GPa)$	10.76	80	3.5
$G_{12}(GPa)$	3.16	33.33	1.296
$G_{13}(GPa)$	2.94	33.33	1.296
$G_{23}(GPa)$	3.89	33.33	1.296
ν_{12}	0.46	0.2	0.35
ν_{13}	0.1628	0.2	0.35
ν_{23}	0.285	0.2	0.35

Analytical formulas, RoHM and Halpin-Tsai equations, were also used to predict the effective elastic constants of the hybrid composite. RoHM was used to determine the axial Young's modulus and Poison's ratio. For the transverse Young's moduli E_2 and E_3 and longitudinal and transverse shear moduli G_{12}, G_{13}, and G_{23}, modified Halpin-Tsai equations were used to predict these elastic constants. Then, the comparison was made between the results obtained from FEA with analytical results. As it is shown later, RoHM results are consistent with FEA results and modified Halpin-Tsai equations agree with reasonable accuracy with FEA results. RoHM can be stated as,

$$E_1 = E_1^f V_f^f + E^g V_f^g + E^m V^m \tag{6.2}$$

$$\nu_{12} = \nu_{12}^f V_f^f + \nu^g V_f^g + \nu^m V^m \tag{6.3}$$

Where f, g, and m superscripts refer to flax, glass and matrix respectively, and V_f^f, V_f^g and V^m refer to the volume fraction of flax, glass, and epoxy respectively.

The Halpin-Tsai equation for one type of fiber composite is given in Eq.4.55. For the hybrid composite, Halpin-Tsai equations required to be modified to include the elastic constants and volume fractions of all reinforcements. Banerjee proposed the modification to the Halpin-Tsai equations [36]. The modified Halpin-Tsai equation is given below:

$$\frac{M}{M^m} = \frac{1 + \xi(\eta^f V_f^f + \eta^g V_f^g)}{1 - (\eta^f V_f^f + \eta^g V_f^g)} \tag{6.4}$$

where,

$$\eta^f = \frac{\frac{M^f}{M^M} - 1}{\frac{M^f}{M^m} + \xi}$$

$$\eta^g = \frac{\frac{M^g}{M^M} - 1}{\frac{M^g}{M^m} + \xi}$$

Here M refers to transverse Young's moduli (E_2 and E_3) or shear moduli (G_{12}, G_{13} and G_{23}).

6.3.1 Effect of Changing Volume Fraction on the Elastic Constants

The effective elastic constants of composite were determined using FEA and analytical formulas. Results obtained from RoHM and Halpin-Tsai equations, wherever applicable, were compared with FEA results. To study the hybridization effect, it is initially assumed that composite is reinforced only by flax fiber and then decreasing the volume fraction of flax and increasing the volume fraction of glass fiber until the composite is reinforced only

by glass fiber. The glass fiber increment that is used in FEA is 5%. Initially, the overall volume fraction of both fibers assumed to be 40%. The elastic constants of the hybrid composite are plotted in Figs 6.3-6.10 with volume fraction of glass varying from 0 to 40%.

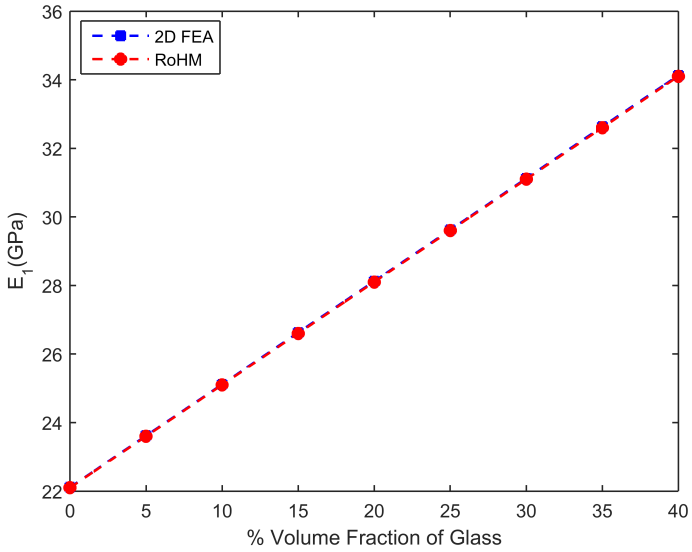

Fig. 6.3: Axial Young's modulus of composite

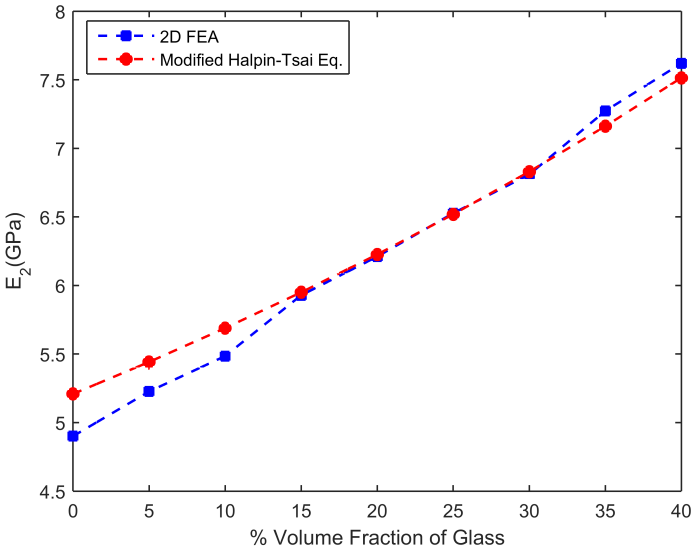

Fig. 6.4: E_2 of composite

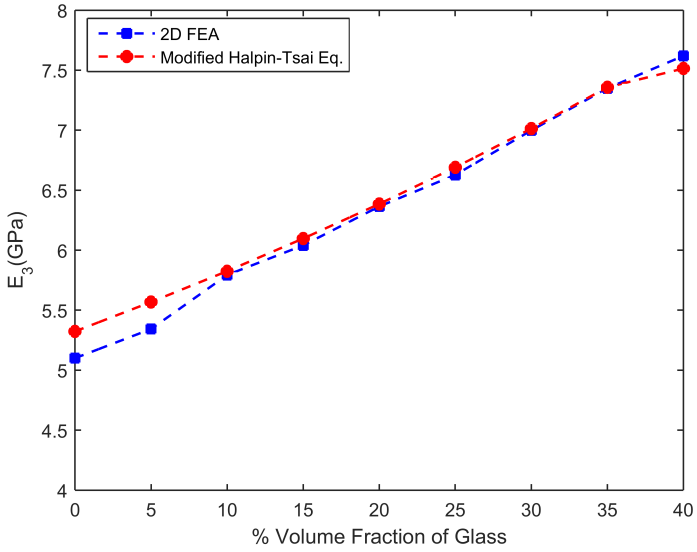

Fig. 6.5: E_3 of composite

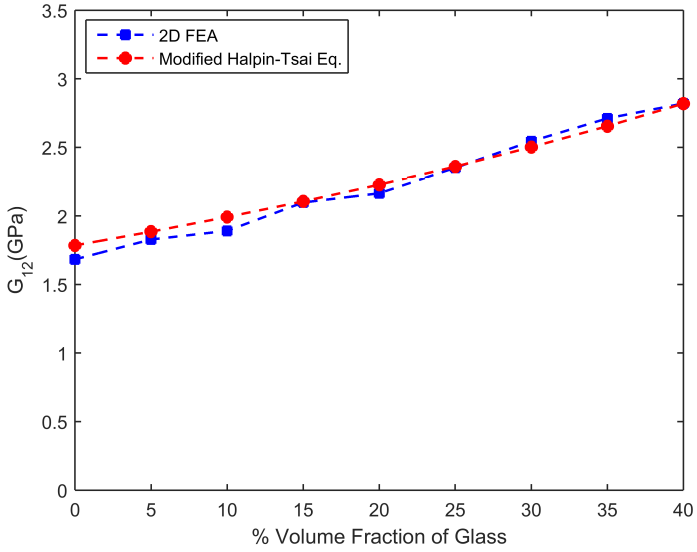

Fig. 6.6: Axial shear modulus of composite

However, during the fabrication of composite samples, it was observed that $V_F = 40\%$ of the hybrid composite gives poor epoxy distribution through composite samples which leads to poor adhesion between fibers and epoxy resin. To overcome this issue, the overall

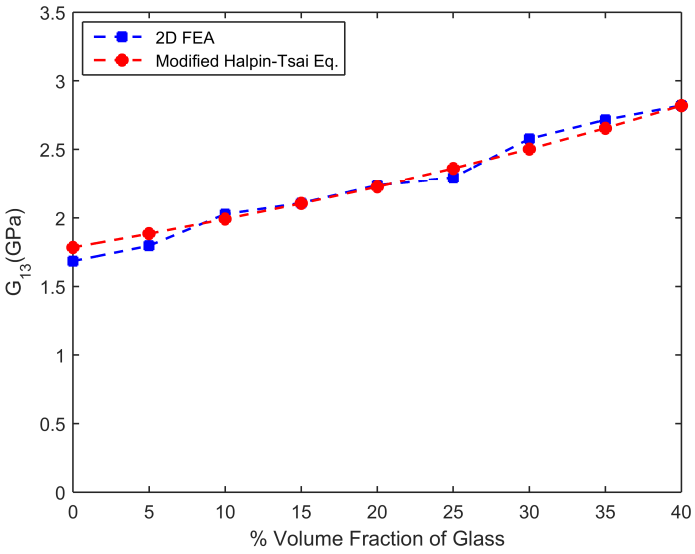

Fig. 6.7: G_{13} of composite

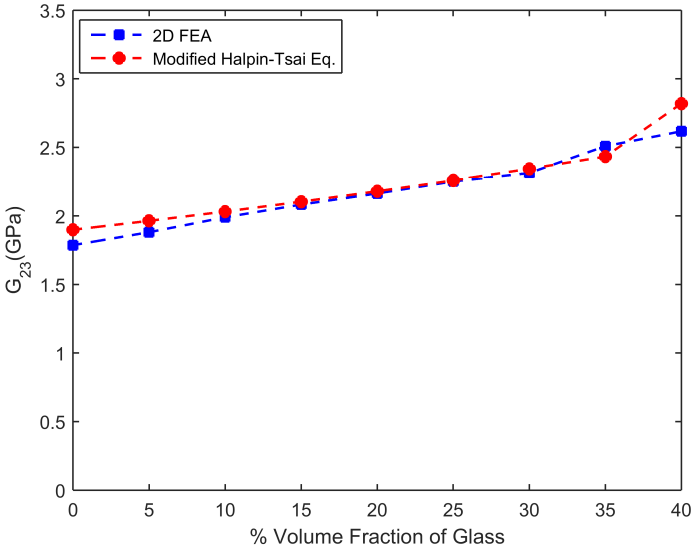

Fig. 6.8: G_{23} of composite

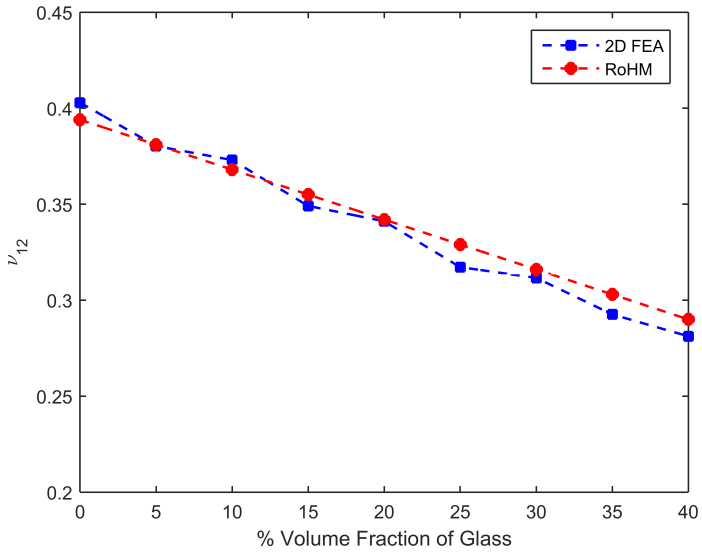

Fig. 6.9: Axial Poisson's ratio of composite

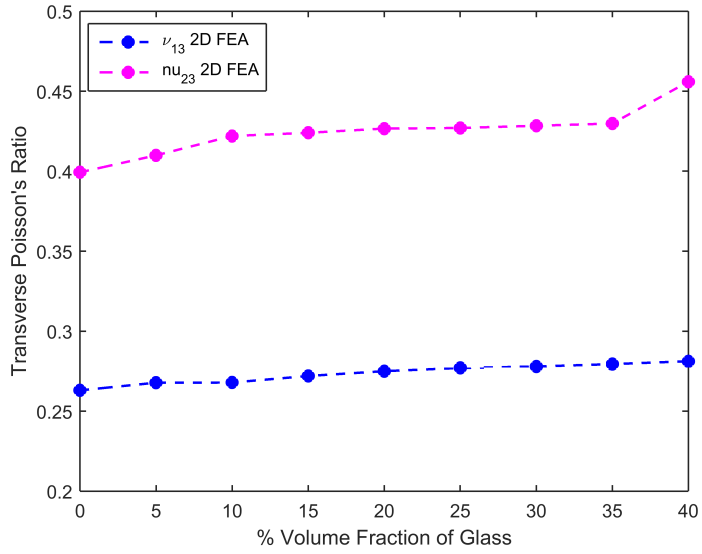

Fig. 6.10: Transverse Poisson's ratios of composite

volume fraction of fibers were reduced gradually until it was ensured that the new volume fraction provides better interfacial adhesion. It was concluded that V_F=30 % gives good interfacial adhesion between fibers and matrix. The following elastic constants are plotted in Figs. 6.11 - 6.18 at $V_F = 30$ % through FEA and analytical equations. The axial Young's modulus calculated at 30 % will be compared with the experimental value.

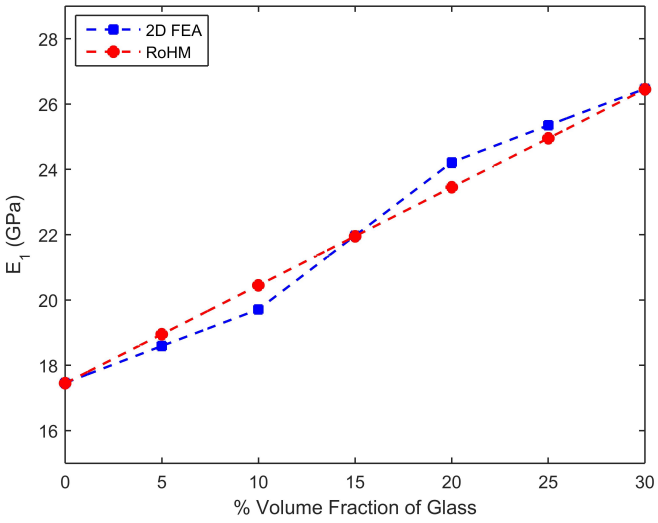

Fig. 6.11: Axial Young's modulus of composite

Observations:

1. Longitudinal elastic constants computed from RoHM are consistent with FEA. Thus, these properties can be calculated using RoHM only if the longitudinal Young's modulus and Poisson's ratio are of interest.

2. Young's and shear moduli in longitudinal and transverse directions increased linearly with increasing the volume fraction of glass fiber.

3. Longitudinal Poisson's ratio (ν_{12}) decreased with increasing the volume fraction of glass fiber. The transverse Poisson's ratio (ν_{13} and ν_{23}) were least effected with increasing the volume fraction of glass fiber.

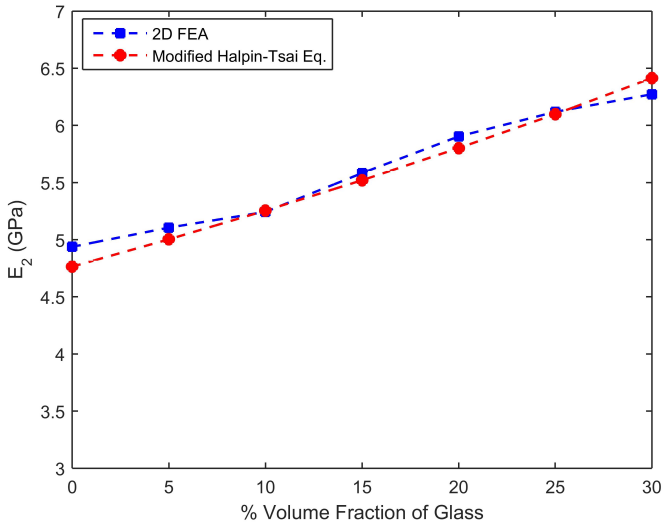

Fig. 6.12: E_2 of composite

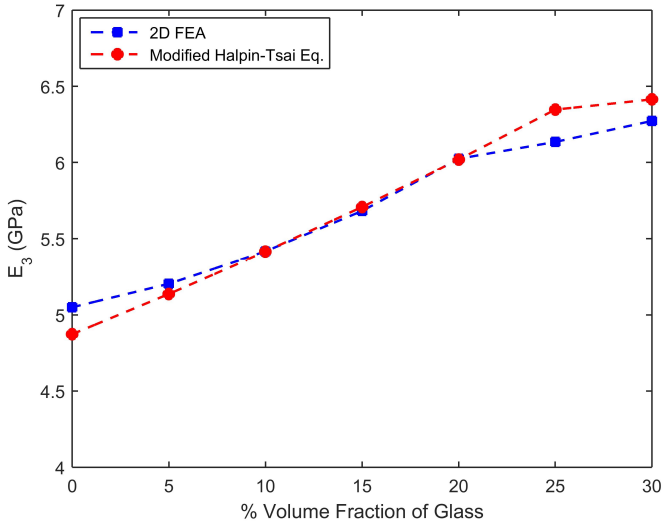

Fig. 6.13: E_3 of composite

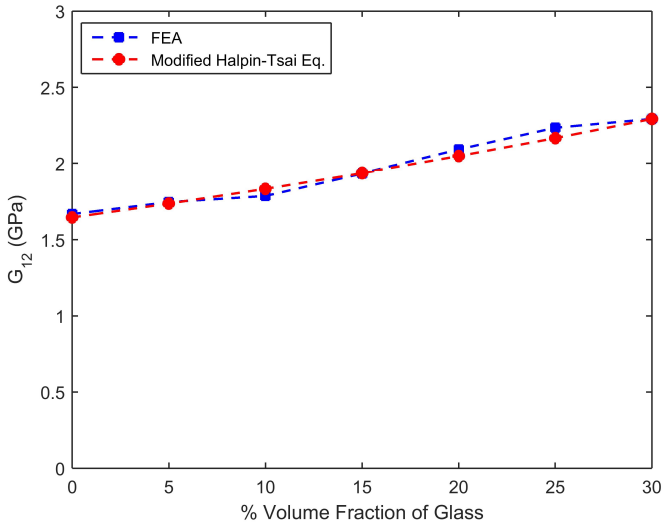

Fig. 6.14: Axial shear modulus of composite

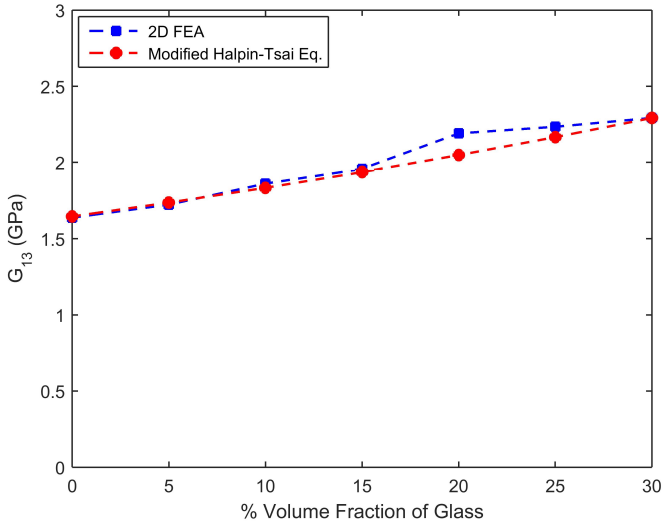

Fig. 6.15: G_{13} of composite

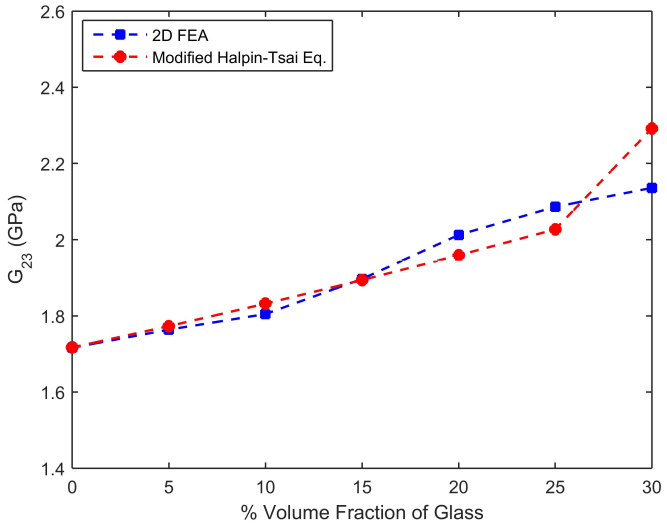

Fig. 6.16: G_{23} of composite

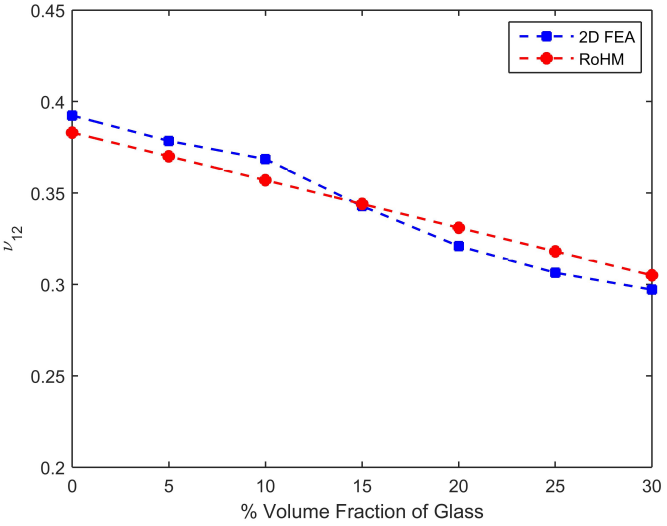

Fig. 6.17: Axial Poisson's ratio of composite

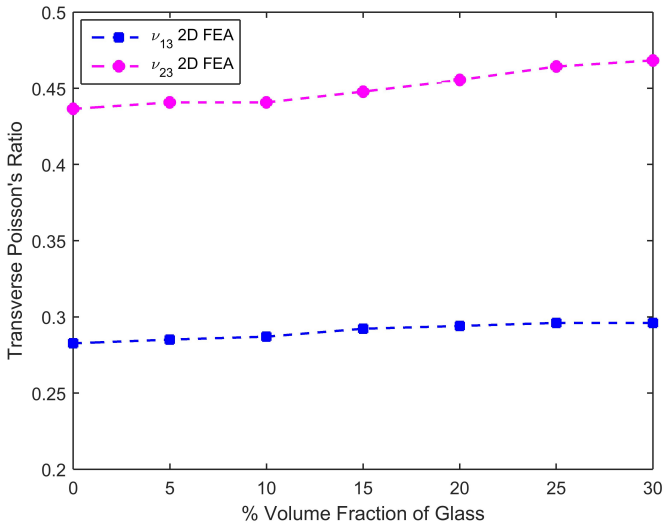

Fig. 6.18: Transverse Poisson's ratios of composite

4. For this particular composite, when the total volume fraction of composite is 30%, it is found that value of ξ in Halpin-Tsai equations which gives a good match with FEA for E_2, E_3, G_{12}, G_{13}, and G_{23} are 1.225, 1.475, 1, 1 and 0.575 respectively.

6.3.2 Comparison between FEA and Analytical Results

The purpose of using analytical equations is to validate the FEA results. In this section, the comparison between FEA and analytical results were made whenever it is applicable. The total volume fraction that is considered in this study is 30 %. Tables 6.3-6.9 show the difference between FEA and analytical results.

Table 6.2: Samples numbering for Composites.

Sample	V_f^f (%)	V_f^g(%)	V_f^t(%)
S1	30	0	30
S2	25	5	30
S3	20	10	30
S4	15	15	30
S5	10	20	30
S6	5	25	30
S7	0	30	30

Table 6.3: Longitudinal Young's moduli (E_1) for various composite samples in GPa units.

Composite Sample	S1	S2	S3	S4	S5	S6	S7
FEA	17.459	18.59	19.71	21.967	24.215	25.348	26.467
RoHM	17.45	18.95	20.45	21.95	23.45	24.95	26.45
% Diff.(absolute)	0.0515	1.918	3.685	0.077	3.21	1.58	0.064

Table 6.4: Transverse Young's moduli (E_2) for various composite samples in GPa units.

Composite Sample	S1	S2	S3	S4	S5	S6	S7
FEA	4.94	5.1	5.24	5.58	5.9	6.11	6.27
Modified Halpin-Tsai	4.764	5	5.254	5.52	5.8	6.1	6.414
% Diff.(absolute)	3.58	2.02	0.205	1.121	1.747	0.335	2.233

Table 6.5: Transverse Young's moduli (E_3) for various composite samples in GPa units.

Composite Sample	S1	S2	S3	S4	S5	S6	S7
FEA	5.05	5.2	5.42	5.68	6.02	6.13	6.27
Modified Halpin-Tsai	4.87	5.137	5.415	5.708	6.019	6.347	6.414
% Diff.(absolute)	3.566	1.298	0.026	0.463	0.0899	3.4	2.232

Table 6.6: Longitudinal Shear moduli (G_{12}) for various composite samples in GPa units.

Composite Sample	S1	S2	S3	S4	S5	S6	S7
FEA	1.67	1.75	1.79	1.93	2.09	2.23	2.29
Modified Halpin-Tsai	1.646	1.737	1.834	1.937	2.048	2.166	2.292
% Diff.(absolute)	1.339	0.561	2.6	0.14	2.126	3.11	0.015

Table 6.7: Transverse Shear moduli (G_{13}) for various composite samples in GPa units.

Composite Sample	S1	S2	S3	S4	S5	S6	S7
FEA	1.64	1.72	1.86	1.96	2.19	2.23	2.29
Modified Halpin-Tsai	1.646	1.737	1.837	1.937	2.048	2.166	2.292
% Diff.(absolute)	0.5	0.784	1.496	1.074	6.743	3.1	0.0173

Table 6.8: Transverse Shear moduli (G_{23}) for various composite samples in GPa units.

Composite Sample	S1	S2	S3	S4	S5	S6	S7
FEA	1.72	1.76	1.8	1.9	2.01	2.09	2.14
Modified Halpin-Tsai	1.717	1.773	1.832	1.894	1.959	2.027	2.292
% Diff.(absolute)	0.034	0.518	1.5	0.153	2.69	2.882	7.051

Table 6.9: Longitudinal Poisson's ratio (ν_{12}) for composite.

Composite Sample	S1	S2	S3	S4	S5	S6	S7
FEA	0.392	0.378	0.368	0.343	0.321	0.306	0.297
RoHM	0.383	0.37	0.357	0.344	0.331	0.318	0.305
% Diff.(absolute)	2.417	2.25	3.16	0.334	3.09	3.71	2.615

6.3.3 Effect of Changing Fiber Locations on the Elastic Constants

Flax and glass fibers were placed in different locations inside the SG. The SG that is used for this study is shown in Fig.6.11. $V_f^f = 15\%$ and $V_f^g = 15\%$ are used for this study. It was observed that elastic constants do not depend on the variability of fiber locations. However, many research papers have shown that location of two different fibers in the matrix have influence on tensile strength of composite. For example, this paper showed changing fiber locations has influence on the tensile strength of the hybrid composite but not on the Young's modulus [20]. The effect of fiber locations on tensile strength are shown in next chapter using experiment.

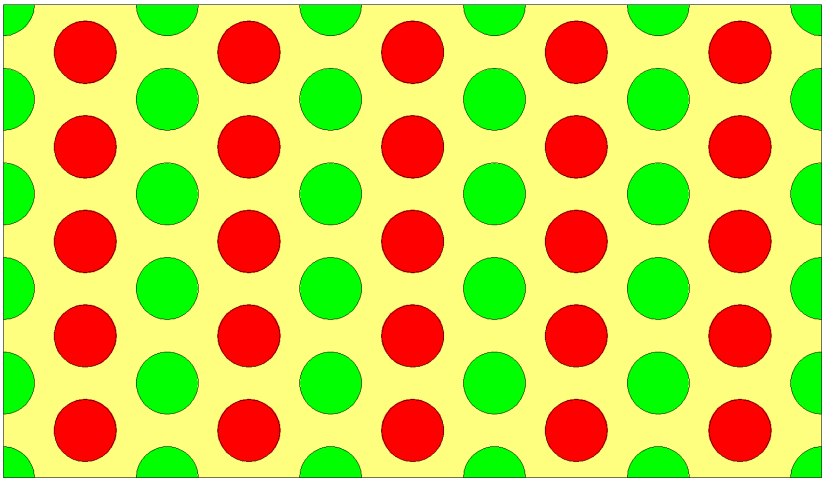

Fig. 6.19: SG that used to investigate the effect of fiber locations on the elastic constants

CHAPTER 7

Experimentation

7.1 Introduction

In chapter 6, elastic constants of flax/E-glass fiber reinforced epoxy resin are calculated for different volume fractions of flax and E-glass fiber. Also, the effect of fiber locations on the elastic constants are determined. In this chapter, Young's modulus and tensile strength of different stacking sequence of fiber layers of hybrid composite are evaluated through tensile tests. FEA and analytical results are compared with experimental results. This chapter also presents the water absorption properties of flax fiber composite, glass fiber composite, and flax/glass fiber hybrid composite due to immersing composite specimens in de-ionized water for a week. The influence of immersing composite specimens in de-ionized water on the tensile properties is also presented. The comparison between dry and wet specimens properties are made. Also, it shows the impact strength of single fiber composites and various stacking sequence of flax and E-glass fiber layers hybrid composite. The impact strength of composites are conducted from Charpy impact test of notched specimen. The volume fraction combinations of flax, E-glass, and epoxy resin that is used in fabrication of hybrid composite specimens are 15%, 15%, and 70% respectively.

7.2 Materials and Experimental Methods

7.2.1 Materials

Polymer Selection

Composites are generally comprised of a polymeric matrix and reinforcing fibers. Because polymers are softer, lighter than fibers and fibers are stronger than polymers , the combination of a polymeric matrix and fibers provides a high strength to weight ratio of

the resulting composite. However, selection of polymeric resin for natural fiber composites must be chosen carefully. It is because of the hydrophilic nature of all natural fibers and most of common matrix polymers. The hydrophilic behavior of natural fibers is due to their chemical structure- hemicellulose and pectin are considered very hydrophilic. The combination of hydrophilic polymer with natural fiber can lead to poor adhesion between the fibers and matrix and dimensional instability of composite. Because the mechanical properties of composites depend on the properties of composite constituents and surface adhesion between fibers and polymer, the ineffective interfaces between fibers and matrix can affect the mechanical properties of composites. The poor adhesion problem can be solved by applying chemical or physical treatment on natural fibers or modifying the chemical composition of the polymer matrix. Hoverer, these treatments have a negative impact on economical aspect of natural fiber composites manufacturing.

Many kinds of polymers have been used as matrices for natural fibers. Polymers can be divided into two types, thermoplastic and thermoset. The structure of thermoplastic polymers comprises of one or two dimensional molecular, so this explain why thermoplastic polymers have the tendency of becoming soft at elevated temperatures and rolling back their properties through cooling. In contrast, thermoplastic polymers can be categorized as highly cross-linked polymers which can be cured using only heat, pressure, or heat and pressure. This structure of thermoset polymers offer good mechanical properties such as strength and modulus [73]. Thermoplastic matrices that are considered in this study are polypropylene (PP), low-density polyethylene (LDPE), and high-density polyethylene (HDPE), whereas thermosetting matrices that are considered in this study are polyester and epoxy.

Thermoplastic polymers have many advantages over thermoset polymers. Thermoplastic polymers are flexible, having low density, and better impact property than thermoset polymers. However, the use of thermoplastic polymers are restricted to nonstructural applications due to their low tensile strength and modulus. Other drawbacks of using thermoplastic polymers as matrices to natural fibers are that they have high viscosity and high processing temperature. Process temperature is a restricting factor of natural fiber

composites. Because thermoplastics are naturally in a solid state, they must be heated to the melting point. Although natural fibers can withstand temperature up to 200°C for short-period but exposing natural fibers to high temperature for long time can lead to poor interfacial adhesion and embitterment of the cellulose components [9, 74]. On the other hand, thermoset polymers have lower viscosity, better tensile strength and modulus, higher corrosion resistance, and they can be cured at lower temperature than most of thermoplastic matrices. Also, thermosets are considered less hydrophilic and therefore less problematic. For example, epoxy resins have high performance and resistance to environmental degradation and good adhesion to fibers. As compared epoxy resins to polyester, epoxy have better bonding strength and moisture resistance than polyester and this is why epoxy resin is used to reinforce flax/E-glass fiber composite. Table 7.1 and Table 7.2 show the properties of thermoplastic and thermosets that are considered in this study [9].

Table 7.1: Properties of thermoplastic polymers

Property	PP	LPDE	HDPE
Density (g/cm^3)	0.899-0.92	0.91-0.9125	0.94-0.96
Water Absorption % (24 hrs at 20°C)	0.01-0.02	<0.015	0.01-0.2
T_g (°C)	-10 to -23	-125	-133 to -100
T_m (°C)	160-176	105-116	120-140
Tensile Strength (MPa)	26-41.4	40-78	14.5-38
Young's Modulus (GPa)	0.95-1.77	0.055-0.38	0.4-1.5
Elongation (%)	15-700	90-800	2-130
Izod Impact Strength (J/m)	21.4-276	>854	26.7-1068

The epoxy resin that is used in this work is PT2050 and hardener B1. The epoxy resin brought from PTMW industries. Density of epoxy resin is 1.14 g/cc and density of hardener is 0.96 g/cc. The resin and hardener are mixed in 100:27 proportion according to manufacturer's specification. The density of mixed epoxy and hardener is 1.1 g/cc.

Fibers

The flax fibers used in this study were obtained from Easy Composites Ltd in the

Table 7.2: Properties of thermoset polymers

Property	Polester	Epoxy
Density (g/cm^3)	1.2-1.5	1.1-1.4
Water Absorption (24 hrs at 20°C)	0.1-0.3	0.1-0.4
Tensile Strength (MPa)	40-90	35-100
Young's Modulus (GPa)	2-4.5	3-6
Elongation (%)	2	1-6
Izod Impact Strength (J/cm)	0.15-3.2	0.3

United Kingdom. The flax fibers known as Biotex Flax and they come in unidirectional fabric. The E-glass fibers used in this study are unidirectional knitted fabric C72-5208 obtained from Fiberglass Supply in WA. The properties of these two fibers as provided by sellers are shown in Tables 7.3 and 7.4.

Table 7.3: Flax fiber properties

Density	1.5 g/cc
Diameter	20 μm
Young's Modulus	50 GPa
Tensile Strength	500 MPa
Failure Strain	2 %

Table 7.4: E-Glass fiber properties

Density	2.62 g/cc
Diameter	17 μm
Young's Modulus	80 GPa
Tensile Strength	3100-3800 MPa
Failure Strain	2%

7.2.2 Experimental

Fabrication of Composite Specimens for Tensile Testing

The tensile composite specimens were fabricated by compression molding to obtain the

least amount of voids inside the composite specimens. Pressure was applied to the upper and bottom parts of the mold by tightening the clamps. The mixed fibers with epoxy was left in the oven for curing at 80°C for 12 hours. During the fabrication of composites, it was found that 30% total volume fraction of fibers yield better epoxy distribution. Volume fraction of flax, E-glass, and epoxy are 15%, 15% and 70% respectively. Flax and E-glass fiber layers were placed in four different stacking sequences to investigate the effect of fiber locations on the tensile modulus and strength of the hybrid composite experimentally. Table 7.5 shows type of composite and the staking sequence that is considered in this study. Where F and G refer to flax and glass fiber consequently and the numbers after letters refer to number of layers.

Table 7.5: Stacking sequence of flax and glass fibers in tensile composite specimens

Specimen	Type of composite	Stacking sequence
C1	Hybrid composite	F2-G2-F2
C2	Hybrid composite	G-F4-G
C3	Hybrid composite	G-F2-G-F2
C4	Hybrid composite	G2-F4

Fabrication of Composite Specimens for Impact Testing

The impact specimens were manufactured using vacuum assisted resin transfer modeling (VARTM). After the VARTM set-up is completed, epoxy resin is added to the flax and E-glass fiber layers using hand lay-up technique. The mixture was then placed into VARTM set-up under vacuum pressure and at 80°C for 12 hours. The total volume fraction of fiber is 30 %. For hybrid composite specimens, the volume fraction of flax, glass, and epoxy that is considered in this study are 15%, 15%, and 70 % respectively. To study the effect of stacking sequence on the impact strength of hybrid composite, flax and glass fiber layers were put in six different locations. Table 7.6 presents type of composites and arranging of flax and E-glass layers from the top the bottom of specimens. The top surface of specimen is meant to be the notched surface.

Table 7.6: Stacking sequence of flax and glass fibers in impact composite specimens

Specimen	Type of composite	Stacking sequence
C1	Flax fiber Composite	F40
C2	Hybrid composite	F10-G10-F10
C3	Hybrid composite	G5-F20-G5
C4	Hybrid composite	G-F2-...-G-F2
C5	Hybrid composite	F2-G...-F2-G
C6	Hybrid composite	G10-F20
C7	Hybrid composite	F20-G10
C8	Glass fiber composite	G20

7.3 Experimental Setup

7.3.1 Experimental Set-up for Tensile Tests

The experimental setup for tensile test requires load cell, extensometer or strain gage, and Vernier to measure force, strain, and specimen dimensions respectively. Tensile tests were performed on Tinius Olsen tensile tester. Epsilon extensor was used to measure the strain. When tensile tests are carried out on Tinios Olsen machine, force-extension curve or stress-strain curve are generally obtained through the Navigation software provided by the manufacturer of this machine.

Load Cell Calibration

The load cell of Tinios Olsen machine calibrated and the grips alignment where checked. To verify the calibration, ten aluminum samples were tested according to ASTM E38 standard. The cross-head speed is 0.034 in/min. The tests were carried out until the complete failure of the aluminum samples. The published value of tensile modulus of aluminum is 68.9 GPa. The calculated values of tensile modulus from tensile testing are shown in Table 7.7. The achieved values from tensile testing are very close to the published values.

7.3.2 Experiential Set-up for Impact Tests

The experimental setup for impact test needs impact tester and Vernier to measure the break energy and the specimen dimensions respectively. Impact tests were carried out

Table 7.7: Tensile properties of aluminum samples

Sample	Young's Modulus (GPa)
1	67.28
2	65.53
3	63.313
4	65.12
5	68.56
6	62.24
7	64.93
8	65.61
9	67.45
10	63.871
Average	65.39 ± 0.621285

on Instron SI-1A impact machine in SMASH lab. The capacity of the tester is 33 J when pendulum released from low latch position and 81.3 J when it is released from high latch position.

7.4 Test set-up

7.4.1 Water Absorption Test

The moisture absorption properties of flax fiber composite, glass fiber composite, and flax/E-glass fiber hybrid composite were investigated in accordance with ASTM D570-98. Five specimens at least were used for each test sample. First, the specimens were sanded before immersing them in water to make the surfaces and edges smooth and free from cracks. After that, the specimens were placed in an oven at 50°C until they were completely dried. Then, they were allowed to cool to room temperature.

Water absorption tests were carried out by immersing composite specimens in a de-ionized water bath at room temperature (23°C). The composite samples were immersed in de-ioned water for a week. The percentage weight gain of the specimens was measured every 24 hours for a week. For every 24 hours, the specimens were taken out from the water container. Water on the surfaces of the samples was removed with a clean dry cloth. Then, the specimens were weighed to the closest 0.1 gram.

To investigate the effect of changing flax and glass fiber layer locations in composite samples on water uptake, E-glass and flax fibers were placed in four different locations. Table 7.8 shows the staking sequence of fiber layers that is considered in this work.

Table 7.8: Stacking sequence of flax and E-glass fiber layers in water absorption composite specimens

Specimen	Type of composite	Stacking sequence
C1	Flax fiber Composite	F8
C2	Hybrid composite	F2-G2-F2
C3	Hybrid composite	G-F4-G
C4	Hybrid composite	G-F2-G-F2
C5	Hybrid composite	G2-F4
C6	Glass fiber composite	G4

The percentage of moisture uptake in the composite specimens can be calculated from the mass difference between the specimens immersed in water and dry specimens using the bellow equation:

$$\Delta M = \frac{m_w - m_d}{m_d} X 100\% \tag{7.1}$$

Where ΔM, M_d, and M_w refer to the percentage of water absorption, mass of dry sample, and mass of immersed sample respectively.

Mechanism of Water Absorption

Moisture absorption in polymeric composite is shown to be govern by three major mechanism [75–77] . These mechanisms include,

1. Diffusion of water molecules inside the micro gaps between polymer chains.

2. Capillary transport of water molecules into the voids, gaps, and flaws at the interfacial regions between fibers and the polymeric resin. These voids, gaps, and flaws occur due to the poor wetability and impregnation during fabrication of composite samples.

3. Transport of water molecule by micro cracks in the matrix, formed during swelling of fibers.

7.4.2 Tensile Test

All the tensile specimens were fabricated in accordance with the ASTM D3039 standard. Five tensile specimens were tested for each test sample. The recommended geometry for 0° unidirectional composite is a constant rectangular cross-sectional shape. The recommended dimensions of the specimens are 250 mm x 15 mm and the thickness is determined by ply stacking lay-up. For highly unidirectional composite, it is recommended to use tapered tabs at the ends of specimens. Tabs were made from glass fabric and they have a geometry of 56 mm x 15mm x 2mm. The speed of the test is 2 mm/min. The tests were performed until the complete failure of composite specimens.

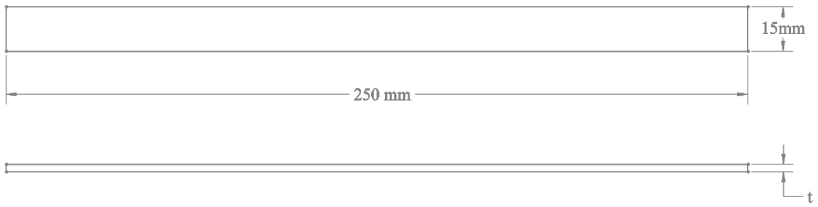

Fig. 7.1: ASTM D3039 standard specimen for unidirectional fiber composites

Glass Tabs

According to ASTM D3039 standard for unidirectional composite, the specimen has a simple rectangle shape of 250 mm x 15 mm x 1 mm. Adding tabs to the ends of the specimens are necessary for two reasons. First, the axial load is applied into the composite specimen through shear forces along the ends of the specimens. Shear forces developed from frictional forces between grip faces and the gripped surfaces of the specimen. Flat or

smooth grips surfaces produce minimal surface damage but they give low friction coefficient between grips and specimen. Thus, flat or smooth grips are unfavorable because specimen may slip without failing. Therefore, grips with coarse surfaces must be used to prevent sliding of specimen. Because coarse surfaces of grips produce permanent surface damage at the gripped regions of the specimens, premature failure may occur in the gripped regions. For this reason, tabs must be added onto the ends of the specimens in the gripped regions to prevent the undesired failure of specimens. Second, they increase the area of the loading regions and therefore reduce the stress concentration. Tabs are usually tapered at the gage section ends to minimize stress concentration and to assure a valid failure within the gage length of the specimen. Tabs are glued to the ends of the specimen using adhesives.

In this work, tabs were made from glass fabric reinforced epoxy resin. Selection of adhesive is also important. The adhesive must be chosen to be able to transmit the load from tabs to the specimen through shear. Firstly, tabs were glued to specimen using PT2050 and hardener B1 epoxy resin. During tensile testing, epoxy failed at the surfaces between tabs and composite specimen before the complete failure of the specimen. Several methods were attempted to solve this problem. First, it was thought that adhesives failed due to the smooth surfaces of tabs and the bonded surfaces of the composite specimen. The tabbed surfaces of the specimens were roughened to create rough surface and then bonded to the tabs. Unfortunately, the surface roughness was not enough to prevent damage of adhesive. Then, two types of adhesives with high shear and peel stresses were used, 3M Scotch-Weld Epoxy Adhesive 2216 B/A Translucent and 3M Scotch-Weld Epoxy Adhesive 2216 B/A Gray. The same problem was occurred for 3M Scotch-Weld Epoxy Adhesive 2216 B/A Translucent. Fortunately, the problem was solved when 3M Scotch-Weld Epoxy Adhesive 2216 B/A Gray was used without roughening the surfaces of tabs and the specimens.

7.4.3 Impact Test

Flax fiber composite, E-glass fiber composite, and flax/E-glass fiber hybrid composite

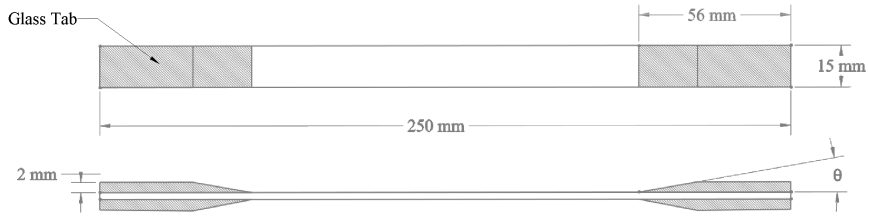

Fig. 7.2: Composite tensile specimen with glass tabs

impact specimens were fabricated according to ASTM E23. ASTM E23 is originally written for Charpy impact tests of notched material specimens. Because there is no ASTM standard available for Charpy impact tests of notched composite specimens, the ASTM E23 was here modified to accommodate composite materials. The recommended geometry of standard is 55 mm x 10 mm x 10 mm. V-notch was made on the surface of the impact specimen. The depth of the notch is 2 mm. Figs. 7.4 -7.11 show the V-notched impact specimen of flax fiber composite, glass fiber composite, and various fiber placement of flax and glass fiber composites. The brown regions represent the flax fibers layers and yellow regions represent the E-glass fiber layers. Five specimens were used for each tests.

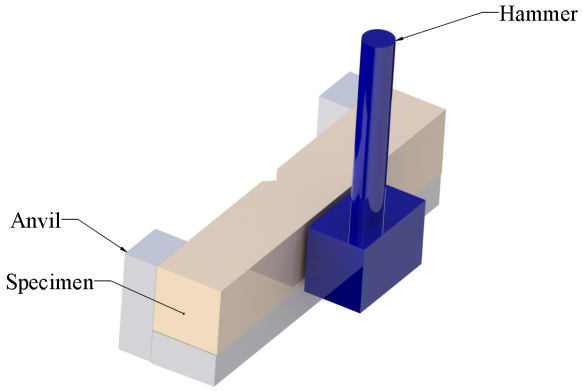

Fig. 7.3: Charpy impact test of notched specimen

Fig. 7.4: F40

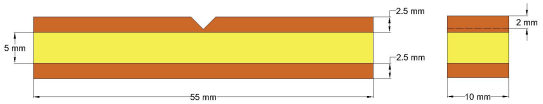

Fig. 7.5: F10-G10-F10

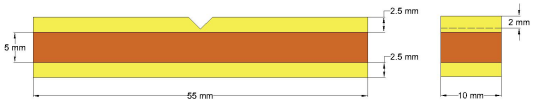

Fig. 7.6: G5-F20-G5

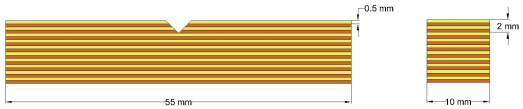

Fig. 7.7: G-F2-...-G-F2

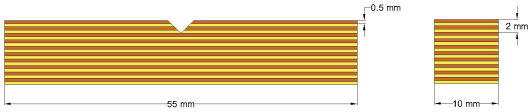

Fig. 7.8: F2-G-...-F2-G

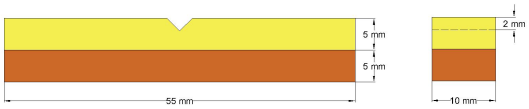

Fig. 7.9: G10-F20

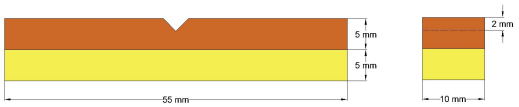

Fig. 7.10: F20-G10

Fig. 7.11: G20

7.5 Results and Discussion

7.5.1 Sorption Properties

Table7.9 and Fig.7.12 show the calculated values from the water absorption testing of flax fiber composite, E-glass fiber composite, and different stacking sequence of flax/E-glass fiber hybrid composite.

Observations:

- It can be clearly observed that flax fiber composite absorbs more water than other composites. In another hand, glass fiber composite absorbs the least amount of water compared to other composites.
- The water absorption of pure flax fiber composite is greatly improved with introducing glass fiber. Water absorption property of flax fiber composite reduced by 36-71 % with incorporation of only 15% glass fiber volume fraction.
- The best design of natural/synthetic fiber hybrid composite that can assure the minimum amount of moisture absorption is when synthetic fiber placed in the extreme positions. This is due to the fact that natural fibers absorb much more water than

Table 7.9: Calculated water uptake and corresponding stacking staking sequence of hybrid composites

Specimen	24hrs	48hrs	72 hrs	96 hrs	120 hrs	144 hrs	168 hrs
C1	2.42±0.355	3.28±0.57	3.76±0.45	4.48±0.7	4.84±0.616	5.34±0.677	5.82±0.668
C2	2.296 ± 0.3	2.588±0.24	2.78±0.3	3.14±0.25	3.27±0.37	3.27±0.36	3.75±0.255
C3	1.17±0.279	1.287±0.079	1.3±0.081	1.3±0.081	1.3±0.081	1.3±0.081	1.686±0.329
C4	1.384±0.04	1.384±0.04	1.939±0.3	1.939±0.3	1.939±0.3	2.08±0.06	2.08±0.06
C5	1.19±0.08	1.76±0.48	2.03±0.37	2.266±0.294	2.266±0.294	2.39±0.167	2.39±0.167
C6	0	0.6±0.008	0.6±0.008	0.6±0.008	0.6±0.008	0.6±0.008	0.6±0.008

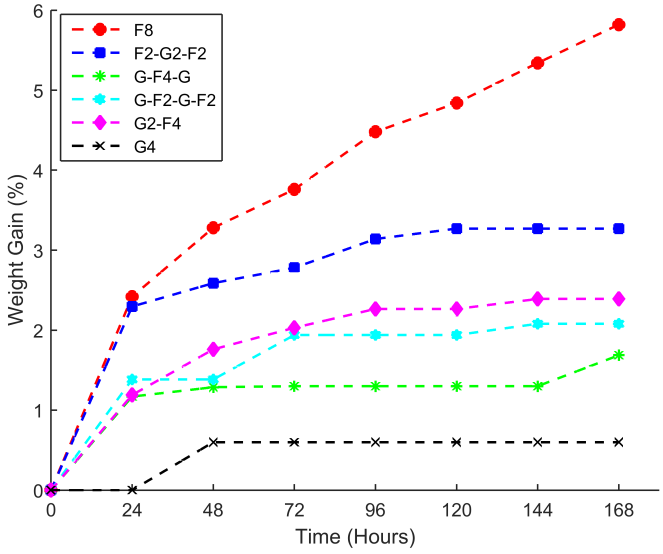

Fig. 7.12: Water absorption curves at room temperature for different samples

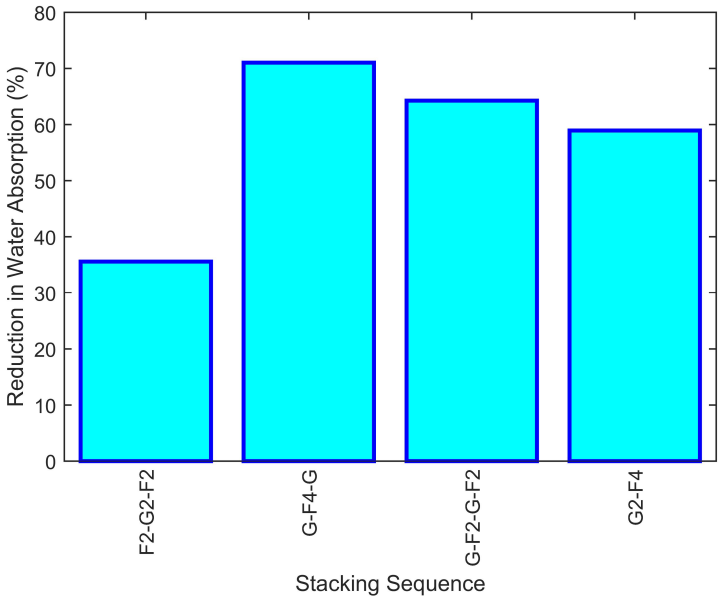

Fig. 7.13: Percent reduction in water absorption

synthetic fibers. When synthetic fiber located in the extreme surfaces of composite sample, the moisture absorption behavior is improved due to the barrier provided by the more impermeable synthetic fiber.

- Change in color of composite specimens occurred due to subjecting specimens to aqueous environment. Fig.7.14 shows the difference in color between dry and wet specimens. The wet specimen is on the left.

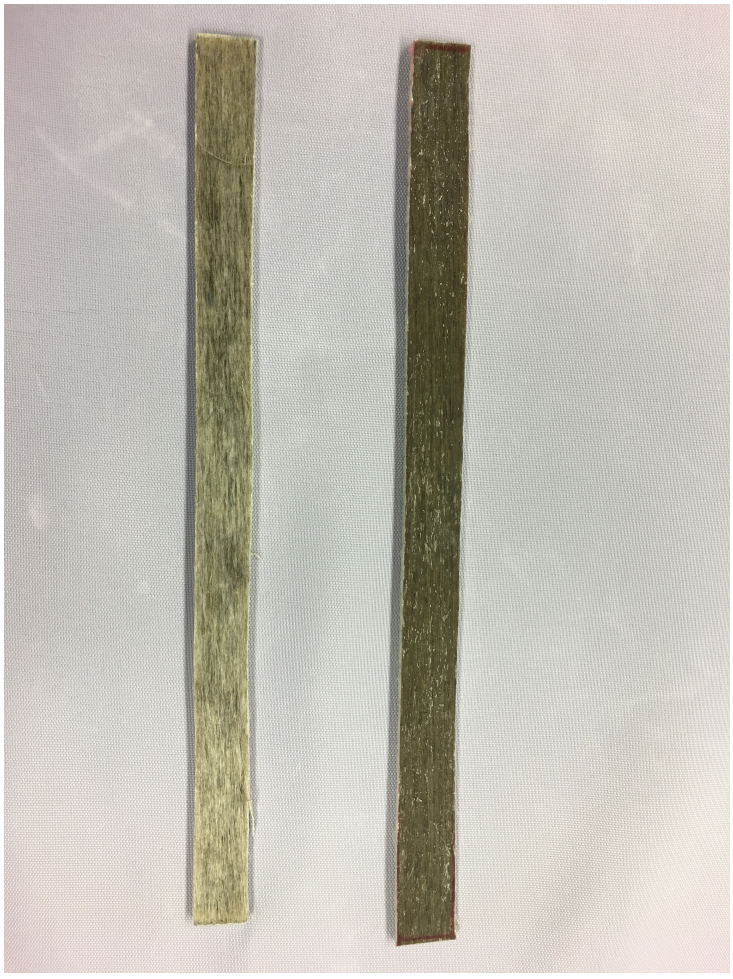

Fig. 7.14: Difference in color between dry and wet specimens

7.5.2 Tensile Properties

Tensile testing was performed on dry and wet specimens. The effect of subjecting composite specimens to water aging on tensile properties is given. The comparison between dry and wet specimens are made.

Tensile Properties for Dry Specimens

Table 7.10 and Figs. 7.15 and 7.16 show the results for tensile testing of dry specimens. The tested specimens are flax/E-glass fiber reinforced hybrid composite. Flax and E-glass fibers are placed in four different locations to show the effect of changing fiber locations on the tensile properties.

Table 7.10: Tensile properties of dry specimens

Panel Configuration	Young's Modulus(GPa)	Tensile Strength(MPa)
F2-G2-F2	23.25±1.61	327.37±16.73
G-F4-G	23.32 ±0.99	360.44 ±6.4
G-F2-G-F2	23.68 ± 1.184	358.656 ±9.69
G2-F4	25.47 ±0.33	308.39 ±5.53

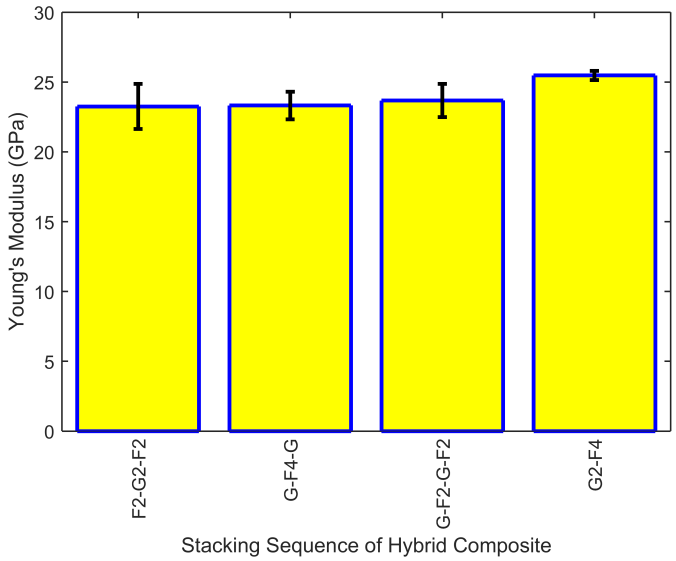

Fig. 7.15: Young's modulus of dry specimens of hybrid composites

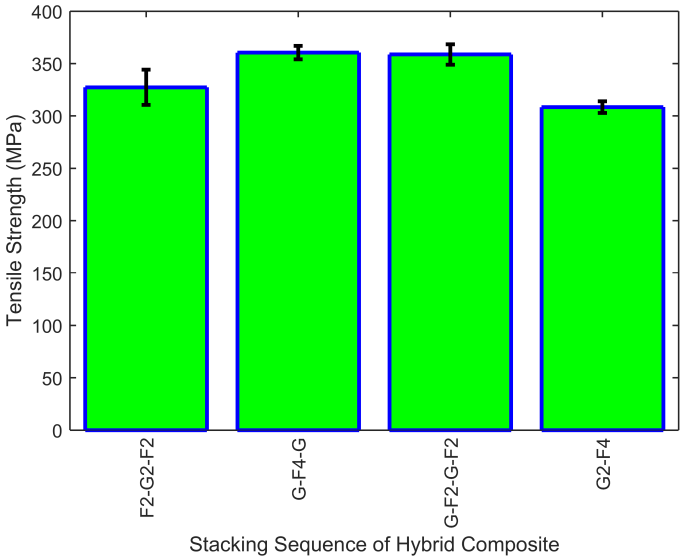

Fig. 7.16: Tensile strength of dry specimens of hybrid composite

Observations:

- Changing flax and glass fiber locations does not show significant effect on Young's modulus of composite. However, it shows noticeable effect on tensile strength. Tensile strength of G-F4-G and G-F2-G-F2 stacking sequence is nearly 110% greater than that of F2-G2-F2 and G-F2-G-F2 stacking sequence. As it is noticed from flax fiber, the surface of flax fiber is rough. SEM images showed that flax fiber has twisted structure with defects. The rough surface of flax fiber and the twisted structure of flax fiber play a noticeable rule in the adhesion between flax fiber layers and glass fiber layers. When the glass fiber placed on the top and bottom positions or on the consecutive order with flax fiber, the adhesion between flax and glass fiber layers improved and led to improve the stress transfer efficiency on the interface between flax fiber and

E-glass fibers. The enhanced interfaces among fiber layers of composite led to higher tensile strength.

- The best design is when glass fibers placed in the top and bottom surfaces of specimen or when glass and flax fiber placed in consecutive orders (G-F2-G-F2). In another hand, the worst design is when flax fiber placed on one side of the specimen and glass fiber placed on another side (G2-F4) or when flax fiber put on the top and bottom surfaces of the specimen (F2-G2-F2).

- During the tensile testing, it was observed that flax fiber failed first. When flax fiber failed, the load transfered to glass fibers. The composite failure eventually occurred due to the failure of glass fibers.

Comparison Between FEA and Analytical results with Experimental Results

In chapter 6, axial Young's modulus of unidirectional fiber composite were determined for different flax and glass fiber content using FEA and analytical equations. In this section, longitudinal Young's modulus calculated from tensile testing is compared with those obtained from FEA and analytical equations at 15%, 15%, and 70% volume fractions of flax, glass, and epoxy resin respectively. The purpose of comparison is to validate the experimental results and to show whether hybridization E-glass fiber with flax fiber have an effect on tensile modulus of composite. Tables 7.11 and 7.12and Fig. 7.17 display the difference between FEA, analytical, and experimental results for different stacking sequence of flax/E-glass fiber reinforced epoxy resin. The shown values are in GPa units.

Table 7.11: Comparison between experimental and FEA results for various stacking sequence of composite specimens

Stacking Sequence	F2-G2-F2	G-F4-G	G-F2-G-F2	G2-F4
Exp.	23.25	23.32	23.68	25.47
FEA	21.967	21.967	21.967	21.967
% Diff.(absolute)	5.84	6.16	7.8	15.95

Observation:

Table 7.12: Comparison between experimental and analytical results for various stacking sequence of composite specimens

Stacking Sequence	F2-G2-F2	G-F4-G	G-F2-G-F2	G2-F4
Exp.	23.25	23.32	23.68	25.47
RoHM	21.95	21.95	21.95	21.95
% Diff.(absolute)	5.92	6.24	7.88	16.04

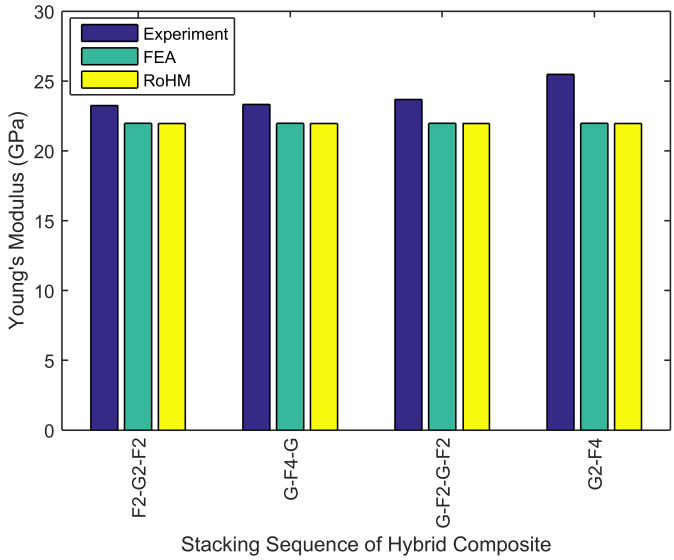

Fig. 7.17: Calculated Young's modulus of various stacking sequence of hybrid composite from tensile testing, FEA, and RoHM

- It can be concluded from the above Tables 7.11 and 7.12 and Fig. 7.17 that Young's modulus values obtained from tensile testing are greater than those predicted from FEA and RoHM. In other words, flax/E-glass fiber reinforced epoxy resin showed positive hybrid effect because Young's modulus achieved from tensile testing is higher than that determined from RoHM. Several authors have shown that hybridization of glass fiber with a natural fiber can lead to get a positive hybrid effect. For instance, this research article showed a positive hybrid effect due to hybridization of glass fibers with natural fibers to reinforce polymeric resin [20].

7.5.3 Effect of Moisture Absorption on Tensile Properties

Tensile properties of wet specimen for various stacking sequences of flax and glass fibers are shown in Table 7.13. (exposure time is 168hrs at 23°C).

Table 7.13: Tensile properties of wet specimens

Panel Configuration	Young's Modulus(GPa)	Tensile Strength(MPa)
F2-G2-F2	21.27±1.88	354.99±13.75
G-F4-G	22.748 ±1.06	379.18 ±18.243
G-F2-G-F2	22.086 ± 1.022	379.11 ±13.76
G2-F4	20.77±1.398	340.8 ±15.38

Tensile modulus and strength of dry and wet specimens versus stacking sequence of flax and E-glass fiber layers are shown in Figs. 7.18 and 7.19.(Exposure time is 168hrs at 23°C)

Observation:

- Young's modulus was decreased after water immersion of 168 hrs. The reductions in Young's modulus due to immersing of hybrid composite specimens in de-ionized water can be attributed to the plasticization of composite specimens. Young's modulus

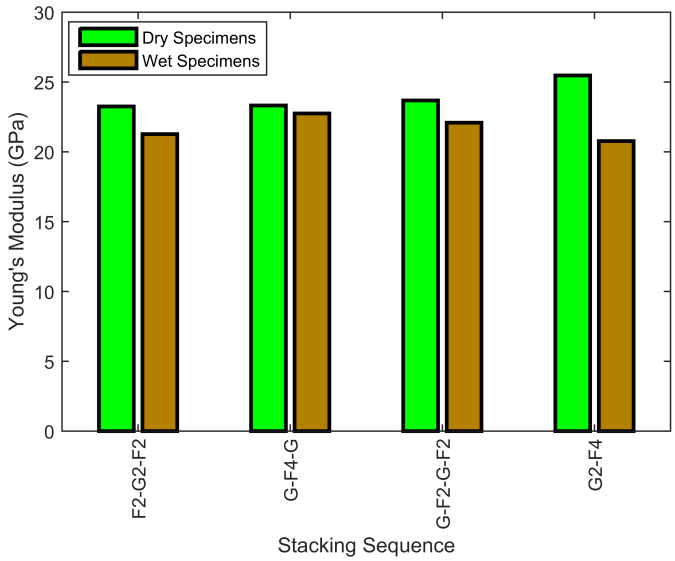

Fig. 7.18: Young's Modulus of dry and wet specimens

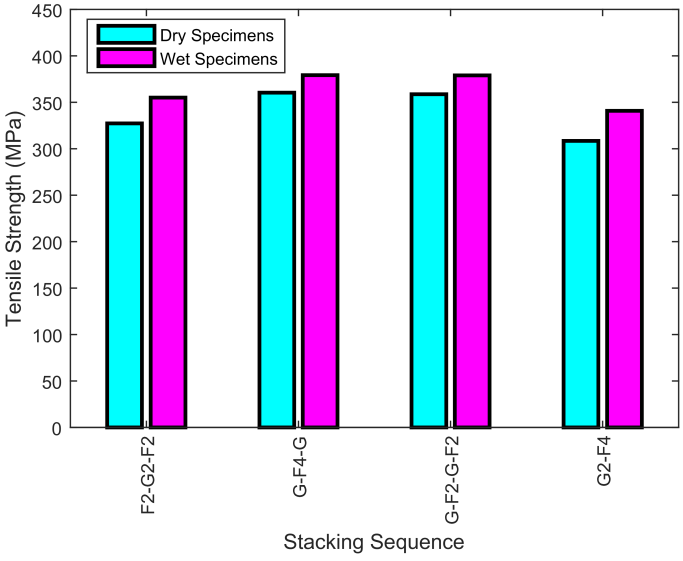

Fig. 7.19: Tensile strength of dry and wet specimens

decreased by 9.3%, 2.5%, 7.2%, and 22.62% for F2-G2-F2, G-F4-G, G-F2-G-F2, and G2-F4 stacking sequence respectively.

- As it can be noticed from Fig.7.19, tensile strength of hybrid composite was increased after immersion in water. Tensile strength increased by 7.78%, 5%, 5.4, and 9.5 for F2-G2-F2, G-F4-G, G-F2-G-F2, and G2-F4 stacking sequence respectively. This increase in tensile strength can be attributed for two probable reasons. First, this increase may imply further cross-linking or other mechanisms happened during immersion in water leading to improve composite strength [78]. Second, it can be contributed to the swelling of the fibers as a result of subjecting them to water immersion. The void or gaps between fibers and epoxy resin that can appear during fabrication of composite samples due to shrinkage of epoxy resin or poor adhesion regions between fibers and matrix can be filled up and therefore can lead to improve the tensile strength of composite [79]. Similar observations have been reported in these research articles [75, 78, 79]

7.5.4 Impact Properties

Table 7.14 and Fig.7.20 displays the result of impact testing. The tested specimens are flax fiber reinforced epoxy resin, E-glass fiber reinforced epoxy resin, and various stacking sequence of flax/E-glass fiber reinforced epoxy resin. The results are given in terms of impact strength (kJ/m^2). Impact strength has been used to refer to the amount of energy absorbed before fracture over the cross-section area of specimen. Percent increase in impact strength due to adding glass fiber to flax fiber is shown in Fig. 7.21.

Observations:

- It can be clearly seen that flax fiber composite has very low impact strength compared to glass fiber composite. The impact strength of glass composite is approximately 11 times larger than that of flax fiber composite.

- The impact strength of pure flax fiber is extremely improved with the incorporation of glass fiber. Compared to flax fiber composite, the impact strength of the hybrid

Table 7.14: Results from Charpy impact testing

Panel Configuration	Impact strength (kJ/m^2)
F40	33.8 ±2.541
F10-G10-F10	179.89 ± 5.27
G5-F20-G5	201.9 ± 8.17
G-F2-...-G-F2	185.14 ± 8.73
F2-G-...-F2-G	205.55 ±6.74
G10-F20	169.05 ± 11.282
F20-G10	206.62 ± 12.1
G20	375.29±8

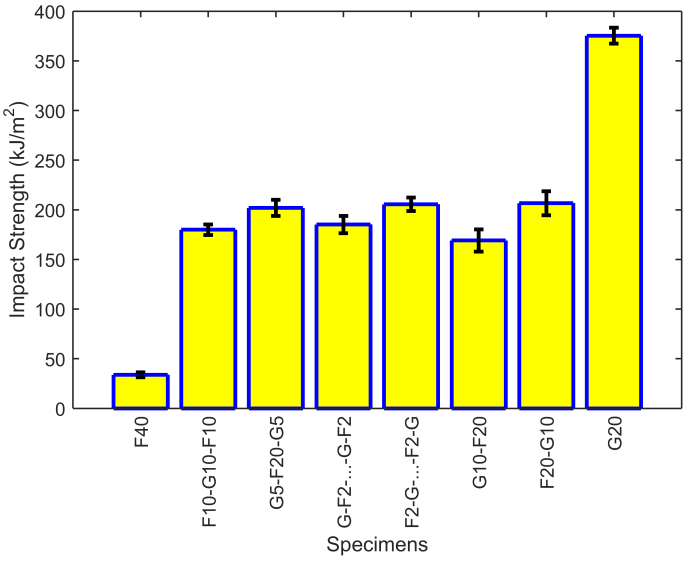

Fig. 7.20: Impact strength for various specimens

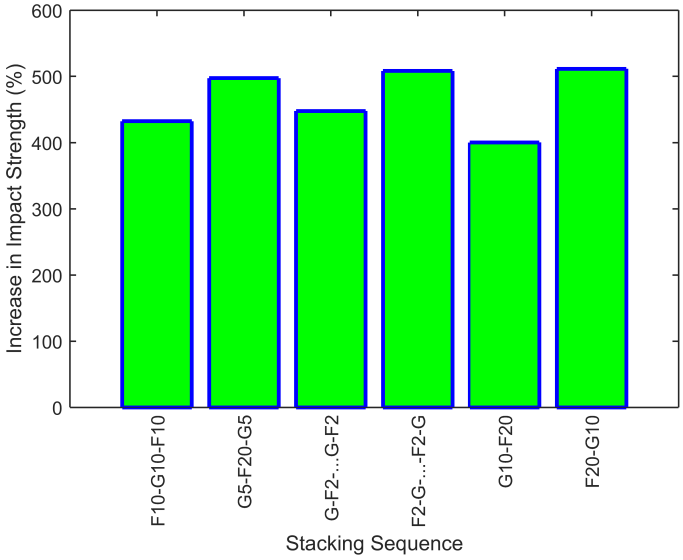

Fig. 7.21: Percent Increase in Impact strength for various fiber layer stacking sequence of hybrid composite compared to flax fiber composite

composite increased by 400-511 % with incorporation of only 15% glass fiber volume fraction.

- Delamination between flax and glass fiber occurred. The occurrence of delamination may be attributed to the big mismatch in impact properties between epoxy resin, flax fibers, and glass fibers. It may also be attributed to the week bonding between the fiber layers. The Delamination between fiber layers was obviously seemed as the major mechanisms in the impact absorption of the hybrid composites.

- The effect of changing fiber layer locations inside the specimen on the impact toughness can be clearly noticed. The best design for impact specimen of hybrid composite is when glass fiber placed in the first position to be having hit by impact machine hammer. This can be attributed to the stiff structure of glass fiber.

CHAPTER 8

Summary, Conclusions and Future Research

8.1 Summary of Work Performed

As a part of this thesis, micormechanical analysis of SG of unidirectional flax/E-glass fiber reinforced epoxy resin was performed to predict the effective properties of composite. A two step homogenization was performed, the first step includes determining the elastic constants of flax fiber at the microscopic scale and the second step is to find the elastic constants of unidirectional flax/glass fiber reinforced hybrid composite. The homogenized properties of flax fiber and flax/E-glass fiber composite were found using FEA and analytical equations. In FEA, SwiftComp tool was used to predict the homogenized properties of composite. SwiftComp is based on MSG theory which is developed by Yu, W. The analytical equations include RoHM and Halpin-Tsai equations, RoHM is used to find the longitudinal Young's modulus and Poisson's ration and Halpin-Tsai equations were used to find the transverse Young's and shear moduli. The effect of changing volume fractions of both fibers with maintaining the total volume fraction the same on the effective properties were investigated using FEA and analytical equations. The effect of changing flax/glass fiber locations on the elastic constants of composite was also investigated using FEA. The FEA results, whenever applicable, was compared with analytical results.

Young's modulus and tensile strength of the unidirectional flax/E-glass hybrid composite were obtained from tensile testing. Young's modulus and tensile strength of composite were calculated for different fiber locations. The Young's modulus values obtained from tensile testing were compared with those obtained from FEA and analytical equations. To investigate the effect of water absorption on Young's modulus and tensile strength of composite, various locations of flax and E-glass fiber composites specimens were immersed in de-ionized water for a week. The weight gain of composite specimens due to immersing

them in water were calculated every 24 hrs. Impact properties of flax fiber composite, E-glass fiber composite, and different stacking sequence of fiber layers of flax/E-glass fiber hybrid composite were determined from Charpy impact test.

8.2 Summary of Findings and Conclusion

Micro-Structure of Flax Fiber

1. It was observed from the scanning election microscope (SEM) that cross-section of flax fiber exhibit irregular shape of 5-7 sides. The length of each side is not the same. Therefore, numerical modeling of flax fiber is challenging because there is no exact shape can describe the cross-section of the fiber. The cross-sectional area of flax fiber measured from SEM had an equivalent circular diameter of 20 μ on average.

Numerical Modeling of Flax Fiber and Flax/E-Glass Fiber Composite

- The effective properties of flax/E-glass fiber reinforced epoxy resin were computed using FEA and analytical equations. In FEA, it is assumed that both fibers are distributed in a hexagonal pattern, perfectly bonded to the epoxy resin, and fibers have circular cross-section with the same radii. Mesh refinement study have been followed until it was made sure that further refinements do not change the results. It is possible to achieve accurate estimates of the elastic constants from FEA. Also, quite accurate estimation of stresses such as the stresses at the interface between the fibers and the matrix can be obtained. Analytical equations include RoHM and Halpin-Tsai equations are also used to predict the elastic constants of the hybrid composite. The assumptions that have been involved in the analytical equations do not necessarily meet the requirements of the exact elasticity solutions. Therefore, the results obtained from analytical equations are approximate. The longitudinal Young's modulus and Poisson's ratio were predicted using RoHM. RoHM is based on Voigt model. In Voigt model, it is assumed that fibers and the matrix experience the same elongation in the

longitudinal direction and fiber and matrix subjected to σ_1. In other words, fibers and matrix are assumed to be under uniform strain in the longitudinal direction. Due to the applied axial stress, the composite tends to stretch in the longitudinal direction and contract in the transverse direction due to the Poisson's effects. It is found that the longitudinal Young's modulus and Poisson's ratio predicted from RoHM are very close to FEA results over different combinations of flax and E-glass fiber volume fractions. Therefore, RoHM can be used instead of FEA if the longitudinal Young's modulus and Poisson's ratio are only of interest. Halpin-Tsai relations are used to predict the transverse Young's moduli and longitudinal and transverse shear moduli of the hybrid composite. Halpin-Tsai model is based on the self-consistent method provided by Hill. Halpin-Tsai equations derived based on the geometry and the orientation of the reinforcement and the elastic constants of the reinforcement and the matrix. The usage of the equations is limited to one type of fibers embedded in a matrix. To use Halpin Tsai equations for hybrid composites, modifications have been proposed by Banerjee et al. [36]. It was found that the elastic constants predicted from Halpin-Tsai equations gives a discrepancy compared to FEA results. The source of the discrepancy is because Halpin-Tsai equations rely on the aspect ratio of the reinforcement. To minimize the difference between FEA and Halpin-Tsai results, the ξ term in the Halpin-Tsai equations can be iteratively changed until the results obtained from Halpin-Tsai equations are very close to FEA results.

- The homogenized properties of flax fiber were obtained using finite element modeling and analytical equations, with varying flax fiber constituent contents and microfibril orientation in S2 layer. It was observed that Young's modulus in axial and transverse direction increased linearly with increasing the cellulose content of S2 layer from 64% to 71%. Other elastic constant were observed to be least effected with changing the cellulose content. The longitudinal Young's modulus of flax fiber decreased linearly and the longitudinal Poisson's ratio increased with increasing the microfibril angle from 6° - 10°. Other elastic constants were least effected with increasing the microfibril

angle.

- It was seen that flax fiber has orthotropic properties while glass fiber and epoxy exhibit isotropic properties. Therefore, combination of flax and glass fiber to reinforce epoxy resin resulted in a composite with orthotropic properties.

- It was deduced that adding glass fiber to flax fiber lead to increase the elastic constants of composite. It was observed that Young's and shear moduli in axial and transverse directions increased linearly with increasing the content of glass fiber. However, the axial Poisson's ratio decreased with increasing the content of glass fiber.

- It was concluded that changing flax and glass fiber locations inside SG showed no effect on the elastic constants of the hybrid composite.

Tensile, Impact, and Water Absorption Properties of Unidirectional Flax/Glass Fiber Composite

- The water absorption test showed that flax fiber composite absorbs more water than glass fiber composite. Five specimens of each of flax fiber composite, glass fiber composite, and four various location of flax/E-glass fiber hybrid composite were immersed in de-ionized water for a week. The considered location of flax and glass fibers are flax in the top and bottom surfaces of the specimen while glass fibers are in the middle (F2-G2-F2), glass fiber in the extreme positions of the specimens and flax fibers in the middle (G-F4-G), glass and flax fibers placed in consecutive orders (G-F2-G-F2), and glass fibers in one side of the specimen and flax fiber in the other side (G2-F4). G and F refer to glass fiber and flax fiber respectively and the number after the G and F letters represent the number of layers. It was seen that flax fiber composite absorbs water nearly 10 times more than glass fiber composite. Therefore, hybridization of glass fiber with flax fiber can lead to minimize the water absorption properties of the hybrid composite. Reduction of 36-71 % was achieved when 15% percent of glass fiber added to flax fiber. It was seen that changing the stacking sequence of flax and

glass fibers had an effect on water absorption of the hybrid composite. G-F4-G absorbed the least amount of water compare to other hybrid composite while F2-G2-F2 absorbed more water than other hybrid composite.

- Young's modulus and tensile strength of unidirectional flax/E-glass fiber reinforced epoxy resin were evaluated from tensile testing. Four different locations of flax and glass fiber layers were used during the fabrication of the hybrid specimens to investigate the effect of changing fiber locations on the tensile properties. The considered locations of flax and glass fibers are flax in the top and bottom surfaces of the specimen while glass fibers are in the middle (F2-G2-F2), glass fiber in the extreme positions of the specimens and flax fibers in the middle (G-F4-G), glass and flax fibers placed in consecutive orders (G-F2-G-F2), and glass fibers in one side of the specimen and flax fiber in the other side (G2-F4). G and F refer to glass fiber and flax fiber respectively and the number after the G and F letters represent the number of layers. It was obtained that varying flax and glass fiber locations have insignificant effect on Young's modulus. However, changing fiber locations have noticeable effect on tensile strength of hybrid composite. It was seen that the tensile strength of G-F4-G and G-F2-G-F2 stacking sequence is approximately 110% greater than that of F2-G2-F2 and G2-F4.

- An increase in tensile strength was achieved after the hybrid composite specimen were immersed in de-ionized water at room temperature for a week. Tensile strength increased by 7.78%, 5%, 5.4%, and 9.5% for F2-G2-F2, G-F4-G, G-F2-G-F2, and G2-F4 staking sequence of hybrid composite. This increase in tensile strength can be justified by two reasons. This increase occurred due to further cross-linking happened or swelling of fibers fill up the voids or gap between fibers and the matrix. However, Young's modulus reduced when the hybrid composite specimens immersed in water. Young's modulus dropped by 9.3%, 2.5%, 7.2%, and 22.6% for F2-G2-F2, G-F4,G, G-F2-G-F2, and G2-F4 respectively.

- Charpy impact test were performed on notched specimen of flax fiber composite, E-glass fiber composite, and flax/E-glass fiber composite. To study the effect of changing fiber placement on the impact properties, flax and glass fiber were placed in various locations. The locations of flax and glass fibers that are considered in this study are flax in the top and bottom surfaces of the specimen while glass fibers are in the middle (F10-G10-F10), glass fiber in the extreme positions of the specimens and flax fibers in the middle (G5-F20-G5), glass and flax fibers placed in consecutive orders (G-F2-...-G-F2) and (F2-G-...-F2-G), and glass fibers in one side of the specimen and flax fiber in the other side (G10-F20) and (F20-G10). The top surface meant to be the notched surface. It was observed that flax fiber composite had very low impact strength compared to glass fiber composite. The impact strength of glass fiber is about 1100% greater than that of flax fiber. Therefore, adding glass fiber to flax fiber improved the impact strength. The impact strength of flax fiber increased by 400-511% when 15% volume fraction of glass fiber added. The effect of changing of fiber locations on impact properties was observed. It was concluded that the best design of the hybrid composite when glass fiber placed in the first position to be having hit by impact machine hammer.

- From water absorption, tensile, and impact tests, it was concluded that the best design of flax/E-glass fiber reinforced epoxy resin is when glass fibers placed in the top and bottom surfaces of the specimen and flax fiber in the middle.

8.3 Suggestions For Future Work

- Experimental testing of flax fiber will be required to do. This can help to validate the numerical and analytical results.

- The effect of considering irregular cross-section shape of flax fiber on the effective properties of the hybrid composite will be required to model.

- Damage model of unit cell containing voids in matrix and imperfect bonding between fibers and matrix will be suggested to model the damage behavior of the composite.
- Immersion of flax fiber composite, glass fiber composite, and flax/E-glass fiber hybrid composite specimen in de-ionized water until the saturation will be suggested to find the saturation time of each composite type and to study the effect of immersing composite specimens until saturation on mechanical performance of composite.
- Charpy impact test of wet specimen will be required to perform to study the effect of water aging on the impact strength of composite.
- Flexural testing of different fiber placement of flax/E-glass reinforced epoxy resin will be suggested. This can show the effect of varying fiber locations on the flexural properties of the hybrid composite.

REFERENCES

[1] Mallick, P. K., *Fiber-reinforced composites: materials, manufacturing, and design*, CRC press, 2007.

[2] Morye, S. and Wool, R., "Mechanical properties of glass/flax hybrid composites based on a novel modified soybean oil matrix material," *Polymer Composites*, Vol. 26, No. 4, 2005, pp. 407–416.

[3] Yang, Y., Boom, R., Irion, B., van Heerden, D.-J., Kuiper, P., and de Wit, H., "Recycling of composite materials," *Chemical Engineering and Processing: Process Intensification*, Vol. 51, 2012, pp. 53–68.

[4] Joshi, S. V., Drzal, L., Mohanty, A., and Arora, S., "Are natural fiber composites environmentally superior to glass fiber reinforced composites?" *Composites Part A: Applied science and manufacturing*, Vol. 35, No. 3, 2004, pp. 371–376.

[5] Kalia, S., Kaith, B., and Kaur, I., *Cellulose fibers: bio-and nano-polymer composites: green chemistry and technology*, Springer Science & Business Media, 2011.

[6] Nunna, S., Chandra, P. R., Shrivastava, S., and Jalan, A., "A review on mechanical behavior of natural fiber based hybrid composites," *Journal of Reinforced Plastics and Composites*, Vol. 31, No. 11, 2012, pp. 759–769.

[7] Wambua, P., Ivens, J., and Verpoest, I., "Natural fibres: can they replace glass in fibre reinforced plastics?" *composites science and technology*, Vol. 63, No. 9, 2003, pp. 1259–1264.

[8] Mishra, S., Mohanty, A., Drzal, L., Misra, M., Parija, S., Nayak, S., and Tripathy, S., "Studies on mechanical performance of biofibre/glass reinforced polyester hybrid composites," *Composites Science and Technology*, Vol. 63, No. 10, 2003, pp. 1377–1385.

[9] Holbery, J. and Houston, D., "Natural-fiber-reinforced polymer composites in automotive applications," *Jom*, Vol. 58, No. 11, 2006, pp. 80–86.

[10] Mohanty, A., Misra, M., and Hinrichsen, G., "Biofibres, biodegradable polymers and biocomposites: an overview," *Macromolecular materials and engineering*, Vol. 276, No. 1, 2000, pp. 1–24.

[11] Arbelaiz, A., Fernandez, B., Cantero, G., Llano-Ponte, R., Valea, A., and Mondragon, I., "Mechanical properties of flax fibre/polypropylene composites. Influence of fibre/matrix modification and glass fibre hybridization," *Composites Part A: Applied Science and Manufacturing*, Vol. 36, No. 12, 2005, pp. 1637–1644.

[12] Bodros, E., Pillin, I., Montrelay, N., and Baley, C., "Could biopolymers reinforced by randomly scattered flax fibre be used in structural applications?" *Composites Science and Technology*, Vol. 67, No. 3, 2007, pp. 462–470.

[13] Burgueño, R., Quagliata, M. J., Mohanty, A. K., Mehta, G., Drzal, L. T., and Misra, M., "Load-bearing natural fiber composite cellular beams and panels," *Composites Part A: applied science and manufacturing*, Vol. 35, No. 6, 2004, pp. 645–656.

[14] Burgueno, R., Quagliata, M. J., Mohanty, A. K., Mehta, G., Drzal, L. T., and Misra, M., "Hybrid biofiber-based composites for structural cellular plates," *Composites Part A: applied science and manufacturing*, Vol. 36, No. 5, 2005, pp. 581–593.

[15] Davoodi, M., Sapuan, S., Ahmad, D., Ali, A., Khalina, A., and Jonoobi, M., "Mechanical properties of hybrid kenaf/glass reinforced epoxy composite for passenger car bumper beam," *Materials & Design*, Vol. 31, No. 10, 2010, pp. 4927–4932.

[16] Almeida, J. H. S., Amico, S. C., Botelho, E. C., and Amado, F. D. R., "Hybridization effect on the mechanical properties of curaua/glass fiber composites," *Composites Part B: Engineering*, Vol. 55, 2013, pp. 492–497.

[17] Swolfs, Y., Gorbatikh, L., and Verpoest, I., "Fibre hybridisation in polymer composites: a review," *Composites Part A: Applied Science and Manufacturing*, Vol. 67, 2014, pp. 181–200.

[18] Jawaid, M. and Khalil, H. A., "Cellulosic/synthetic fibre reinforced polymer hybrid composites: A review," *Carbohydrate Polymers*, Vol. 86, No. 1, 2011, pp. 1–18.

[19] Sreekala, M., George, J., Kumaran, M., and Thomas, S., "The mechanical performance of hybrid phenol-formaldehyde-based composites reinforced with glass and oil palm fibres," *Composites science and technology*, Vol. 62, No. 3, 2002, pp. 339–353.

[20] Zhang, Y., Li, Y., Ma, H., and Yu, T., "Tensile and interfacial properties of unidirectional flax/glass fiber reinforced hybrid composites," *Composites Science and Technology*, Vol. 88, 2013, pp. 172–177.

[21] Kim, D.-H., Kim, H.-G., and Kim, H.-S., "Design optimization and manufacture of hybrid glass/carbon fiber reinforced composite bumper beam for automobile vehicle," *Composite Structures*, Vol. 131, 2015, pp. 742–752.

[22] Swolfs, Y., Verpoest, I., and Gorbatikh, L., "Maximising the hybrid effect in unidirectional hybrid composites," *Materials & Design*, Vol. 93, 2016, pp. 39–45.

[23] Dittenber, D. B. and GangaRao, H. V., "Critical review of recent publications on use of natural composites in infrastructure," *Composites Part A: Applied Science and Manufacturing*, Vol. 43, No. 8, 2012, pp. 1419–1429.

[24] Shah, D. U., Schubel, P. J., and Clifford, M. J., "Can flax replace E-glass in structural composites? A small wind turbine blade case study," *Composites Part B: Engineering*, Vol. 52, 2013, pp. 172–181.

[25] Yan, L., Chouw, N., and Jayaraman, K., "Flax fibre and its composites–A review," *Composites Part B: Engineering*, Vol. 56, 2014, pp. 296–317.

[26] Gururaja, M. and Rao, A. H., "A review on recent applications and future prospectus of hybrid composites," *International Journal of Soft Computing and Engineering (IJSCE)*, Vol. 1, No. 6, 2012, pp. 352–355.

[27] Fu, S.-Y., Lauke, B., Mäder, E., Yue, C.-Y., Hu, X., and Mai, Y.-W., "Hybrid effects on tensile properties of hybrid short-glass-fiber-and short-carbon-fiber-reinforced polypropylene composites," *Journal of materials science*, Vol. 36, No. 5, 2001, pp. 1243–1251.

[28] Ashori, A., "Wood–plastic composites as promising green-composites for automotive industries!" *Bioresource Technology*, Vol. 99, No. 11, 2008, pp. 4661–4667.

[29] Pickering, K. L., Efendy, M. A., and Le, T. M., "A review of recent developments in natural fibre composites and their mechanical performance," *Composites Part A: Applied Science and Manufacturing*, Vol. 83, 2016, pp. 98–112.

[30] Gurunathan, T., Mohanty, S., and Nayak, S. K., "A review of the recent developments in biocomposites based on natural fibres and their application perspectives," *Composites Part A: Applied Science and Manufacturing*, Vol. 77, 2015, pp. 1–25.

[31] Bourmaud, A., Morvan, C., Bouali, A., Placet, V., Perre, P., and Baley, C., "Relationships between micro-fibrillar angle, mechanical properties and biochemical composition of flax fibers," *Industrial Crops and Products*, Vol. 44, 2013, pp. 343–351.

[32] Baley, C., "Analysis of the flax fibres tensile behaviour and analysis of the tensile stiffness increase," *Composites Part A: Applied Science and Manufacturing*, Vol. 33, No. 7, 2002, pp. 939–948.

[33] Naik, L. and Fronk, T. H., "Weibull distribution analysis of the tensile strength of the kenaf bast fiber," *Fibers and Polymers*, Vol. 17, No. 10, 2016, pp. 1696–1701.

[34] Charlet, K., Baley, C., Morvan, C., Jernot, J., Gomina, M., and Bréard, J., "Characteristics of Hermès flax fibres as a function of their location in the stem and properties of the derived unidirectional composites," *Composites Part A: Applied Science and Manufacturing*, Vol. 38, No. 8, 2007, pp. 1912–1921.

[35] Placet, V., Trivaudey, F., Cisse, O., Gucheret-Retel, V., and Boubakar, M. L., "Diameter dependence of the apparent tensile modulus of hemp fibres: A morphological, structural or ultrastructural effect?" *Composites Part A: Applied Science and Manufacturing*, Vol. 43, No. 2, 2012, pp. 275–287.

[36] Banerjee, S. and Sankar, B. V., "Mechanical properties of hybrid composites using finite element method based micromechanics," *Composites Part B: Engineering*, Vol. 58, 2014, pp. 318–327.

[37] Singh, B., Gupta, M., and Verma, A., "Mechanical behaviour of particulate hybrid composite laminates as potential building materials," *Construction and Building Materials*, Vol. 9, No. 1, 1995, pp. 39–44.

[38] Thomas, S. and Pothan, L. A., *Natural fibre reinforced polymer composites: from macro to nanoscale*, Archives contemporaines, 2009.

[39] Jarukumjorn, K. and Suppakarn, N., "Effect of glass fiber hybridization on properties of sisal fiber–polypropylene composites," *Composites Part B: Engineering*, Vol. 40, No. 7, 2009, pp. 623–627.

[40] Panthapulakkal, S. and Sain, M., "Injection-molded short hemp fiber/glass fiber-reinforced polypropylene hybrid compositesMechanical, water absorption and thermal properties," *Journal of Applied Polymer Science*, Vol. 103, No. 4, 2007, pp. 2432–2441.

[41] Hariharan, A. B. A. and Khalil, H. A., "Lignocellulose-based hybrid bilayer laminate composite: Part I-Studies on tensile and impact behavior of oil palm fiber-glass fiber-reinforced epoxy resin," *Journal of Composite Materials*, Vol. 39, No. 8, 2005, pp. 663–684.

[42] Pothan, L. A., Thomas, S., and George, J., "Tensile and Impact Properties of Banana Fibre/Glass Fibre Hybrid Polyester Composites," *12th International Conference on Composite Materials, Paris, France*, Vol. 1267, 1999.

[43] Idicula, M., Neelakantan, N., Oommen, Z., Joseph, K., and Thomas, S., "A study of the mechanical properties of randomly oriented short banana and sisal hybrid fiber reinforced polyester composites," *Journal of applied polymer science*, Vol. 96, No. 5, 2005, pp. 1699–1709.

[44] Jacob, M., Thomas, S., and Varughese, K. T., "Mechanical properties of sisal/oil palm hybrid fiber reinforced natural rubber composites," *Composites Science and Technology*, Vol. 64, No. 7, 2004, pp. 955–965.

[45] Jawaid, M., Khalil, H. A., and Bakar, A. A., "Mechanical performance of oil palm empty fruit bunches/jute fibres reinforced epoxy hybrid composites," *Materials Science and Engineering: A*, Vol. 527, No. 29, 2010, pp. 7944–7949.

[46] Venkateshwaran, N., ElayaPerumal, A., Alavudeen, A., and Thiruchitrambalam, M., "Mechanical and water absorption behaviour of banana/sisal reinforced hybrid composites," *Materials & Design*, Vol. 32, No. 7, 2011, pp. 4017–4021.

[47] Tajvidi, M., "Static and dynamic mechanical properties of a kenaf fiber–wood flour/polypropylene hybrid composite," *Journal of applied polymer science*, Vol. 98, No. 2, 2005, pp. 665–672.

[48] Sun, C. and Vaidya, R., "Prediction of composite properties from a representative volume element," *Composites Science and Technology*, Vol. 56, No. 2, 1996, pp. 171–179.

[49] LLorca, J., González, C., Molina-Aldareguía, J. M., Segurado, J., Seltzer, R., Sket, F., Rodríguez, M., Sádaba, S., Muñoz, R., and Canal, L. P., "Multiscale modeling of composite materials: a roadmap towards virtual testing," *Advanced Materials*, Vol. 23, No. 44, 2011, pp. 5130–5147.

[50] Yu, W., "A unified theory for constitutive modeling of composites," *Journal of Mechanics of Materials and Structures*, Vol. 11, No. 4, 2016, pp. 379–411.

[51] Bensoussan, A., Lions, J.-L., and Papanicolaou, G., *Asymptotic analysis for periodic structures*, Vol. 5, North-Holland Publishing Company Amsterdam, 1978.

[52] Hodges, D. and Danielson, D., "Nonlinear beam kinematics by decomposition of the rotation tensor," *J Appl Mech*, Vol. 54, No. 6, 1987, pp. 258–262.

[53] Simmonds, J. G., *A brief on tensor analysis*, Springer Science & Business Media, 2012.

[54] Yu, W. and Hodges, D. H., "A geometrically nonlinear shear deformation theory for composite shells," *TRANSACTIONS-AMERICAN SOCIETY OF MECHANICAL ENGINEERS JOURNAL OF APPLIED MECHANICS*, Vol. 71, No. 1, 2004, pp. 1–9.

[55] Yu, W., Hodges, D. H., and Ho, J. C., "Variational asymptotic beam sectional analysis–an updated version," *International Journal of Engineering Science*, Vol. 59, 2012, pp. 40–64.

[56] Pietraszkiewicz, W. and Eremeyev, V., "On natural strain measures of the non-linear micropolar continuum," *International Journal of Solids and Structures*, Vol. 46, No. 3, 2009, pp. 774–787.

[57] Halpin, J. and Kardos, J., "The Halpin-Tsai equations: a review," *Polymer Engineering & Science*, Vol. 16, No. 5, 1976, pp. 344–352.

[58] Pickering, K., *Properties and performance of natural-fibre composites*, Elsevier, 2008.

[59] Stamboulis, A., Baillie, C., and Peijs, T., "Effects of environmental conditions on mechanical and physical properties of flax fibers," *Composites Part A: Applied Science and Manufacturing*, Vol. 32, No. 8, 2001, pp. 1105–1115.

[60] Madsen, B. and Gamstedt, E. K., "Wood versus plant fibers: similarities and differences in composite applications," *Advances in Materials Science and Engineering*, Vol. 2013, 2013.

[61] Gassan, J., Chate, A., and Bledzki, A. K., "Calculation of elastic properties of natural fibers," *Journal of materials science*, Vol. 36, No. 15, 2001, pp. 3715–3720.

[62] Qing, H. and Mishnaevsky, L., "3D hierarchical computational model of wood as a cellular material with fibril reinforced, heterogeneous multiple layers," *Mechanics of Materials*, Vol. 41, No. 9, 2009, pp. 1034–1049.

[63] Gierlinger, N. and Schwanninger, M., "Chemical imaging of poplar wood cell walls by confocal Raman microscopy," *Plant Physiology*, Vol. 140, No. 4, 2006, pp. 1246–1254.

[64] Sun, Z., Zhao, X., Wang, X., and Ma, J., "Multiscale modeling of the elastic properties of natural fibers based on a generalized method of cells and laminate analogy approach," *Cellulose*, Vol. 21, No. 3, 2014, pp. 1135–1141.

[65] Célino, A., Fréour, S., Jacquemin, F., and Casari, P., "The hygroscopic behavior of plant fibers: A review," *Frontiers in chemistry*, Vol. 1, 2013.

[66] Klemm, D., Heublein, B., Fink, H.-P., and Bohn, A., "Cellulose: fascinating biopolymer and sustainable raw material," *Angewandte Chemie International Edition*, Vol. 44, No. 22, 2005, pp. 3358–3393.

[67] Gibson, L. J., "The hierarchical structure and mechanics of plant materials," *Journal of the Royal Society Interface*, Vol. 9, No. 76, 2012, pp. 2749–2766.

[68] Martone, P. T., Estevez, J. M., Lu, F., Ruel, K., Denny, M. W., Somerville, C., and Ralph, J., "Discovery of lignin in seaweed reveals convergent evolution of cell-wall architecture," *Current Biology*, Vol. 19, No. 2, 2009, pp. 169–175.

[69] Gargulak, J. D., Lebo, S. E., and McNally, T. J., "Lignin," *Kirk-Othmer encyclopedia of chemical technology*, 2001.

[70] Bhatia, M. S., Deshmukh, R., Choudhari, P., and Bhatia, N. M., "Chemical modification of pectins, characterization and evaluation for drug delivery," *Scientia Pharmaceutica*, Vol. 76, No. 4, 2008, pp. 775–784.

[71] Komuraiah, A., Kumar, N. S., and Prasad, B. D., "Chemical composition of natural fibers and its influence on their mechanical properties," *Mechanics of composite materials*, Vol. 50, No. 3, 2014, pp. 359–376.

[72] Hewitt, R. and De Malherbe, M., "An approximation for the longitudinal shear modulus of continuous fibre composites," *Journal of Composite Materials*, Vol. 4, No. 2, 1970, pp. 280–282.

[73] Mohammed, L., Ansari, M. N., Pua, G., Jawaid, M., and Islam, M. S., "A review on natural fiber reinforced polymer composite and its applications," *International Journal of Polymer Science*, Vol. 2015, 2015.

[74] Saheb, D. N., Jog, J., et al., "Natural fiber polymer composites: a review," *Advances in polymer technology*, Vol. 18, No. 4, 1999, pp. 351–363.

[75] Karmaker, A., Hoffmann, A., and Hinrichsen, G., "Influence of water uptake on the mechanical properties of jute fiber-reinforced polypropylene," *Journal of Applied Polymer Science*, Vol. 54, No. 12, 1994, pp. 1803–1807.

[76] Espert, A., Vilaplana, F., and Karlsson, S., "Comparison of water absorption in natural cellulosic fibres from wood and one-year crops in polypropylene composites and its influence on their mechanical properties," *Composites Part A: Applied science and manufacturing*, Vol. 35, No. 11, 2004, pp. 1267–1276.

[77] Thwe, M. M. and Liao, K., "Effects of environmental aging on the mechanical properties of bamboo–glass fiber reinforced polymer matrix hybrid composites," *Composites Part A: Applied Science and Manufacturing*, Vol. 33, No. 1, 2002, pp. 43–52.

[78] Dhakal, H., Zhang, Z., and Richardson, M., "Effect of water absorption on the mechanical properties of hemp fibre reinforced unsaturated polyester composites," *Composites Science and Technology*, Vol. 67, No. 7, 2007, pp. 1674–1683.

[79] Muñoz, E. and Garcia-Manrique, J., "Water absorption behaviour and its effect on the mechanical properties of flax fibre reinforced bioepoxy composites," *International Journal of Polymer Science*, Vol. 2015, 2015.